From the:

Biomedizinisches Centrum München, Ludwig-Maximilians-Universität München

Dissertation
zum Erwerb des Doctor of Philosophy (Ph.D.) an der
Medizinischen Fakultät der
Ludwig-Maximilians-Universität zu München

The role of DNA sequence in S. cerevisiae nucleosome organisation as implemented by chromatin remodelers and general regulatory factors

Submitted by

Toby Barnes

from

London, UK

2022

First evaluator (1. TAC member): PD Dr. Philipp Korber

Second evaluator (2. TAC member): Dr. Tobias Straub

Third evaluator: Prof. Andreas Ladurner

Fourth evaluator: Prof. Dr. Robert Schneider

Dean: Prof. Dr. med. Thomas Gudermann

Date of oral defence: 23.03.2023

Table of content

Table of content 3

Abstract (English): 5

List of figures 6

List of tables 7

List of abbreviations 8

1. Introduction 9

1.1 Structural organisation of DNA 9
1.1.1 The discovery of chromatin 9
1.1.2 Composition of a nucleosome 9
1.1.3 Histone H1 and core variants in *S. cerevisiae* 11
1.1.4 Higher order structures of chromatin 11

1.2 Nucleosome positioning 12
1.2.1 Background of nucleosome positioning research 13
1.2.2 Determinants of nucleosome positioning 15
1.2.3 Current techniques for studying chromatin organisation 18

1.3 Aims of this study 18

2. Material and Methods 20

2.1 Materials 20
2.1.1 Kits and miscellaneous 20
2.1.2 Instruments 21
2.1.3 Buffers 22

2.2 Methods 25
2.2.1 Purification of *Drosophila melanogaster* embryonic histones 25
2.2.2 Salt Gradient Dialysis (SGD) 25
2.2.3 RSC Purification 26
2.2.4 ATPase assay (based on (Wagner, 2020)) 28
2.2.5 Genome-wide *in vitro* remodelling 28
2.2.6 MNase-seq 28
2.2.7 Illumina Library Preparation 29
2.2.8 Data Processing 29
2.2.9 Nucleosome positioning sequence (NPS) analysis 30
2.2.10 Nucleosome depleting sequences (NDS) analysis 31

3. Results 32

3.1 The direct role of DNA sequence in nucleosome positioning 33
3.1.1 Derivation of nucleosome positioning sequences (NPSs) from MNase-seq data ... 33
3.1.2 Remodeler-specific NPSs 36
3.1.3 Structural basis for remodeler NPSs 38

3.2 The direct role of DNA sequence in nucleosome depletion 40
3.2.1 The active mechanism of nucleosome depletion by poly(dA:dT) tracts *in vivo* 40
3.2.2 Nucleosome depletion by RSC at poly(dA:dT) tracts *in vitro* 47
3.2.3 Remodeler-specific NDSs 50

3.3 Where has the *S. cerevisiae* genome evolved remodeler-specific nucleosome positioning sequences? 53
3.4 The indirect role of DNA sequence on nucleosome organisation 58
3.4.1 RSC cooperation with GRFs *in vitro* 58

4. Discussion 65

4.1 Nucleosome positioning by remodeler-specific reading of DNA sequence 65
4.1.1 Remodeler NPSs 65
4.1.2 NPS – structure discussion 66
4.1.3 Interpreting NPSs 66
4.2 The role of poly(dA:dT) tracts in nucleosome depletion 67
4.3 The role of GRFs in nucleosome organisation by RSC 69
4.3.1 NFR generation but no array formation 69

Bibliography 71

Appendix A: 86

Acknowledgements 88

Affidavit 89

Confirmation of congruency 90

List of publications 91

Curriculum vitae 92

Abstract (English):

Well-defined organisation of nucleosomes at promoter regions across the *S. cerevisiae* genome is a prerequisite for proper and efficient transcription and thereby for the viability of the organism. Such organisation involves depletion of promoter nucleosomes and precise positioning of flanking nucleosomes, extending into the gene body. This patterning is achieved through the combined action of several ATP-dependent chromatin remodeling complexes, capable of evicting, sliding, editing and regularly spacing nucleosomes in response to different stimuli.

In this study, we focused on the role of DNA sequence in directing remodeler-mediated chromatin remodeling, both through its direct readout by remodelers as well as through its indirect role, via determining the binding site of general regulatory factors. Using the combination of a unique genome-wide *in vitro* reconstitution system and novel bioinformatic workflows, we determined that different chromatin remodeler types differentially process DNA shape/mechanics into nucleosome positions. These remodeler-specific preferences were found to be reflected in published structural data, generating testable hypotheses for future mutation studies of remodeler function. We also show the reverse, i.e., that remodelers may differentially process DNA sequence information with regard to nucleosome depletion.

We elaborated further that nucleosome depletion at poly(dA:dT) tracts is predominantly an active process, catalysed by the essential remodeler RSC, in contrast to the historical view that such tracts intrinsically exclude nucleosome formation to the extent observed *in vivo*. We show that such a depletion by RSC occurs with a bias toward the 5’ direction of poly(dA) and 3’ of poly(dT) tracts, regardless of genomic context, and that it scales with tract length. In addition to direct stimulation by poly(dA:dT) tracts, we show that RSC cooperates with general regulatory factors in nucleosome depletion proximal to their binding sites, although without directional input by these factors. Whilst this cooperation has been shown to be necessary for nucleosome depletion at most general regulatory factor binding sites *in vivo*, we show *in vitro* that it’s also sufficient.

We provide an overview of the organisation of DNA sequence determinants of nucleosome organisation at promoters, finding that remodeler-intrinsic preferences for nucleosome positioning generally underpin *in vivo* organisation when both poly(dA:dT) tracts and general regulatory factor binding sites are also present. In the absence of either element the position of remodeler-preferred nucleosome positioning sequences appear shifted relative to the depleted region, and depletion in the absence of either sequence element suggests an unexplored mechanism.

Together, this study contributes to our collective understanding of how different remodelers, DNA sequence elements and general regulatory factors cooperate in the determination of nucleosome positioning and depletion in yeast, as a model for eukaryotic chromatin regulation in general.

List of figures

Figure 1 – Chromatin under a microscope 9
Figure 2 – X-ray crystal structure of a nucleosome core particle (NCP) 10
Figure 3 – Model of *in vivo* chromatin compaction 12
Figure 4 – Stereotypical NDR-array pattern of *S. cerevisiae* promoter nucleosome organisation 14
Figure 5 – Genome-wide *in vitro* reconstitution of nucleosome positioning 32
Figure 6 – Overview of bioinformatic workflow used to define NPSs 34
Figure 7 – INO80 NPS shape profiles are consistent across a range of criteria. 35
Figure 8 – Chromatin remodelers differentially process DNA sequence information into nucleosome positioning. 36
Figure 9 – Randomly selected *S. cerevisiae* sequences show no distinct rigidity profile 37
Figure 10 – Average nucleosome dyad positions *in vivo* do not reflect any one remodeler's intrinsic preferences for positioning nucleosomes 38
Figure 11 – Shape/mechanic profiles of remodeler-specific NPSs reflect functionally crucial remodeler-DNA interactions 38
Figure 12 – Nucleosome depletion over poly(dA:dT) tracts in promoter regions is less pronounced *in vitro* than *in vivo*, especially if monitored without MNase 41
Figure 13 – Alternative visualisation of data shown in Figure 7, showing greater nucleosome depletion over promoter region poly(dA:dT) tracts *in vivo* vs *in vitro* 43
Figure 14 – Nucleosome depletion over poly(dA:dT) tracts scales with tract length and appeara similar *in vitro* vs *in vivo* with MNase-seq, but not with ODM-seq 44
Figure 15 – Differential nucleosome depletion over poly(dA) tracts *in vivo* vs *in vitro* is more pronounced in promoter regions, vs non-promoter regions 45
Figure 16 – *S. cerevisiae* promoters have developed a particular poly(dA)/poly(dT) tract distribution which argues for active and directional nucleosome depletion 46
Figure 17 - RSC directionally depletes nucleosomes from poly(dA) tracts *in vitro.* .. 47
Figure 18 - Nucleosome depletion at poly(dA) tracts scales with tract length. 48
Figure 19 – RSC does not deplete nucleosomes from poly(dG) tracts *in vitro.* 49
Figure 20 – Our usual RSC concentrations are sufficient to reach the system's steady state. 50
Figure 21 – Overview of bioinformatic workflow used to generate NDSs 51
Figure 22 - Chromatin remodelers differentially process DNA sequence information into nucleosome depletion. 52
Figure 23 – Pairwise comparisons of remodeler-specific NPS and *in vivo* dyad overlaps 54
Figure 24 – NPS distributions and *in vivo* MNase-seq coverage at different promoter classes 56
Figure 25 - GRFs alone guide NDR formation by RSC but do not in a directional way. 59
Figure 26 - GRFs alone do not cause nucleosome depletion at GRF PWMs. 60
Figure 27 – Nucleosome depletion at different classes of GRF sites in response to RSC ± GRF addition *in vitro* 61
Figure 28 – Distribution of DNA sequence elements contributing to nucleosome organisation around *in vivo* NFRs 63

List of tables

Table 1 – Overview of main *S. cerevisiae* chromatin remodeling complexes. 17

Table 2 – Overlap of remodeler-specific NPSs with *in vivo* dyad positions. NPSs as in Figure 8, but overlapping dyads from different replicates only counted once. 55

Table 3 – Percentage of +1 *in vivo* nucleosome dyads at each promoter class within 20 bp of an NPS dyad for each remodeler 57

Table 4 – Response of Kubik et. al., (2018) GRF site classes to factor addition *in vitro* vs factor ablation *in vivo.* '+' indicates response to the stimulus (NFR formation *in vitro* vs NFR filling *in vivo*), whilst '-' indicates no response. 62

Table 5 – Primary RSC *in vitro* reconstitution dataset TBPool1 & TBPool2 86

List of abbreviations

NFR	Nucleosome free region
NPS	Nucleosome positioning sequence
NDS	Nucleosome depleting sequence
SGD	Salt gradient dialysis
YPD	Yeast extract peptone dextrose (media)
EDTA	Ethylenediaminetetraacetic acid
EGTA	Ethylene Glycol Tetraacetic Acid
TAE	Tris + acetate + EDTA (buffer)
GRF	General regulatory factor
MNase	Micrococcal nuclease
NCP	Nucleosome core particle
NRL	Nucleosome repeat length

1. Introduction

1.1 Structural organisation of DNA

1.1.1 The discovery of chromatin

All eukaryotic life depends on the information stored in strands of deoxyribonucleic acid (DNA), forming the 'blueprint' of each cell. DNA exists in the nucleus, condensed into a structure called 'chromatin' (from the Greek word *chroma*, meaning colour) which was first observed in the late 19th century by Walther Flemming (1882) and named as such for its' ability to bind basic dyes. Almost a century later, it was discovered that chromatin consists of repeats of a core unit, termed the 'nucleosome'. Early electron microscopy work visualised the nucleosome as 'beads-on-a-string', akin to thread wrapping twice round a spool and connecting to the next via unwound 'linker' regions (**Figure 1**) (Kornberg, 1977; Olins & Olins, 2003; Woodcock et al., 1976). Combining this imagery with data from limited nuclease digestion experiments (Kornberg & Thomas, 1974), led to the conclusion that nucleosomes are a complex of four histone dimers (the 'spool'), forming an octamer, wrapped in ~200 bp DNA (the 'thread') (Kornberg, 1974). The name 'nucleosome' was given to these particles to reflect their nuclear origin (Oudet et al., 1975).

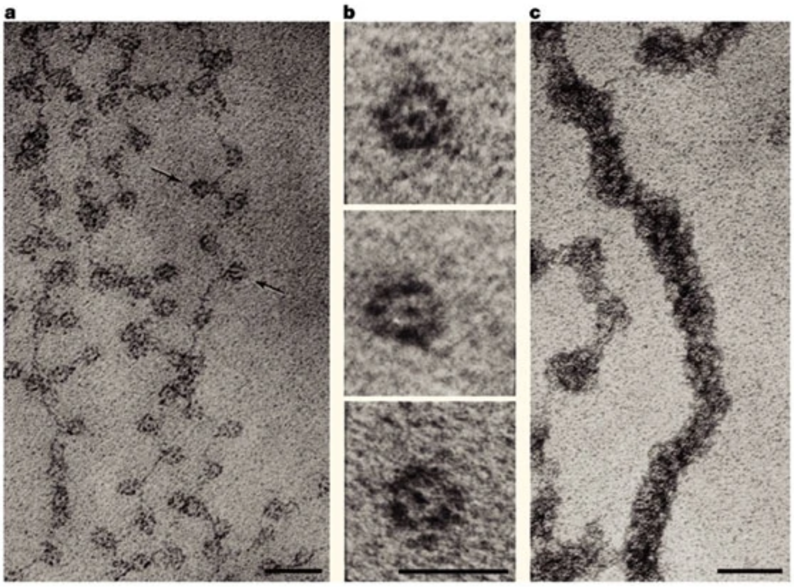

Figure 1 – Chromatin under a microscope

Electron microscopy of chromatin under varying conditions. (a) Nucleosomes assembled on a chromatin fiber, resembling 'beads-on-a-string' at low ionic strength. (b) Mononucleosomes isolated via nuclease digest of chromatin. (c) Heteochromatin in the form of a '30-nm fiber' at moderate ionic strength. Figure taken from (Olins & Olins, 2003), with permission.

1.1.2 Composition of a nucleosome

More specifically, a so-called 'canonical' nucleosome (**Figure 2**) has been shown to consist of two copies each of the histone proteins H2A, H2B, H3 and H4 (Luger et al., 1997). These histone proteins are similarly structured, each forming a motif termed the 'histone-fold', formed by 3 alpha helices (Arents et al., 1991). In addition, they all possess disordered N-terminal ‘tails’ (H2A also has a C-terminal ‘tail’), which are subjected to a wide range of post-translational modifications (PTMs), such as methylation, ubiquitination, ADP-ribosylation, acetylation and phosphorylation (Ame et al., 2004; Berger, 2002; Kuo & Allis, 1998; Peterson & Laniel, 2004; Zhang, 2003; Zhao & Shilatifard, 2019) The assembly of these proteins into the histone octamer begins with the formation of H2A-H2B and H3-H4 heterodimers, before the H3-H4 dimers further join to form a tetramer, either side of which a H2A-H2B dimer binds to form the full octamer (Arents et al., 1991). Around the octamer, 147 bp DNA are wrapped, corresponding to ~1.65 full rotations, a process driven primarily by electrostatic interactions between the positively charged histone proteins and negatively charged DNA phosphate backbone (Luger et al., 1997). The central base pair of the nucleosome is referred to as the dyad position, from which nucleosomal positions are annotated in 10 bp steps as super-helical locations (SHLs), e.g., SHL±1, SHL±2, and so on, with the dyad also known as SHL0 (Klug et al., 1980). This nucleosome structure comprising of 147 bp DNA is referred to as the nucleosome core particle (NCP), whilst the term nucleosome originally includes linker DNA flanking the NCP.

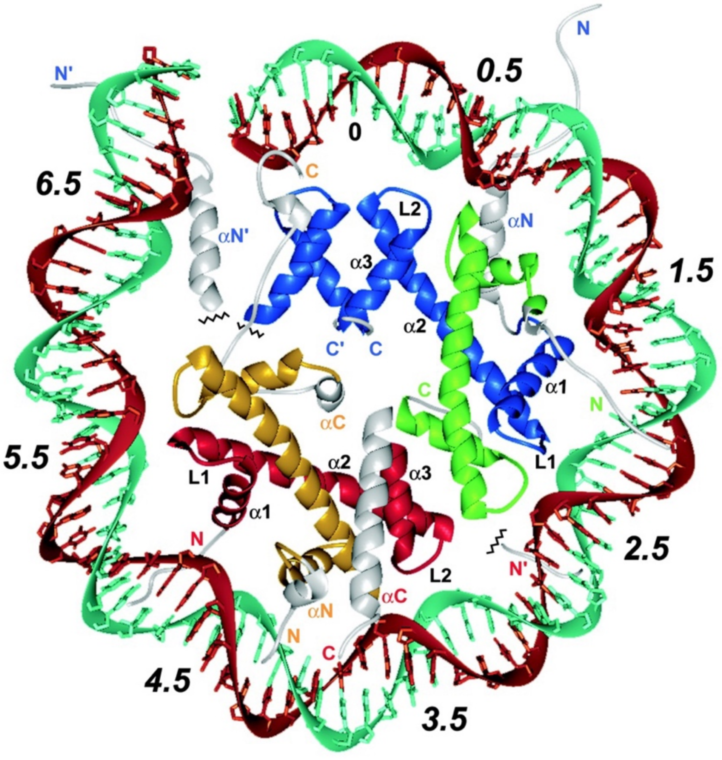

Figure 2 – X-ray crystal structure of a nucleosome core particle (NCP)

View of a NCP from above, centered on the dyad axis and only showing the top half the structure for simpler visualisation of histone and DNA organisation. DNA strands are shown in brown and cyan, whilst histone fold domains are coloured yellow, red, blue, and green for H2A, H2B, H3 and H4, respectively. Histone-fold extensions and N-terminal tails are coloured in white. The nucleosome dyad is labelled (0), and superhelical locations (SHLs) indicated from 0.5 – 6.5. Substructures of H2B and H3 histone domains (α1-3, L1/2), extensions (αN/αC) and N/C-terminal tails (N, C, N’, C’) are annotated. Figure 1b from (Davey et al., 2002), taken with permission.

1.1.3 Histone H1 and core variants in *S. cerevisiae*

Beyond the canonical core histones, a fifth type of histone proteins exists, known as the H1 ‘linker’ histone. This histone protein binds ~20 bp linker DNA proximal to the nucleosome dyad, increasing the structure’s stability and forming a so-called ‘chromatosome’, which promotes compaction of the chromatin fiber (Bednar et al., 1998; Clark & Kimura, 1990; Simpson, 1978). The histone H1 family contains many different variants, depending on the organism and cell type, although the *Saccharomyces cerevisiae* genome only encodes one variant – Hho1. Deletion of the *HHO1* gene proved to be non-lethal, although gene expression changes implicated Hho1 in transcriptional regulation (Ushinsky et al., 1997), and mapping of Hho1 binding genome-wide revealed a role in repression of meiosis (Bryant et al., 2012). Additionally, whilst higher eukaryotes have many different histone variants, exponentially increasing the complexity of their ‘epigenetic code’ (Talbert & Henikoff, 2021), *S. cerevisiae* only possesses two. One of these is the H2A variant H2A.Z (in *S. cerevisiae* called Htz1), which is also non-essential but plays a role in transcriptional regulation and telomere silencing, with null mutants displaying a reduced resilience to stress (Jackson et al., 1996; Meneghini et al., 2003; Santisteban et al., 2011). The other *S. cerevisiae* histone variant is Cse4, an essential protein which replaces histone H3 at centromeres and regulates chromosome segregation, via phosphorylation by Cdc7 (Meluh et al., 1998; Mishra et al., 2021; Stoler et al., 1995).

1.1.4 Higher order structures of chromatin

The variety of available histone variants and PTMs represent the building blocks of the chromatin fiber and complexity is further generated by heterogeneity of nucleosome positioning both along the fiber and in a 3D space. Historically, chromatin was believed to exist in 2 distinct states: euchromatin, corresponding to the ‘beads-on-a-string’ structure observed in early microscopy experiments, and heterochromatin, a more compact chromatin configuration. The exact nature of this higher order structure is still somewhat unclear. A so-called ’30-nm fiber’ was discovered (Finch & Klug, 1976), described as a ‘solenoid’ arrangement, and a ‘zig-zag’ conformation was later offered as an alternative (Woodcock et al., 1984). Indeed, evidence for the latter has been provided by more recent cryo-electron microscopy (cryo-EM) structures (Garcia-Saez et al., 2018; Song et al., 2014), although a lack of evidence for its *in vivo* existence casts doubt upon the physiological relevance of such a ’30-nm’ fiber (Eltsov et al., 2008; Nishino et al., 2012; Ricci et al., 2015; Tremethick, 2007). Instead, *in vivo* observations of chromatin compaction usually describe a ‘sea of nucleosomes’ structure, or ‘liquid-like chromatin droplet’, maybe formed through liquid-liquid phase separation (LLPS) (**Figure 3**) (Gibson et al., 2019; Maeshima, Ide, et al., 2016; Maeshima, Rogge, et al., 2016; Rippe, 2022). It’s been suggested that the self-interacting properties of this globular chromatin structure are the driving force behind further condensation into interphase chromosomes, with histone variants, PTMs and additional chromatin binding factors conferring functional and structural properties (Hansen et al., 2018), such as Structural Maintenance of Chromosomes (SMC) complexes which promote an ATP-dependent loop-extrusion mechanism in metaphase (via condensins) and interphase (via cohesins and CTCF) (Mirny et al., 2019).

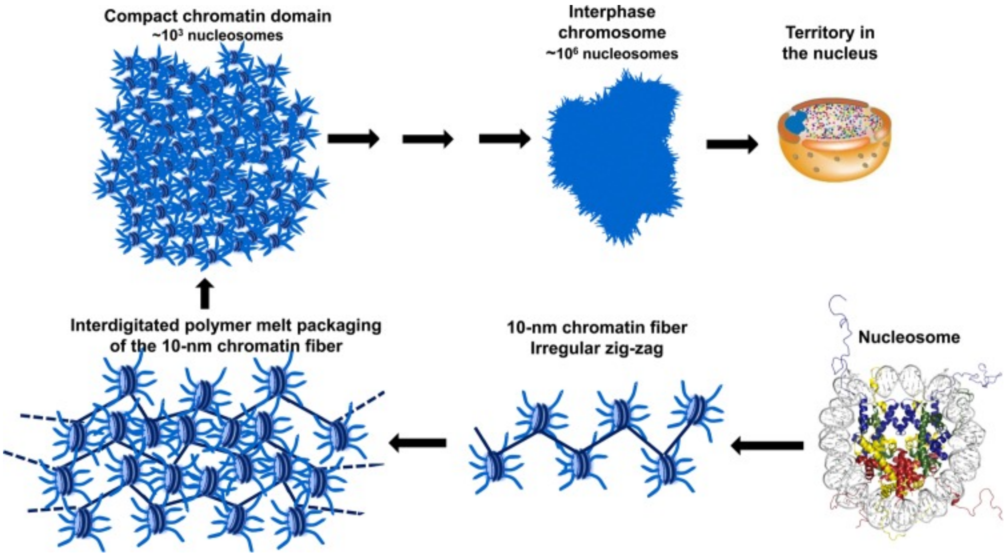
Compact chromatin domain
~10^3 nucleosomes
Interphase chromosome
~10^6 nucleosomes
Territory in the nucleus
Interdigitated polymer melt packaging of the 10-nm chromatin fiber
10-nm chromatin fiber
Irregular zig-zag
Nucleosome

Figure 3 – Model of *in vivo* chromatin compaction

In vivo observations fit a model where chromatin fibers pack irregularly into droplet-like structures (referred to here as a polymer melt), capable of further condensing through intra-globular interactions, with histone variants, PTMs and chromatin binding proteins conveying functional and structural properties. Figure taken from (Hansen et al., 2018) with permission.

1.2 Nucleosome positioning

Nucleosome positioning is an important feature of the chromatin fiber, with a major regulatory role in processes requiring factors to bind to DNA, namely transcription, replication, repair of damaged DNA and cell differentiation (Azmi et al., 2017; Echigoya et al., 2020; Kujirai & Kurumizaka, 2020; Soria et al., 2012). For instance, early *in vitro* work has shown nucleosomes to be inhibitory to transcription initiation (Knezetic & Luse, 1986; Workman & Roeder, 1987), although with variable conclusions regarding their impact on elongation (Izban & Luse, 1991; Lorch et al., 1987; Morse, 1989). It was later shown that elongation factors, e.g., TFIIS play an important role in promoting transcription elongation through the nucleosome (Kireeva et al., 2005). More recently, RNA polymerase II (RNAPII) has been shown to pause on nucleosomes *in vivo* (Churchman & Weissman, 2011; Kwak et al., 2013; Ramachandran et al., 2017), whilst cryo-EM structures of the RNAPII-nucleosome complex reveal that RNAPII stalls at sites of major histone-DNA contacts (Farnung et al., 2018; Hall et al., 2009; Kujirai et al., 2018), which must be disrupted to allow RNAPII to progress through the nucleosome. As such, variables which affect the strength of these interactions, such as histone variants, histone tail PTMs and mutations have an impact on the efficiency of transcription (Bintu et al., 2012; Chen et al., 2019; Di Cerbo et al., 2014; Hsieh et al., 2010; Rudnizky et al., 2016; Tropberger et al., 2013). Thus, nucleosomes represent a barrier to transcription initiation and elongation and understanding their position along the DNA fiber helps us to understand the complex regulation of gene expression.

1.2.1 Background of nucleosome positioning research

1.2.1.1 History of monitoring nucleosome positioning

The monitoring of nucleosome positioning was initially limited to measuring the distance between NCPs. This was achieved by limited digestion of chromatin with micrococcal nuclease (MNase) (Heins et al., 1967), as DNA within the NCP was found to be protected against digestion compared to linker DNA, producing fragments which when separated via electrophoresis produced a ‘ladder’ of regular spacing (Noll, 1974). From the ladder, the size and distance between NCPs could be calculated, termed the nucleosome repeat length (NRL). The NRL in *S. cerevisiae* was estimated to be ~165 bp (Thomas & Furber, 1976), consisting of a 147 bp nucleosome and 18 bp linker DNA. This number varies depending on species, cell type and transcription level of the chromatin region (Chereji et al., 2018; Perisic et al., 2010; Van Holde, 2012).

With the advent and increased commercial availability of Next-Generation sequencing (NGS), the pairing of this technology with MNase digestion allowed the mapping of nucleosomes to precise DNA locations genome-wide (Albert et al., 2007; Johnson et al., 2006; Schones et al., 2008), a technique called ‘MNase-seq’, which forms the basis of many modern day genomic mapping workflows.

1.2.1.2 Promoter nucleosome organisation

High-resolution nucleosome maps have revealed that most *S. cerevisiae* genes are depleted of nucleosomes in their promoter, a so-called nucleosome-free region (NFR), or nucleosome depleted region (NDR), with well positioned nucleosomes upstream (-1 nucleosome) and downstream (+1 nucleosome), followed by a regularly occurring array of nucleosomes toward the gene body (Yuan et al., 2005). The same basic ‘stereotypical’ nucleosome patterning was later discovered at active genes in humans (Barski et al., 2007) and flies (Mavrich et al., 2008), and was present even in lowly expressed genes in yeast (Albert et al., 2007; Lee et al., 2007; Mavrich et al., 2008). Furthermore, promoter NFR formation and proper ±1 nucleosome positioning was correlated with increased binding of the transcription factor TATA-binding protein (TBP) and RNAPII, linking promoter nucleosome organisation to transcription initiation (Kubik et al., 2018). Taken together, these results suggest that the stereotypical nucleosome organisation observed at promoters is necessary but not sufficient, at least at most genes, for efficient transcription.

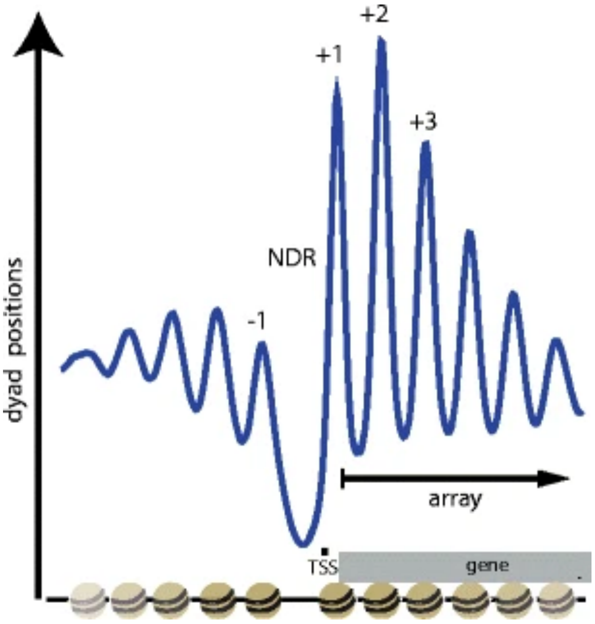

Figure 4 – Stereotypical NDR-array pattern of *S. cerevisiae* promoter nucleosome organisation

Composite plot of nucleosome dyad positions, aligned to *S. cerevisiae* TSSs. The promoter NDR with flanking nucleosomes, downstream array and TSS position are indicated. Figure from (Lieleg et al., 2015), with permission.

1.2.1.3 NFRs vs NDRs

Upon the first genome-wide mapping of nucleosome positions in yeast, the term 'nucleosome-free region' was coined (Yuan et al., 2005). The observation of low mapping signal in an NFR was interpreted to be due to the absence of a nucleosome at such locations, and such named to reflect this interpretation. However, later work has contested the notion that such NFRs are truly absent of nucleosomes, with the detection of non-canonical or unstable 'fragile' nucleosomes (FNs) in promoters (Jin et al., 2009; Kubik et al., 2015). Thus, there has been a shift in recent years toward the nomenclature of 'nucleosome-depleted region', with the connotation that NDR nucleosome occupancies exist on a continuum, rather than zero occupancy as the term NFR implies.

An alternative to this quantitative definition has been offered by Frank Pugh, who reserves the term NFR for locations which are hard-wired to be constitutively and truly nucleosome-free as seen by the lack of cross-linkable histones in these regions as would be expected for canonical nucleosomes (Lai & Pugh, 2017; Rhee et al., 2014; Rossi et al., 2021), rather than NDRs which by this definition are regulated to be occupied by nucleosomes in a repressed state and depleted upon activation of the promoter.

The terms NFR and NDR are often used interchangeably and in this thesis, we use the term NFR largely to remain consistent with our published work (see Results - 3.2.1), where we mostly discussed mechanistically defined NFRs (i.e., the Pugh definition).

1.2.2 Determinants of nucleosome positioning

1.2.2.1 DNA sequence

Given the importance of nucleosome organisation, many studies have explored the variables involved in establishing promoter NFRs and genic arrays. The first of these to be explored was DNA sequence, with researchers finding that nucleosomes preferentially contained repeats of AA, TT and TA dinucleotides at regular 10 bp intervals (Brogaard et al., 2012; Ioshikhes et al., 2006; Moyle-Heyrman et al., 2013; Satchwell et al., 1986; Segal et al., 2006; Wang & Widom, 2005), whilst GC repeats were also observed 5 bp out of phase with the AA, TT and TA repeats. Such arrangement of dinucleotide repeats molds the DNA helical grooves in a manner which favours bending around the histone octamer and has been suggested as a 'genomic code for nucleosome positioning' (Kaplan et al., 2010; Kaplan et al., 2009; Segal et al., 2006). However, whilst this could direct rotational positioning of the nucleosome, i.e., the orientation of the DNA helix as it wraps around the histone core, specific translational positioning, i.e., the exact stretch of DNA sequence wrapped around the histone core, is likely not driven by this dinucleotide repeat arrangement, as shifting the nucleosome in 10 bp increments would still fit the model. Additionally, *in vitro* reconstitutions of nucleosome positioning have shown that DNA sequence alone does not drive *in* vivo-like array formation (Zhang et al., 2011).

Another DNA sequence element linked to promoter nucleosome organisation is the poly(dA:dT) tract, defined as a homopolymeric stretch of adenine or thymine repeats, which are often found in *S. cerevisiae* promoters and associated with NFRs (de Boer & Hughes, 2014; Field et al., 2008; Iyer & Struhl, 1995; Segal & Widom, 2009a; Struhl, 1985; Wu & Li, 2010; Yuan et al., 2005). Historically, poly(dA:dT) tracts have been believed to generate NFRs by intrinsically disfavouring nucleosome formation, as a result of the rigidity of such tracts (Segal & Widom, 2009a, 2009b; Struhl & Segal, 2013). However, in recent years the evidence has been mounting for a predominantly active mechanism of nucleosome depletion at poly(dA:dT) tracts, in yeast via the action of the ATP-dependent chromatin remodeler RSC (Krietenstein et al., 2016; Kubik et al., 2018; Lorch et al., 2014). Additionally, chemical mapping of the *S. pombe* genome revealed an enrichment of poly(dA:dT) tracts within nucleosomes rather than NFRs (Moyle-Heyrman et al., 2013), and transfer of yeast artificial chromosomes (YACs) between different species of yeast revealed that nucleosome positioning was largely dictated by the host cell environment, rather than the DNA sequence (Hughes et al., 2012). Also, DNA sequences generating nucleosomal arrays were found to be species specific, i.e., they only generated arrays in the species they were identified in (Gonzalez et al., 2016). Taken together, these results argue that the role of DNA sequence in determining nucleosome positioning is unlikely implemented by the preferences of histone ocatemers only but also importantly by those of *trans*-factors, which may even be contrary to the histone octamer's.

1.2.2.2 Chromatin remodelers

Beyond the contribution of the DNA sequence itself, nucleosome positioning is also influenced by the action of chromatin remodelers. Remodelers are often large multimeric complexes, with a common helicase-like ATPase domain homologous to that of the *S. cerevisiae* protein Snf2 (Laurent et al., 1992). This so-called Snf2 domain consists of two RecA-like folds which contain motifs required for ATP hydrolysis and coupling of this energy to DNA translocation (Cairns et al., 1994; Smith & Peterson, 2005). Differences in sequence similarity of the Snf2 domain, along with variability in associated domains, has led to classification of remodelers into four subfamilies with varying functionalities: ISWI, CHD, SWI/SNF and INO80 (Flaus et al., 2006). Possible functions of a chromatin remodeler include translocation of a nucleosome along the DNA strand (sliding), disassembly of the nucleosome (eviction), placing nucleosomes at regular distances to each other (spacing) and replacing canonical histones with variants and vice versa (histone exchange) (**Table 1**) (Clapier et al., 2017; Gamarra & Narlikar, 2021; Nodelman & Bowman, 2021).

In *S. cerevisiae*, the ISWI family consists of two ATPases, Isw1 and Isw2, forming three distinct complexes with auxiliary subunits, ISW1a, ISW1b and ISW2 (Kagalwala et al., 2004; Vary et al., 2003). ISW1a and ISW2 have been shown to reconstitute regularly spaced nucleosome arrays (Krietenstein et al., 2016; Tsukiyama et al., 1999), though ISW1a appears to set a tighter spacing, whilst ISW2 appears to be more involved in proper positioning of the +1 nucleosome (Kubik et al., 2019). ISW1b shows weaker sliding and spacing activity and has been linked with facilitating transcription elongation via preventing histone exchange in the gene body (Gangaraju & Bartholomew, 2007a, 2007b; Smolle et al., 2012; Vary et al., 2003).

Only one member of the CHD family is present in *S. cerevisiae*, named Chd1, which is well documented to space nucleosomes (Lusser et al., 2005; Stockdale et al., 2006; Tsukiyama et al., 1999). Indeed, cells lacking both Chd1 and Isw1 were shown to have severely disrupted nucleosome arrays, indicating a role for both remodelers in establishing proper spacing (Ocampo et al., 2016, 2019). Additionally, Chd1 associates with the histone chaperone FACT at transcribed genes, implicating Chd1 in mediating RNAPII progression through a nucleosome during the process of transcription (Farnung et al., 2021; Jeronimo et al., 2021; Simic et al., 2003)

The SWI/SNF family of remodelers in *S. cerevisiae* consists of SWI/SNF and RSC, with the latter being the only essential yeast remodeler (Cairns et al., 1996). Both remodelers are capable of sliding nucleosomes, but also share an activity unique to the SWI/SNF family, the ability to evict nucleosomes (Lorch et al., 1999). RSC is ten times more abundant than SWI/SNF (Ghaemmaghami et al., 2003), and it’s essential nature is likely due to the role it plays in establishing promoter NFRs throughout the majority of the yeast genome, facilitating gene expression (Badis et al., 2008; Hartley & Madhani, 2009; Krietenstein et al., 2016; Kubik et al., 2019; Kubik et al., 2018; Parnell et al., 2008). One mechanism by which RSC establishes NFRs at yeast promoters is by removing nucleosomes from poly(dA:dT) tracts (Lorch et al., 2014), in a 3’-to-5’ direction (Krietenstein et al., 2016).

Two non-mutually exclusive mechanisms of eviction by SWI/SNF-type remodelers have been proposed (Clapier et al., 2017). The first of these involves high levels of ATPase hydrolysis and efficient coupling to DNA translocation (Clapier et al., 2016), allowing simultaneous disruption of multiple DNA-histone interactions, leading to disassembly of the octamer which likely begins with displacement of an H2A-H2B dimer (Lorch et al., 2006; Yang et al., 2007). The alternative mechanism involves sliding a nucleosome into a neighbouring nucleosome and peeling the DNA off the histone octamer, hereby disassembling the neighbouring rather than bound nucleosome (Boeger et al., 2008; Engeholm et al., 2009).

The INO80 family of remodelers in *S. cerevisiae* consists of INO80 and SWR1 (Bao & Shen, 2011; Morrison & Shen, 2009). SWR1 has been shown to replace canonical H2A-H2B dimers with H2A.Z-H2B dimers (Mizuguchi et al., 2004), whilst INO80 may be able to catalyse the reverse, i.e., replace H2A.Z-H2B dimers with canonical H2A-H2B dimers, serving to prevent mislocalisation of this variant outside of promoter nucleosomes (Papamichos-Chronakis et al., 2011), though failure to reproduce this observation casts doubt upon INO80’s histone editing role (Wang et al., 2016). Beyond its histone editing functionality, INO80 is known to slide and space nucleosomes (Udugama et al., 2011; Zhou et al., 2018), and has been implicated in +1 nucleosome positioning (Krietenstein et al., 2016; Kubik et al., 2019). Recent work has shown INO80 to position +1 nucleosomes partially via a direct readout of the DNA shape/mechanics (Oberbeckmann, Krietenstein, et al., 2021).

Table 1 – Overview of main *S. cerevisiae* chromatin remodeling complexes.

Remodeler subfamily	**Remodeler complex**	**Remodeler functions**
ISWI	ISW1a	Sliding, spacing
	ISW1b	Sliding
	ISW2	Sliding, spacing
CHD	Chd1	Sliding, spacing
SWI/SNF	SWI/SNF	Sliding, eviction
	RSC	Sliding, eviction
INO80	INO80	Sliding, spacing, histone variant removal?
	SWR1	Histone variant incorporation

1.2.2.3 General regulatory factors (GRFs)

Another class of proteins with a significant role in chromatin organisation are the general regulatory factors (GRFs). GRFs are sequence-specific DNA binding proteins, with target sites often residing within promotor regions, and are often essential for viability of the organism. Binding of GRFs to their target sites has been shown to contribute to nucleosome exclusion (Bai et al., 2011; Yan et al., 2018) and is required for transcription of several different gene classes (Badis et al., 2008; Challal et al., 2018; Hartley & Madhani, 2009; Hughes et al., 2012; Kubik et al., 2018). They do not possess ATPase activity, so they cannot directly move nucleosomes, rather they rely on co-operation with chromatin remodelers. For instance, INO80, Chd1, ISW1a and ISW2 have been shown to generate regularly spaced arrays phased relative to GRF binding sites (Krietenstein et al., 2016; Oberbeckmann, Niebauer, et al., 2021), and cooperation with Reb1 was shown to improve +1 nucleosome positioning by INO80 (Oberbeckmann, Krietenstein, et al., 2021).

1.2.2.4 Overview of stereotypical NFR-array formation

To summarise, most yeast promoters are characterised by an NFR upstream of the transcription start site (TSS), associated with poly(dA:dT) tracts, GRF binding and eviction of promoter nucleosomes by SWI/SNF-type remodelers like RSC. This increase in chromatin accessibility permits assembly of the pre-initiation complex (PIC) and subsequent transcription initiation. The +1 nucleosome is primarily positioned by INO80 and ISW2, particularly in conjunction with GRFs, although INO80 appears to also directly readout DNA sequence to achieve this. Downstream arrays are primarily the consequence of ISW1a and Chd1 spacing activities, though INO80 and ISW2 are also capable of generating such arrays and ISW1a can also contribute to +1 nucleosome positioning (Parnell et al., 2015).

1.2.3 Current techniques for studying chromatin organisation

Modified versions of MNase-seq have been widely used to study the contribution of chromatin remodelers to nucleosome organisation. For instance, MNase digestion prior to immunoprecipitation of a cross-linked target protein (MNase-ChIP) confers increased specificity and allows precise mapping of histone variants (Albert et al., 2007), histone modifications (Weiner et al., 2015) and transcription factor binding (Henikoff et al., 2011), for example. Alternatively, substituting MNase with a lambda exonuclease and digesting the DNA after immunoprecipitation (ChIP-exo) has been used to precisely identify DNA-protein binding sites (Rhee & Pugh, 2011). Other mapping technologies involve fusing MNase either to a protein of interest to target calcium-dependent DNA cleavage (ChEC-seq) (Zentner et al., 2015), or to Protein-A, allowing MNase cleavage in the vicinity of a DNA-bound protein which has already been tagged with an antibody (CUT&RUN sequencing) (Skene & Henikoff, 2017). MNase-seq has also been performed at a single-cell level (Lai et al., 2018).

These techniques have been used heavily to investigate chromatin organisation *in vivo*, for example through genetic deletions or ablations of remodelers or GRFs (Kubik et al., 2019; Kubik et al., 2018; Ocampo et al., 2016, 2019; Singh et al., 2021). However, it can be very difficult to directly attribute specific contributions to a factor in this manner due to redundancies between factors. In contrast, *in vitro* studies control for this problem with full control of the combination of factors being studied but have previously been limited to non-physiological substrates. These include mono-nucleosomes formed using a synthetic DNA sequence with an abnormally strong affinity for a histone octamer during salt gradient dialysis (SGD) (Widom 601 sequence) (Lorch et al., 2014; Lowary & Widom, 1998), or with nucleosome arrays formed on circular cloning vectors (Clapier et al., 2016). As such, assays utilising these constructs struggle to fully capture the complex combinations of nucleosome organisation determinants present *in vivo*. To address this problem, earlier work from the Korber group involved establishing a completely *in vitro* system whereby *in vivo*-like nucleosome positioning could be generated in a genome-wide way with the use of purified factors (Krietenstein et al., 2012). With this system, chromatin is assembled via SGD of a genomic plasmid library with purified histone octamers. In the presence of ATP, addition of different combinations of purified remodelers and GRFs to this SGD chromatin, followed by MNase-seq, revealed that RSC generates NFRs at promoter poly(dA:dT) tracts, INO80 reads DNA sequence to position the +1 nucleosome, ISW2 requires cooperation with GRFs to position the +1 nucleosome, both INO80 and ISW2 space downstream nucleosome arrays and ISW1a generates a tighter spaced array of *in vivo*-like repeat length (Krietenstein et al., 2016). Importantly, all these mechanisms observed in the purified system are consistent with and can explain *in vivo* observations of respective remodeler mutants.

1.3 Aims of this study

In our study, we attempted to address some open questions arising from previous applications of this *in vitro* reconstitution approach (Krietenstein et al., 2016). For example, do any remodelers other than INO80 directly read DNA sequence information to position nucleosomes, and if so, how? Does RSC specifically deplete nucleosomes from *S. cerevisiae* promoter poly(dA:dT) tracts and do any other sequence features stimulate this activity? Do any other remodelers read DNA sequence for nucleosome depletion? Does RSC cooperate with GRFs for nucleosome depletion? We approached these questions by utilising the genome-wide reconstitution system previously described (Krietenstein et al., 2016), adding combinations of RSC and the GRFs Abf1, Rap1 and

Reb1 to SGD chromatin, followed by MNase-seq to monitor nucleosome positioning at poly(dA:dT) tracts, *in vivo* +1 nucleosome positions, promoter NFR centers and GRF binding sites. We also developed existing and novel bioinformatic workflows to probe for DNA sequence determinants of nucleosome organisation changes, before applying them to previously published data for other remodelers (Oberbeckmann, Krietenstein, et al., 2021; Oberbeckmann, Niebauer, et al., 2021).

2. Material and Methods

2.1 Materials

2.1.1 Kits and miscellaneous

Product	Source
NEBNext Multiplex Oligos for Illumina	NEB
AMPure XP (beads for PCR cleanup)	Beckman Coulter
100 bp DNA ladder	NEB
1 kb DNA ladder	NEB
Creatine kinase	Roche
DNA 1000 bioanalyzer kit	Agilent
DNA HS bioanalyzer kit	Agilent
Micrococcal nuclease	Sigma
Qubit dsDNA HS assay kit	ThermoFisher
Plaque agarose	Biozym
Universal agarose	Bio&Sell
PureLink Gel extraction kit	Invitrogen
B-mercaptoethanol	Serva
Orange G	Sigma
Glycogen (20 mg/mL)	Roche
Proteinase K	Qiagen
EDTA-free protease inhibitor tablets	Roche
Econo-pac chromatography columns	Bio-Rad
IgG Sepharose 6 Fast Flow affinity resin	GE Healthcare
Calmodulin affinity resin	Agilent
Quick Start Bradford Protein Assay	Bio-Rad
Ethidium bromide	VWR
Polyethylenamine	Sigma
Polyethylenglycol 6000	Sigma
Ampicillin	Roth
Adenosine triphosphate (ATP)	Sigma
Bovine serum albumin (BSA)	Sigma

Ammonium sulfate (NH_4SO_2)	Merck
Dithiothreoitol (DTT)	Roth
EDTA	ITW
EGTA	Roth
Ethanol	Sigma
Glycerol	Sigma
Hepes	Serva
IGEPAL CA630	Sigma
KCl	VWR
$MgCl_2$	VWR
NaCl	Serva
2-Propanol	Sigma
Sodium dodecyl sulfate (SDS)	Serva
Potassium acetate (KOAc)	Sigma
NP-40	Sigma
MgAc	Sigma
Phosphoenol pyruvate (PEP)	Sigma
Lactate dehydrogenase (LDH)	Sigma
NADH	Sigma
Tween-20	Sigma
$CaCl_2$	Sigma
Tris	Diagonal

2.1.2 Instruments

Product	Source
ProFlex PCR system	ThermoFisher
ThermoMixer C	Eppendorf
Centrifuge 5424 R	Eppendorf
Centrifuge 5810 R	Eppendorf
6875 Freezer/Mill High Capacity	SPEXSamplePrep
Optima XPN-80 Ultracentrifuge	Beckman Coulter
Avanti JXN-26	Beckman Coulter

New Brunswick Innova 44	Eppendorf
Multitron	Infors HT

2.1.3 Buffers

Buffer name	Recipe
Histone lysis buffer	15 mM K·HEPES pH 7.5 10 mM KCl 5 mM $MgCl_2$ 0.1 mM EDTA 0.5 mM EGTA 1 mM DTT 0.2 mM PMSF 10 % glycerol
SGD buffer	10 mM Tris·HCl pH 7.6 2 M NaCl 1 mM EDTA 0.05% IGEPAL CA630 0.2 µg/µL BSA
High salt buffer	10 mM Tris·HCl pH 7.6 2 M NaCl 1 mM EDTA 0.05% IGEPAL CA630 14.3 mM β-mercaptoethanol
Low salt buffer	10 mM Tris·HCl pH 7.6 50 mM NaCl 1 mM EDTA 0.05% IGEPAL CA630 1.4 mM β-mercaptoethanol
YPD medium	10 g/L yeast extract 20 g/L peptone 20 g/L dextrose
RSC lysis buffer (2x)	100 mM Tris-HCl pH 8 500 mM KOAc

	40% glycerol 20 mM EDTA 1 mM DTT
IgG purification high salt buffer	10 mM Tris-HCl 400 mM KOAc 0.1% NP-40 10% glycerol 0.5 mM EDTA 0.5 mM DTT
IgG purification low salt buffer	10 mM Tris-HCl 200 mM KOAc 0.1% NP-40 10% glycerol 0.5 mM EDTA 0.5 mM DTT
CBP buffer	25 mM Tris-HCl 250 mM KOAc 1 mM MgAc 1 mM imidazole 2 mM $CaCl_2$ 10% glycerol 0.1% NP-40 0.5 mM DTT
Calmodulin purification wash buffer 1	25 mM Tris-HCl 400 mM KOAc 1 mM MgAc 1 mM Imidazole 2 mM $CaCl_2$ 10% glycerol 0.1% NP-40 0.5 mM DTT
Calmodulin purification wash buffer 2	25 mM Tris-HCl 150 mM NaCl

	2 mM $CaCl_2$ 10% glycerol 0.1% NP-40 0.5 mM DTT
RSC elution buffer	25 mM Tris-HCl 150 mM NaCl 2 mM EDTA 3 mM EGTA 10% glycerol 0.1% NP-40 0.5 mM DTT
ATPase assay buffer	25 mM Tris-HCl pH 8.0 100 mM NaCl 1.5 mM MgOAc 0.1 mM Na-EDTA pH 8.0 10% v/v glycerol 0.2 mg/mL BSA 1 mM DTT 2 mM Mg^{2+}-ATP 15.5 U/mL pyruvate kinase 3 mM PEP 15.5 U/mL lactate dehydrogenase 0.6 mM NADH
4x Shifting Mix	80 mM HEPES-NaOH pH 7.5 12 mM MgCl2 10 mM ATP (in 0.1 M HEPES-NaOH pH 7.5) 40 mM creatine phosphate 10 mM DTT 2 mM EGTA 48% (v/v) glycerol
Buffer E	20 mM HEPES-NaOH pH 7.5 350 mM NaCl 0.1% TWEEN-20

	1 mM DTT 10% glycerol
Buffer D	20 mM HEPES-KOH pH 7.5 80 mM KCl 1 mM EGTA 10% glycerol
STOP buffer	0.1 M EDTA 2% SDS
1x TAE buffer	40 mM Tris 20 mM acetic acid 1 mM EDTA
4x Quick Ligation Buffer (QLB)	250 mM Tris-HCl pH 7.4 40 mM $MgCl_2$ 4 mM DTT 6 mM ATP 30% polyethylene glycol (PEG6000))

2.2 Methods

2.2.1 Purification of *Drosophila melanogaster* embryonic histones

Purification of *D. melanogaster* embryonic histones was carried out as previously described (Krietenstein et al., 2012; Oberbeckmann, Krietenstein, et al., 2021; Simon & Felsenfeld, 1979). In preparation, *D. melanogaster* embryos between 0-12 hours old (OregonR strain) were collected to a total of 50 g, before dechorionation with 25% sodium hypochlorite-based commercial bleach for 2 mins. They were then washed with cold dH_2O and resuspended with cold 40 mL lysis buffer (15 mM K·HEPES pH 7.5, 10 mM KCl, 5 mM $MgCl_2$, 0.1 mM EDTA, 0.5 mM EGTA, 1 mM DTT, 0.2 mM PMSF, 10 % glycerol). Subsequent purification was carried out by Iris Langstein (Korber group) and Nikolas Eggers (Becker group), from the Molecular Biology Division of the Biomedical Center, LMU.

2.2.2 Salt Gradient Dialysis (SGD)

Preparation of chromatin through salt gradient dialysis was performed as described previously (Krietenstein et al., 2012; Oberbeckmann, Krietenstein, et al., 2021). Briefly, 10 µg DNA genomic plasmid library DNA was mixed with purified *D. melanogaster* histone octamers in 100 µL SGD buffer (10 mM Tris·HCl, pH 7.6, 2 M NaCl, 1 mM EDTA, 0.05% IGEPAL CA630, 0.2 µg/µL BSA). The quantity of histones added varied depending on the desired chromatin density, or 'assembly degree', but 4 µg histones per 10 µg DNA was typical for a 'medium' assembly degree, with 2 µg and 8 µg used for ‘low’ and ‘high’ assembly degrees, respectively. The *S. cerevisiae* DNA source was a plasmid library previously described (Jones et al., 2008), and amplified according to Krietenstein et al., 2012 by Andrea Schmid, using a clonal glycerol stock collection (Open Biosystems, pGP546). *S. pombe* and *E. coli* libraries were generated via limited Sau3A or AluI digestion of respective genomic DNA and blunt end-cloning into vector pJET1.2 (ThermoFisher), also by Andrea Schmid (Oberbeckmann, Niebauer, et al., 2021). Samples were transferred to Slide-A-Lyzer MINI dialysis devices (3.5K MWCO, 0.1 mL, ThermoFisher), pre-soaked in dH2O, and added to a 3 L beaker containing 300 mL high salt buffer (10 mM Tris·HCl pH 7.6, 2 M NaCl, 1 mM EDTA, 0.05% IGEPAL CA630, 14.3 mM β-mercaptoethanol). Using a peristaltic pump, 3 L low salt buffer (10 mM Tris·HCl pH 7.6, 50 mM NaCl, 1 mM EDTA, 0.05% IGEPAL CA630, 1.4 mM β-mercaptoethanol) were gradually added to this beaker over 16 hours at 30 °C, whilst being stirred. Once this dialysis step was completed, a further 1-hour dialysis against 1 L low salt buffer was performed at room temperature. The DNA concentration of the resulting SGD chromatin was then determined via Nanodrop and stored at 4 °C until use. Chromatin was used fresh (i.e., within a week of preparation) and success of assembly was determined by MNase digest of an aliquot to visualise ladder extent.

2.2.3 RSC Purification

Purification of RSC was taught by Christoph Kurat and performed using a published protocol (Wittmeyer et al., 2004), with minor adaptations detailed here.

2.2.3.1 Yeast cell culture

The following incubations were at 30 °C, unless specified. An *S. cerevisiae* strain with a TAP-tag (Tandem Affinity Purification) on the Rsc2 subunit of the RSC complex was obtained from Christoph Kurat and stored as a glycerol stock at -80 °C. Cells were scraped from the frozen stock and restreaked onto a fresh YPD plate, then grown overnight. A single colony was then used to inoculate 50 mL 1x YPD media and again left to culture overnigt. 5 mL of this ‘starter’ culture were then added per 2 L 1x YPD media, with the addition of 33 ug/mL ampicillin (1/3 normal working concentration, to reduce the risk of bacterial contamination) and left for a final overnight incubation. Typically, 6 L yeast culture were processed at any one time for ease of handling and processing. Cells were harvested at late log/early stationary phase, as determined by a plateau in OD_{600} measurements. Harvest was performed by centrifugation at 4.5k rpm for 20 mins at room temperature, using a JLA-8 rotor (Beckman Coulter Life Sciences).

2.2.3.2 Preparing ‘popcorn’

The resulting cell pellet was gently resuspended in 2x Lysis Buffer (100 mM Tris-HCl pH 8, 500 mM KOAc 40% glycerol, 20 mM EDTA, 1 mM DTT, 1 EDTA-free protease inhibitor tablet (Roche)/50 mL) at a 1:1 v/v ratio. Either by using a 25 mL pipette or by piercing the bottom of a 50 mL Falcon tube with a needle, the cell suspension was dripped into a Dewar of liquid nitrogen, creating shock-frozen cell paste that looked like ‘popcorn’. This was then collected with a sieve and quickly transferred to 50 mL tubes, pre-cooled on dry ice, for storage at -80 °C until ready to lyse.

2.2.3.3 Cell lysis

The cells were lysed using a freezer mill (SPEXSamplePrep 6875 High Capacity) under the following conditions: 6 cycles, 2 min pre-cool, 2 min run time, 1 min cool time, rate 15 cycles per second (CPS), 20 min total. Typically, 2 runs were required to lyse cells from 6 L culture. The resulting powder was transferred to pre-cooled 50 mL tubes for storage at -80 °C until ready for purification.

2.2.3.4 Lysate preparation

Powdered yeast lysate was thawed on ice and 1x Lysis Buffer was added at a 1:1 v/v ratio. The mixture was then centrifuged for 10 mins at ~12k RCF at 4 °C with a JA-25.50 rotor (Beckman Coulter Life Sciences). To achieve high-salt extraction of chromatin bound proteins, 3M KOAc was added slowly (important!) to the supernatant whilst stirring at 4 °C, to bring the sample's KOAc concentration up to 400 mM, assuming the supernatant was at 250 mM. Next, 10% polyethylenimine (v/v) pH 7.2 was added dropwise to a final concentration of 0.1%, to precipitate nucleic acids. The mixture was then centrifuged at ~200k RCF for 45 mins at 4 °C with a Ti45 rotor (Beckman Coulter Life Sciences).

2.2.3.5 IgG-Sepharose Affinity Chromatography

As the lysate was being centrifuged, 1.25 mL IgG 80% slurry corresponding to 1 mL IgG beads (IgG Sepharose 6 Fast Flow, GE Healthcare) were washed twice by addition of 25 mL 1x Lysis Buffer without protease inhibitors, followed by a 2 min spin at ~1k RCF in a tabletop centrifuge (Eppendorf 5804R) to collect the beads. On the third wash, 40 mL 1x Lysis buffer was added, and the mixture was partitioned equally into 4x 50 mL tubes before harvesting the beads. This step accommodated for the volume of supernatant retrieved from the lysate ultracentrifugation step (2.2.3.4) and could be adjusted as needed. Next, the supernatant from the lysate ultracentrifugation was collected by careful pipetting, so as not to collect lipids from the top layer or to disturb the pellet, added to the IgG bead-containing tubes, and incubated on rollers at 4 °C for 2 h.

The samples were loaded into a gravity flow column (Econo-Pac Chromatography Columns, Bio-Rad) and washed with 50 mL high salt buffer (10 mM Tris-HCl, 400 mM KOAc, 0.1% NP-40, 10% glycerol, 0.5 mM EDTA, 0.5 mM DTT) with protease inhibitors (1 tablet/50 mL, as in Lysis Buffer). This was followed by another 50 mL high salt buffer wash but without protease inhibitors. A third wash was performed with 50 mL low salt buffer (identical to high salt buffer, albeit 200 mM KOAc) without inhibitors. Once the column emptied, it was capped, then 1 mL low salt buffer and 100 µL TEV protease (1 mg/mL, Christoph Kurat) were added. The column's lid was placed and wrapped in parafilm prior to an overnight incubation on a rotating wheel at 4 °C. The following day, the sample was eluted in 5x 1 mL fractions by addition of low salt buffer, followed by gentle mixing and several minutes incubation, before pooling all fractions.

2.2.3.6 Calmodulin Affinity Chromatography

To the TEV eluate, 1 M $CaCl_2$ was added to a final concentration of 3 mM, followed by 3 volumes of CBP buffer (25 mM Tris-HCl, 250 mM KOAc, 1 mM MgAc, 1 mM imidazole, 2 mM $CaCl_2$, 10% glycerol, 0.1% NP-40, 0.5 mM DTT and protease inhibitors). 2 mL 50% calmodulin affinity resin slurry (Agilent), corresponding to 1 mL resin, was washed 3 times in CBP buffer as described for IgG resin and incubated with the eluate for 2 hours at 4 °C. Then, this mixture was applied to a gravity flow column and washed with 50 mL wash buffer 1 (25 mM Tris-HCl, 400 mM KOAc, 1 mM MgAc, 1 mM Imidazole, 2 mM $CaCl_2$, 10% glycerol, 0.1% NP-40, 0.5 mM DTT). The second wash used wash buffer 2 (25 mM Tris-HCl, 150 mM NaCl, 2 mM $CaCl_2$, 10% glycerol, 0.1% NP-40, 0.5 mM DTT). The bound proteins were then eluted in 10x 500 µL fractions using RSC elution buffer (25 mM Tris-HCl, 150 mM NaCl, 2 mM EDTA, 3 mM EGTA, 10% glycerol, 0.1% NP-40, 0.5 mM DTT). Protein containing fractions were determined via Bradford Assay (Bio-Rad) and pooled before aliquotizing and freezing in liquid nitrogen, for storage at -80 °C.

2.2.4 ATPase assay (based on (Wagner, 2020))

ATP hydrolysis by RSC was assessed as previously described (Forne et al., 2012). The ATPase assay was conducted in a reaction buffer of final composition 25 mM Tris-HCl pH 8.0, 100 mM NaCl, 1.5 mM MgOAc, 0.1 mM Na-EDTA pH 8.0, 10% v/v glycerol, 0.2 mg/ml BSA, 1 mM DTT, 2 mM Mg^{2+}-ATP, 500 ng circular plasmid DNA (pJet1.2), 15.5 U/mL pyruvate kinase, 3 mM PEP, 15.5 U/mL lactate dehydrogenase, 0.6 mM NADH and various concentrations of RSC. A Biotek PowerWave HT 384 well plate reader was used to measure NADH absorption at 340 nm over 30 mins in flat-bottom, uncoated 384 well plates (Greiner).

2.2.5 Genome-wide *in vitro* remodelling

Remodelling reactions were performed in 100 µL and assembled at room temperature. A mock remodelling reaction, i.e., without addition of remodeler or other factor, also referred to as ‘SGD’ sample downstream, was set up by mixing 28 µL dH2O, 25 µL 4x Shifting Mix (80 mM HEPES-NaOH pH 7.5, 12 mM MgCl2, 10 mM ATP (in 0.1 M HEPES-NaOH pH 7.5), 40 mM creatine phosphate, 10 mM DTT, 2 mM EGTA, 48% (v/v) glycerol), 23 µL Buffer E (20 mM HEPES-NaOH pH 7.5, 350 mM NaCl, 0.1% TWEEN-20, 1 mM DTT, 10% glycerol), 10 µL Buffer D (20 mM HEPES-KOH pH 7.5, 80 mM KCl, 1 mM EGTA, 10% glycerol) and 4 µL 0.25 M ammonium sulfate. This was vortexed and spun down in a microcentrifuge, prior to the addition of 10 µL SGD chromatin (using a 20 µL pipet rather than 10 µL, to help reduce shearing). The reaction mixture was mixed gently by flicking the tube and spinning down once more before incubation for 2 h at 30 °C. Reactions were stopped by addition of 0.8 units apyrase (NEB) and incubated for 15 min before proceeding to MNase digestion. When adding purified factors to the sample, creatine kinase (Roche Applied Science) was added to a final concentration of 20 ng/µL and dH20 volume was reduced accordingly. Information for each individual sample can be found in Appendix Table 1.

2.2.6 MNase-seq

To remodelled (or mock) chromatin, 2 µL 75 mM $CaCl_2$ were added (final concentration 1.5 mM) in tandem with 2 µL/100 units MNase (Sigma), as a premix. Mixtures were quickly (important!) vortexed and spun down, before exactly 5 min incubation at 30 °C. MNase digestion was stopped by addition of 12 µL STOP buffer (0.1 M EDTA, 2% SDS). Next, 5 µL proteinase K (20 mg/mL, Bioline) were added and gently mixed before samples were incubated for 45 min at 37 °C. Purification of the resulting mononucleosomal DNA fragments was achieved via ethanol precipitation. To each sample 2 µL glycogen (20 mg/mL, Roche), 5 µL 5 M NaCl and 325 µL 100% ethanol were added, followed by 10 min on ice and a 20 min spin at 21k RCF and 4 °C in a tabletop centrifuge (Eppendorf). Pellets were washed with 800 µL room temperature 70% ethanol and spun at room temperature for 4 min. Supernatants were then aspirated, and pellets were air dried briefly prior to resuspension in 15 µL 5 mM Tris-HCl pH 8. Samples were electrophoresed on

1.5% agarose gels in 1x TAE buffer (40 mM Tris, 20 mM acetic acid, 1 mM EDTA) at 100V for 1-1.5 hours. Mononucleosomal DNA bands were visualised on a UV sample tray and excised from the gel with a scalpel, to be purified (PureLink Quick Gel Extraction Kit, Invitrogen) and stored at -20 °C until library preparation.

2.2.7 Illumina Library Preparation

2.2.7.1 Adapter Ligation

DNA concentrations were determined via Qubit (ThermoFisher) and 10-50 ng were used for library preparation. All reagents were purchased from NEB either individually or as part of the NEBNext Multiplex Oligos for Illumina Kit unless stated, except 4x Quick Ligation Buffer (QLB) which was made in-house. In a 25 µL reaction were mixed 6.25 µL 4x QLB (250 mM Tris-HCl pH 7.4, 40 mM $MgCl_2$, 4 mM DTT, 6 mM ATP, 30% polyethylene glycol (PEG6000)), 1.25 µL T4 DNA Polymerase, 1.25 µL T4 PNK and 1 µL dNTPs (10 mM). The sample DNA was added, and the volume made up to 24.75 µL with dH2O before addition of 0.25 µL Taq DNA Polymerase. In a thermal cycler (ProFlex PCR System, ThermoFisher) the samples were incubated for 15 min at 12 °C, 15 min at 37 °C, then 20 min at 72 °C. Next, 1 µL T4 DNA Ligase Buffer, 1.5 µL 15 µM NEB adapter and 2 µL T4 Ligase were mixed in, before incubating for 15 min at 25 °C. Finally, 2 µL USER enzyme were added and samples held for 15 min at 37 °C. 70 µL AMPure XP beads (Beckman Coulter) were added to each sample, gently mixed and incubated at room temp for 5 min before placing the sample tubes into magnetic racks. Once the supernatant cleared it was aspirated, and the beads were washed with room temperature 80% ethanol twice before being left to briefly air dry, prior to elution with 20 µL 5 mM Tris HCl pH 8.

2.2.7.2 DNA Indexing

In 50 µL tubes, PCR reactions were assembled with 18 µL adapter ligated mononucleosomal DNA (eluate of 2.2.7.1), 15 µL ddH20, 10 µL 5x Phusion buffer, 1.5 µL dNTPs (10 mM), 2.5 µL Universal Primer, 2.5 µL Index Primer (unique for each sample) and 0.5 µL Phusion Polymerase. Thermal cycling conditions were as follows: 30 sec at 98 °C initiation, 8-10 cycles of 10 sec at 98 °C denaturation, 30 sec at 65 °C annealing and 30 sec at 72 °C extension, before a final extension of 5 min at 72 °C. PCR products were electrophoresed, excised and purified as detailed in 2.2.6. Samples were diluted to 10 nM and pooled for sequencing by Stefan Krebs (LaFuGa, Gene Center, LMU) on an Illumina HiSeq 1500 in 50 bp single-end mode, with library quality being assessed by checking fragment size distribution by Bioanalyzer (Agilent).

2.2.8 Data Processing

Sequencing reads (~5 million/sample) were mapped to the *S. cerevisiae* (Ensembl R64-1-1), *S. pombe* (Ensembl EF2) or *E. coli* (NCBI REL606) genome with Bowtie 2 (Langmead & Salzberg, 2012) and duplicate reads were dropped. In RStudio using GenomicAlignments (Lawrence et al., 2013), reads were shifted by 73 bp and resized to 50 bp to represent an extended dyad for each fragment. Coverages for each sample were generated and aligned to genomic features as indicated in respective plots, such as *in vivo* +1 nucleosome positions (Oberbeckmann, Krietenstein, et al., 2021), Abf1 PWMs (MacIsaac et al., 2006), Rap1 PWMs (Morozov & Siggia, 2007), Reb1 PWMs (Badis et al., 2008) or poly(dA:dT) tracts. MNase-seq composite plots and heatmaps were normalised such that the sum of each alignment window equals 1, and y-axes report normalised dyad density x1000. MNase-seq heatmap colour scales range from the 10th to 90th percentile values, with normalised dyad densities outside of this limited to the min/max of the scale. More details on alignment filtering, sorting and normalisation can be found in the relevant figure legends.

2.2.9 Nucleosome positioning sequence (NPS) analysis

Nucleosome peak calling, principal component analysis (PCA) and DNA shape analysis were performed as previously described (Oberbeckmann, Krietenstein, et al., 2021), with the addition of an orthogonal 'Manual Filtering' approach, described here.

2.2.9.1 Nucleosome Peak Calling – 'Denoised peaks'

Sequencing reads were trimmed to 40 bp extended dyads for nucleosome peak calling. Coverages were calculated, then using the nucleR package (Flores & Orozco, 2011) noise was removed with FFT filtering (parameter pcKeepComp = 0.02), and peaks were detected with a threshold of 99%.

2.2.9.2 Reproducibility Filtering of Peaks

Peak positions in each sample were enlarged to 20 bp and overlapped with all samples of the same experimental condition. Positions where at least 15 bp were common across most replicates (exact number dependent on sample set) were merged and designated reproducible peaks, whilst non-reproducible positions were dropped. Peaks within 250 bp of tile borders (i.e., the boundary where the yeast DNA meets the backbone of the plasmid library) and overlapping a high artifact region of the library (chr**III**, 91-93 kb) were removed. This set of nucleosome peaks were then subjected to either 'Manual Filtering of Nucleosome Peaks' or 'PCA of Nucleosome Peaks' to generate nucleosome positioning sequences (NPSs).

2.2.9.3 Filtering of Nucleosome Peaks by Difference Sets

Reproducible nucleosome peaks from 2 different experimental conditions (usually SGD vs remodeler) were overlapped with each other. Peaks only present in their respective experimental condition (difference set) were designated as sample-specific and separated from those present in both groups (intersection set). Sample-specific peak positions were subjected to 'DNA Shape Analysis'.

2.2.9.4 PCA of Nucleosome Peaks

Nucleosome peak positions generated from 'Peak Filtering' were grouped together and reduced to their dyad positions. 50 bp coverages of sequencing reads for each contributing sample were overlapped with the pool of nucleosome dyad positions, creating a matrix of dimensions *n* samples x *n* nucleosome positions, containing the overlap counts. Considering each count in the matrix as *x,* normalisation was achieved using the formula: normalised occupancy = log2(((x/sum(x)) × 1000) + 0.001). Principal component analysis was performed on this normalised matrix and K-means clustering was used on the resulting principal components. This process was able to group nucleosomes based on similarity in occupancy patterns across experimental conditions. Nucleosome groups determined by this clustering were then analysed for DNA shape features.

2.2.9.5 DNA Shape Analysis

Nucleosome dyad positions were resized to 321 bp, centered on the dyad, and DNA shape features were calculated with the R package DNAshapeR (Chiu et al., 2016). DNA rigidity scores were calculated by determining 'the longest consecutive run of the form A*n*T*m* that contains this position (with the requirement of $n \geq 0$, $m \geq 0$, and $n + m \geq 2$)'(Le Poul et al., 2020).

2.2.10 Nucleosome depleting sequences (NDS) analysis

2.2.10.1 Defining high coverage genomic regions

In order to define nucleosome depleted sequences (NDSs) from MNase-seq data, we focused on regions with generally high coverage, to ensure that local nucleosome depletions were reflective of the genomic environment, rather than of poor local sequencing depth or low plasmid library copy number. To this end, the *S. cerevisiae* genome was binned into 5 kb windows and coverages for each sample in a particular analysis (e.g., SGD vs RSC NDSs) were assigned to each bin. Only bins where the total coverage fell within the 0.5 and 0.99 quantiles were defined as high coverage. Only the bins defined as high coverage for every sample in a comparison were retained and searched for NDSs.

2.2.10.2 Defining NDSs

For each sample in a comparison, the mean coverage was calculated across the common high coverage bins defined in the previous step. Regions where 100 to 350 consecutive base pairs had a coverage below this mean value were defined as nucleosome free regions (NFRs), for their underlying sequences (NDSs) to be analysed. PCA and DNA shape analysis of NDSs was performed in the same way as NPSs, with the exception that the 'Filtering of Nucleosome Peaks by Difference Sets' approach was omitted, as this method was unable to resolve differentially responsive groups of NDSs, whilst PCA and clustering was. See Results - 3.2.3 text for details.

3. Results

In order to investigate the mechanisms by which ATP-dependent chromatin remodellers organise chromatin, our lab employs a unique genome-wide reconstitution system, capable of recapitulating *in-vivo* like nucleosome positioning *in vitro.* This system (**Figure 5**) was published several times (Krietenstein et al., 2016; Krietenstein et al., 2012; Oberbeckmann, Krietenstein, et al., 2021; Oberbeckmann, Niebauer, et al., 2021; Zhang et al., 2011), with gradual optimisations accumulating to greatly develop the approach for use in many potential applications. Notably, the development of superior dialysis chambers (Slide-a-Lyzer, Thermofisher) has permitted the reconstitution of chromatin at higher densities (closer to an *in vivo* state) than previously possible, on a well characterised and defined *S. cerevisiae* genomic plasmid library (Jones et al., 2008), whilst the use of *S. pombe* and *E. coli* libraries allows for independent interrogation of nucleosome positioning determinants which may have evolved to co-localise on the *S. cerevisiae* genome, e.g., poly(dA:dT) tracts and GRF binding sites at promoters. Additionally, whilst the histones used to reconstitute chromatin in this study were always endogenous *D. melanogaster* embryo histone octamers, the use of fully recombinant *S. cerevisiae* or *H. sapiens* octamers has been demonstrated, allowing for control of post translational modifications (PTMs) on histone tails and mutagenesis (Oberbeckmann, Krietenstein, et al., 2021). Likewise, the use of recombinant chromatin remodellers is also possible, although not employed here.

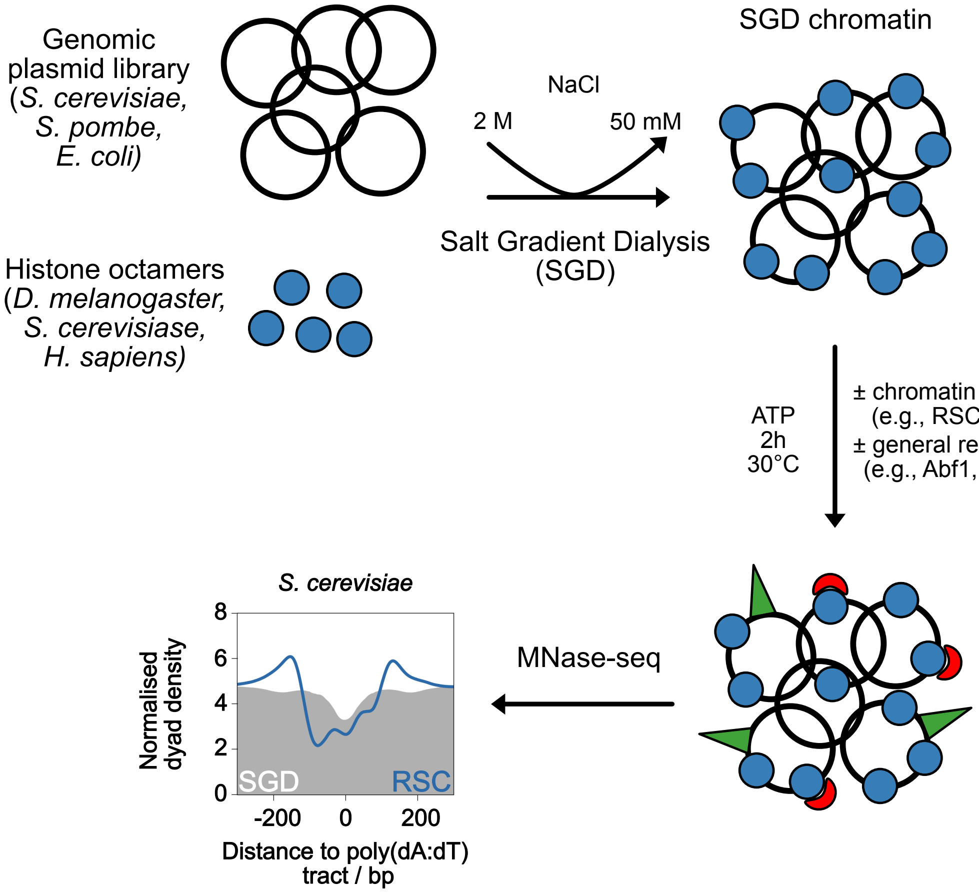
Genomic plasmid library
(*S. cerevisiae,*
S. pombe,
E. coli)
Histone octamers
(*D. melanogaster,*
S. cerevisiase,
H. sapiens)
NaCl
2 M
50 mM
Salt Gradient Dialysis (SGD)
SGD chromatin
ATP
2h
30°C
± chromatin remodeler
(e.g., RSC, INO80)
± general regulatory factor
(e.g., Abf1, Rap1, Reb1)
MNase-seq
S. cerevisiae
Normalised dyad density
8
6
4
2
0
SGD
RSC
-200
0
200
Distance to poly(dA:dT) tract / bp

Figure 5 – Genome-wide *in vitro* reconstitution of nucleosome positioning

Schematic overview of the *in vitro* system we used to study nucleosome positioning by chromatin remodelers. A genomic plasmid library (usually *S. cerevisiae* but *S. pombe* and *E. coli* genomes were also used) was mixed with histone octamers, in this case purified from *D. melanogaster* embryos, but recombinant *S. cerevisiae* and *H. sapiens* octamers have previously been used. The mixture was dialysed from high to low salt concentration (salt gradient dialysis), during which the histones were incorporated into nucleosomes with DNA-dependent 'intrinsic' positioning (SGD chromatin). This chromatin was incubated with combinations of purified ATP-dependent chromatin remodelers and general regulatory factors to reposition nucleosomes, and their resulting positions were determined via MNase-sequencing (MNase-seq). Figure modified after (Oberbeckmann, Krietenstein, et al., 2021).

This project, and our lab's work in general, deals with understanding determinants of nucleosome organisation, which can be conceptualised as a combination of nucleosome positioning, i.e., the location of a nucleosome dyad, and nucleosome depletion, such as the nucleosome free regions (NFRs) observed in *S. cerevisiae* promoters. Importantly, whilst the DNA sequence within a nucleosome defines the position, it does not necessarily determine that a nucleosome is placed there. Likewise, the DNA sequence of an NFR need not necessarily determine its depletion. As such, there are two modes, direct or indirect, by which the DNA sequence can influence nucleosome organisation in its vicinity. As an example for the direct mode, the shape/mechanics of a particular DNA sequence may be directly read out by a chromatin remodeler, which in turn preferentially deposits a nucleosome at or near this sequence. This has so far been demonstrated for INO80 (Oberbeckmann, Krietenstein, et al., 2021), but this mechanism has been so far unexplored for other remodelers. Regarding the indirect mode, the DNA sequence may directly determine just the position of a 'barrier' (e.g., a GRF binding site), to which nucleosomes are phased, then regularly spaced to each other, through a ruler mechanism (Oberbeckmann, Niebauer, et al., 2021). This leads to extensive nucleosome positioning with little or no determining role of the nucleosomal DNA sequence. This ruler mechanism has been demonstrated for INO80, ISW1a, ISW2 and Chd1 so far. The following chapters explore aspects of these nucleosome organisation mechanisms by chromatin remodelers.

3.1 The direct role of DNA sequence in nucleosome positioning

3.1.1 Derivation of nucleosome positioning sequences (NPSs) from MNase-seq data

Oberbeckmann, Krietenstein, et al. (2021) pioneered a bioinformatic approach to determine so-called nucleosome positioning sequences (NPSs) from genome-wide nucleosome positioning by individual factors, e.g. remodellers, as measured by MNase-seq. We have made incremental updates to this workflow, including the addition of an orthogonal method of determining NPS groups and implementing single-end sequencing data to expand the available repertoire of remodeller data (**Figure 6** & **Figure 7**). Details can be found in Methods (2.2.9).

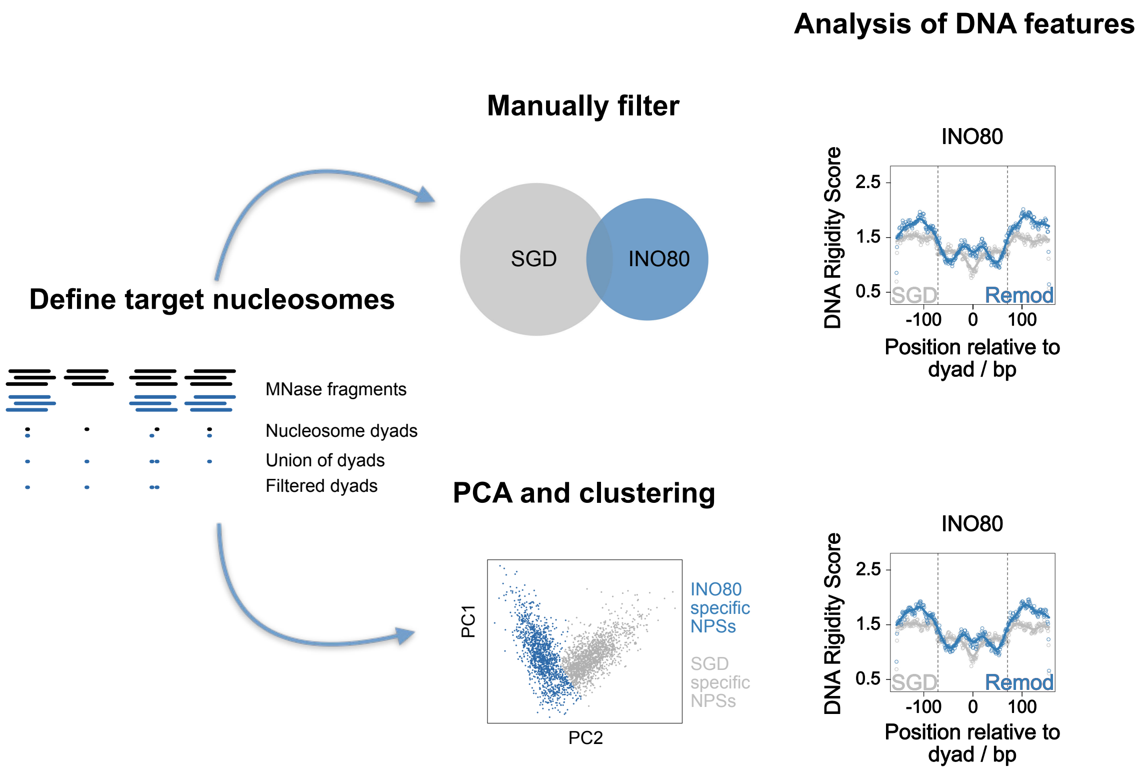
Analysis of DNA features
Manually filter
Define target nucleosomes
SGD
INO80
MNase fragments
Nucleosome dyads
Union of dyads
Filtered dyads
PCA and clustering
PC1
PC2
INO80 specific NPSs
SGD specific NPSs
INO80
DNA Rigidity Score
2.5
1.5
0.5
SGD
Remod
-100
0
100
Position relative to dyad / bp
INO80
DNA Rigidity Score
2.5
1.5
0.5
SGD
Remod
-100
0
100
Position relative to dyad / bp

Figure 6 – Overview of bioinformatic workflow used to define NPSs

Graphical representation of Methods – Nucleosome positioning sequence (NPS) analysis. MNase-sequencing reads from *in vitro* reconstitution experiments with purified factors were aligned to the relevant genome and stacked to determine genomic coverage. Nucleosome dyad positions were called from the coverages, artefactual reads corresponding to a marker used in the *S. cerevisiae* plasmid library were filtered out and peak positions were pooled. Either this pool was directly analysed (**Figure 7**, 'Denoised'), or further filtering was applied to only retain nucleosome dyads reproduced in the majority of replicates of a particular experimental condition. Dyad positions were then either separated into those unique to an experimental group (Filtering of Nucleosome Peaks) or subjected to principle component analysis and K-means clustering (PCA of Nucleosome Peaks). DNA shape/mechanics of NPSs defined by one of these three means were then calculated and visualised as composite plots. Figure modified after (Oberbeckmann, Krietenstein, et al., 2021).

Before using these updated workflows to investigate potential novel NPSs of various remodelers, we confirmed that we could still recapitulate published shape profiles for nucleosomes positioned by INO80 (**Figure 7**). We compared minor groove width (MGW), helical twist (HelT), propeller twist (ProT), roll, electrical potential (EP) and DNA rigidity score profiles of INO80 NPSs (only propeller twist shown here for simplicity of comparison to Oberbeckmann, Krietenstein, et al. (2021)) derived by the previously published workflow (**Figure 7**, 'Paired') to the scores derived from our alternative workflows explored here. Note that the shape profiles displayed in this study are symmetrical, because NPSs were not orientated on a particular strand, e.g., relative to the direction of transcription. Initially, we asked whether we could recapitulate INO80 NPS shape profiles using single end sequencing data, instead of the previously used paired-end data, which would allow the NPS analysis of a wealth of previously generated MNase-seq data for other remodelers. We had previously hypothesised that the greater precision that paired end sequencing provides would be necessary for aligning NPSs well enough to reveal shape features, but evidently this was not the case (**Figure 7**, ‘Denoised’, ‘Filter’ and ‘PCA’ vs ‘Paired’). Next, we attempted to manually filter nucleosome peaks for those reproducible and present in only INO80 as compared to SGD samples and found this to be sufficient to recapitulate the profiles observed after PCA and clustering (**Figure 7**, ‘Filter’ vs ‘PCA’). Oberbeckmann, Niebauer, et al. (2021) observed that INO80 positioned +1 nucleosomes much less clearly *in vitro* at higher chromatin densities, prompting us to ask if this was reflected in a less clear shape profile at such densities. Whilst some mild differences could be observed between shape profiles generated from medium and high-density chromatin samples (**Figure 7**, ‘High Density’ vs rest), key characteristics of the profile were generally well conserved. Finally, we asked if the pool of nucleosome peaks called from each experimental condition would produce a distinct shape profile, without the strict filtering which accompanies the downstream Manual Filter and PCA pipelines. To our surprise, this pool of sequences was already sufficient to recapitulate the distinct profiles seen with much more extensive processing (**Figure 7**, ‘Denoised’). Since this group of sequences requires much less processing to generate and yields many more data points (ca. 9,000 vs ca. 1,000) to feed into downstream analyses, we chose to use the Denoised group of sequences as NPSs in further analyses of different remodelers.

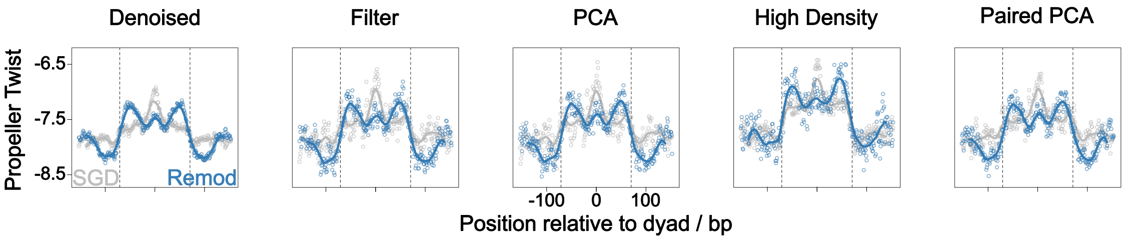

Figure 7 – INO80 NPS shape profiles are consistent across a range of criteria.

Propeller twist profiles for INO80 NPSs defined by various workflows and at different conditions. ‘Denoised’, ‘Filter’ and ‘PCA’ refer to NPSs derived from processing only reads from one end of paired end sequencing data at a medium assembly degree. This involved shifting all read 5’ ends 73 bp to approximate extended dyad positions, rather than precisely determining dyad positions using reads from both ends. This was done to assess the effect of this processing on resolution of the shape profiles. ‘Denoised’ NPSs are simply the pool of all nucleosome peaks defined in each INO80 replicate, with those proximal to tile borders and artefactual regions filtered out. ‘Filter’ and ‘PCA’ NPSs were derived as detailed in Methods (2.2.9), including a common step where only sequences present in most replicates of a condition were kept, a so-called ‘reproducibility’ filter. ‘High Density’ NPSs were generated from single end sequencing of INO80-remodelled high assembly SGD chromatin, also via PCA. ‘Paired PCA’ NPSs were derived from paired end sequencing of INO80-remodelled medium assembly chromatin, using the PCA workflow. Number of sequences plotted in each panel: Denoised – 9,557 x SGD, 9,065 x INO80; Filter – 716 x SGD, 1,037 x INO80; PCA – 695 x SGD, 1,118 x INO80; High Density – 1,135 x SGD, 412 x INO80; Paired PCA – 1,127 x SGD, 1,268 x INO80. Samples used – INO80 (GSM4306398, GSM4306399, GSM4306402, GSM4306406); SGD (GSM4306398, GSM4306400, GSM4306403, GSM4306404), from GEO accession GSE145093 (Oberbeckmann, Krietenstein, et al., 2021).

3.1.2 Remodeler-specific NPSs

Once we confirmed the robustness of INO80's specific NPS shape profiles also using single-end read MNase-sequencing data (**Figure 7**), we turned to previously published data (Oberbeckmann, Niebauer, et al., 2021) and generated new data (**Table 5**) to ask if other chromatin remodelers displayed any DNA shape profile preferences for the positioning of nucleosomes. To this end, we generated NPSs from single-end read MNase-seq data for nucleosome positioning by INO80, RSC, ISW1a, ISW2, Fun30 and Chd1, then performed DNA shape analysis on the resulting sequences. In each analysis, we compared the remodeler samples with their respective matched SGD-only samples. Using the example of DNA Rigidity Score (**Figure 8**), we saw that whilst some characteristics of each remodeler's profile appeared similar (e.g., INO80 vs ISW1a), the profiles generally differed from each other. This shows us that remodelers vary in the manner they directly read DNA sequence and position nucleosomes, providing a first such comparative view.

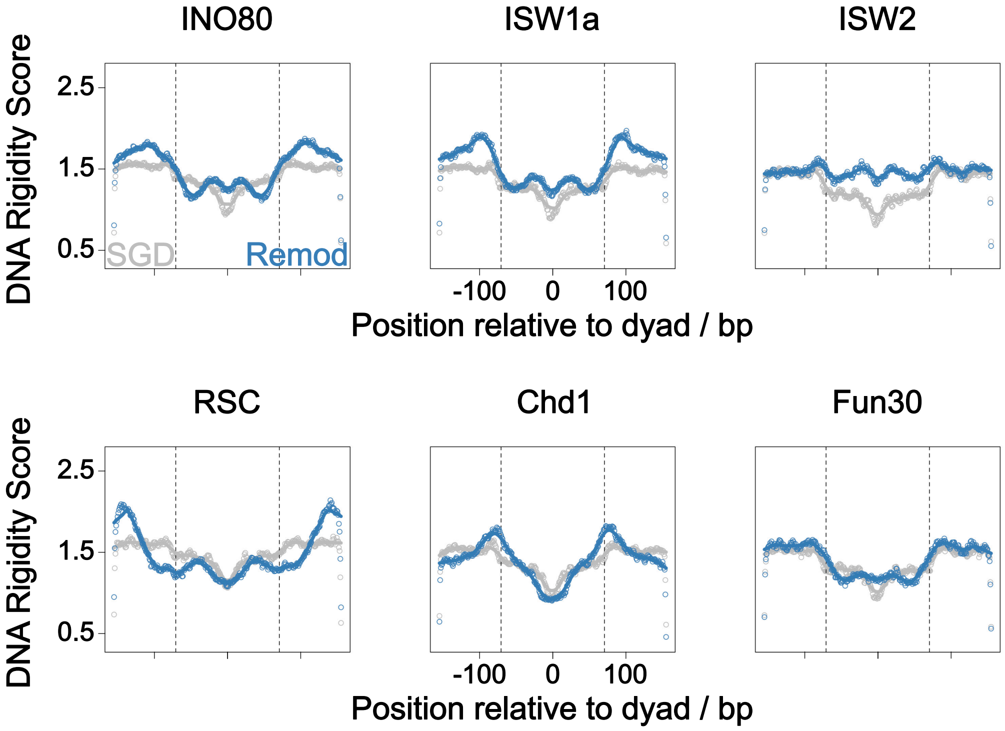

Figure 8 – Chromatin remodelers differentially process DNA sequence information into nucleosome positioning.

Rigidity score profiles of DNA sequences occupied by nucleosomes in SGD chromatin (grey) and SGD chromatin remodelled by the indicated remodeler (blue). See **Figure 6** and Methods - 2.2.9 for details on determining these sequences. Plots are aligned at nucleosome dyad positions and vertical dashed lines indicate the position of theoretical nucleosome core borders at ±73 bp from the dyad. Number of sequences plotted in each panel: INO80 – 14739 x SGD, 12,568 x INO80; ISW1a – 9,219 x SGD, 8,872 x ISW1a; ISW2 – 4,823 x SGD, 5,106 x ISW2; RSC – 8,438 x SGD, 7,611 x RSC; Chd1 – 10,343 x SGD, 9,069 x Chd1; Fun30 – 5,279 x SGD, 5,079 x Fun30. All samples used here were single-end sequencing data, as more single-end than paired-end replicates were available for each remodeler, hence we defined a different number of INO80 NPSs compared to when we used different paired-end samples (**Figure 7**). Samples used: INO80 panel

– SGD (GSM4175544, GSM4175545, GSM4175599, GSM4175600, GSM4175670, GSM4175671), INO80 (GSM4175541, GSM4175542, GSM4175593, GSM4175594, GSM4175661, GSM4175662); RSC panel – SGD (TBPool1_04, TBPool1_042, TBPool2_Univ9), RSC (TBPool1_1, TBPool1_18, TBPool2_Univ1); ISW1a panel – SGD (GSM4175599, GSM4175600, GSM4175670, GSM4175671), ISW1a (GSM4175596, GSM4175597, GSM4175664, GSM4175665); ISW2 panel – SGD (GSM4175670, GSM4175671), ISW2 (GSM4175667, GSM4175668); Fun30 panel – SGD (GSM4175671, GSM4175728), Fun30 (GSM4175659, GSM4175727); Chd1 panel – SGD (GSM4175544, GSM4175545, GSM4175670, GSM4175671), Chd1 (GSM4175538, GSM4175539, GSM4175655, GSM4175656). All samples listed can be found at GEO accession GSE140614 (Oberbeckmann, Niebauer, et al., 2021) or in **Table 5**.

RSC displayed the greatest preference for positioning nucleosomes far away from rigid DNA (~70 bp from the nucleosome border), reflecting that RSC moves nucleosomes away from rigid poly(dA:dT) tracts more strongly than other chromatin remodelers (Barnes & Korber, 2021; Lorch et al., 2014). Interestingly, SGD-derived NPSs also displayed a distinct and well-reproduced profile (**Figure 8**, grey line, all panels), with nucleosomes preferentially assembling on DNA of low rigidity. This finding is consistent with earlier work documenting the lower intrinsic nucleosome formation affinity of DNA containing poly(dA:dT) tracts (Shrader & Crothers, 1990), which are inherently rigid sequences with a high energetic cost for wrapping around a histone octamer (Liu et al., 2021). ISW2 appeared the least discriminative toward DNA sequence, based on the low variance in mean rigidity score. In order to confirm that these rigidity profiles were not dominated by random variance, we also plotted profiles for 10,000 randomly selected 321 bp sequences from the *S. cerevisiae* genome (**Figure 9**). Importantly, the rigidity score profile averaged over all *in vivo* dyad positions (67,935) did not resemble the profile of any particular remodeler. In other words, all-average nucleosome positions *in vivo* are not dominated by any one remodeler's intrinsic preferences.

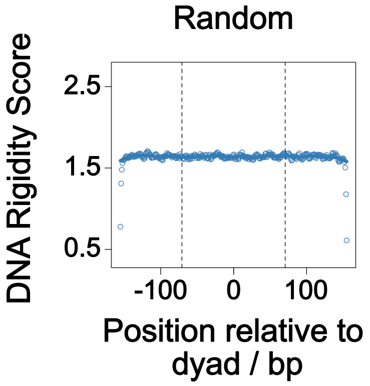

Figure 9 – Randomly selected *S. cerevisiae* sequences show no distinct rigidity profile

DNA rigidity score profile of 10,000 randomly selected *S. cerevisiae* sequences of 321 bp length. Sequences were generated using BEDTools (Quinlan & Hall, 2010). The following code was used: bedtools random -l 321 -n 10000 -g scer.txt -seed 654 > random.bed, where scer.txt was a tab-delimited file containing *S. cerevisiae* chromosome names and lengths, the specific seed number was unimportant but standardised to reuse the same random sequences and random.bed was the output file.

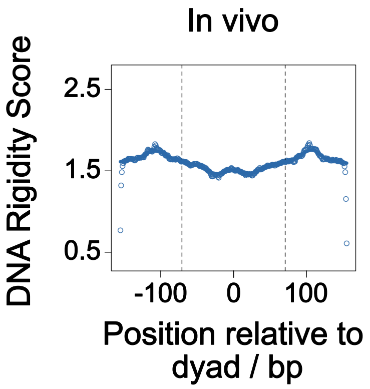

Figure 10 – Average nucleosome dyad positions *in vivo* do not reflect any one remodeler's intrinsic preferences for positioning nucleosomes

DNA rigidity score profile of all *in vivo* dyad positions (67,935) (Oberbeckmann et al., 2019).

3.1.3 Structural basis for remodeler NPSs

Once we determined this array of remodeler-specific NPS shape/mechanic profiles, we turned to the published literature on high-resolution remodeler-nucleosome structures to ask if there was a correlation between NPS profiles and structural information. We first looked to recapitulate the observations by Oberbeckmann, Krietenstein, et. al., (2021), that significant DNA interaction sites crucial for permitting nucleosome translocation by INO80 map to noteworthy regions of the corresponding rigidity profile (**Figure 11**, left panel). It has been shown that INO80 contacts extra-nucleosomal DNA at ~100 bp upstream of the dyad via the HSA helix of the Ino80 motor ATPase subunit situated in the Arp8 module (Brahma et al., 2018; Knoll et al., 2018). This interaction is important for coupling ATP hydrolysis to DNA translocation and facilitating +1 nucleosome positioning *in vitro* (Knoll et al., 2018). It maps to the point of highest rigidity in the NPS profile, implicating extra-nucleosomal rigid DNA in guiding nucleosome positioning by INO80. Additionally, further contacts are made via the ATPase motor and Arp5 grip, broadly at ~60 bp and ~30 bp upstream of the dyad, respectively. Between these contact points lies the region of most flexible DNA in the NPS profile. The accumulation of DNA strain at this region after subsequent rounds of DNA pumping by the core ATPase motor is proposed to be the driving force behind INO80's ability to translocate nucleosomes (Eustermann et al., 2018). Hence, flexible DNA at this region may affect the accumulation of strain and consequently sliding by INO80.

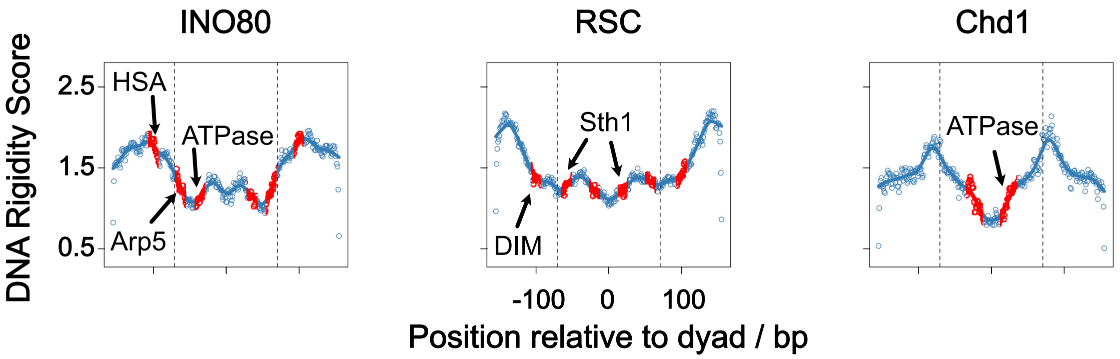

Figure 11 – Shape/mechanic profiles of remodeler-specific NPSs reflect functionally crucial remodeler-DNA interactions

Significant remodeler-DNA interactions (red), derived from high resolution structues, were mapped onto DNA rigidity profiles of INO80, RSC and Chd1 NPSs. Note that NPSs are not oriented by strand and hence display symmetrical rigidity profiles. As such, notable remodeler-DNA contact points are plotted in duplicate. In the case of INO80, highlighted contacts at -100 bp, -60 bp and -30 bp correspond to INO80 pumping the DNA from right to left, i.e., entry DNA is on the right; contacts downstream of the dyad correspond to remodelling in the reverse direction. This can be seen in Oberbeckmann, Krietenstein et. al., (2021), where NPSs at +1 *in vivo* positions, oriented by the direction of transcription, display markedly flatter rigidity score profiles downstream of the dyad. Likewise, RSC contacts displayed at -110 bp, -60 bp and +20 bp correspond to an orientation where DNA enters the RSC complex from the right and exits on the left, with the reverse true for the mirroring contacts. Finally, the Chd1 contact at +20-35 bp corresponds to entry DNA on the right, whilst Chd1 binding to -20-35 bp on a nucleosome would indicate DNA entry from the left. See text for further details on remodeler-DNA interactions.

Next, we cross-referenced the rigidity profile of RSC NPSs with a recently published structure of a RSC-bound nucleosome (Wagner et al., 2020). Whilst the authors were unable to clearly resolve RSC’s DNA-interacting module (DIM) due to its flexibility and therefore variable positioning within the acquired structures, their cross-linking data placed this module at a RSC-DNA contact ~20 – 40 bp upstream of the nucleosome border, in concordance with RSC protecting ~50 bp DNA from MNase digestion (Brahma & Henikoff, 2019). One component of the DIM is the subunit Rsc2 (or its less abundant homolog Rsc1), both of which contain an AT-hook motif, a conserved DNA-binding motif renowned for binding to the minor groove of rigid AT-rich DNA (Aravind & Landsman, 1998; Reeves & Nissen, 1990; Singh et al., 2006). Earlier work on Rsc1 and Rsc2 mutants revealed this motif to be essential for *S. cerevisiae* viability (Cairns et al., 1999). The contact point between the DIM (likely via Rsc1/Rsc2) and the extra-nucleosomal DNA mapped to the bottom of a slope transitioning from high to low rigidity (**Figure 11**, middle panel). As such, the binding affinity of Rsc1/Rsc2 for the extra-nucleosomal DNA may be linked to RSC’s capacity for DNA translocation.

Wagner et al., (2020) also resolved two RSC contacts with intra-nucleosomal DNA at SHL-6 and SHL+2, roughly -60 bp and +20 bp from the nucleosome dyad, respectively. These regions are stacked on top of each other in the 3D nucleosomal structure and represent the interface between Sth1, the core ATPase subunit of RSC, and the nucleosome. Specifically, lobe 1 of Sth1’s ATPase module contacts both locations on the DNA. Adjacent to lobe 1 lies the hinge region, containing the post-HSA domain, then the HSA domain which acts as a binding scaffold for the ARP module. The ARP module has been shown to influence RSC’s remodelling activity by coupling ATPase hydrolysis to DNA translocation (Clapier et al., 2016; Schubert et al., 2013), which Wagner et al. (2020) suggest occurs by modulating the interaction between lobe 1 and the nucleosomal DNA via the hinge region. Indeed, mutations in the post-HSA domain of the hinge region have a marked impact on translocation and ATP hydrolysis by RSC (Clapier et al., 2016; Saha et al., 2002; Szerlong et al., 2008). Taken together, this interface between RSC and the nucleosome potentially represents an important processing step whereby DNA sequence information is read by the remodeler and may modulate ATP hydrolysis and/or translocation via conformational changes in key modules nearby. This interface also maps to slopes trending toward peaks of highest intra-nucleosomal DNA rigidity, which could influence the hydrolysis-translocation coupling mechanism previously discussed, affecting nucleosome sliding at an NPS.

Finally, we compared our results for Chd1 with a recently published structure for a Chd1-bound nucleosome (Nodelman et al., 2022). Chd1 was seen to contact the nucleosome at SHL+2, ~20 bp downstream of the nucleosome dyad. The DNA duplex was distorted toward an A-form geometry accommodating an extra nucleotide on one strand, a perturbation which propagated toward SHL+3, where it was resolved back to a B-form geometry. Thus, this region represents not only the binding interface of Chd1 with the nucleosome, but also the site where structural changes in the DNA are induced, allowing translocation in 1-bp steps (Nodelman & Bowman, 2021; Winger et al., 2018). This region mapped to the Chd1 rigidity profile proximal to the point of highest flexibility over the NPS dyad, trending toward higher rigidity (given the direction of DNA translocation by Chd1). Hence, it may be the case that Chd1 is better able to induce the necessary B-form to A-form transition in the nucleosomal DNA structure with a more flexible substrate, thereby permitting translocation, whilst DNA of greater rigidity at SHL+2 may hinder the same mechanic, leading to increased nucleosome occupancy. This is consistent with the finding that inserting a rigid poly(dA:dT) tract around SHL2.5 greatly reduces sliding by Chd1 on a mononucleosomal substrate *in vitro* (Winger & Bowman, 2017).

3.2 The direct role of DNA sequence in nucleosome depletion

In addition to direct nucleosome positioning by reading specific DNA sequence features, we hypothesised that chromatin remodelers may also exhibit preferences for DNA sequences from which they deplete nucleosomes. This type of mechanism was already known to be deployed by RSC, shown to preferentially displace nucleosomes from poly(dA:dT) tracts *in vitro* (Lorch et al., 2014), notably in a directional manner, 5’ of polyA and 3’ of polyT (Krietenstein et al., 2016). Furthermore, we present evidence for a largely active rather than solely passive mechanism of nucleosome depletion at poly(dA:dT) tracts *in vivo* (Barnes & Korber, 2021), for which RSC is a prime example in yeast.

3.2.1 The active mechanism of nucleosome depletion by poly(dA:dT) tracts *in vivo*

The following chapter elaborates on our published (Barnes & Korber, 2021) data and arguments regarding nucleosome depletion mechanisms at poly(dA:dT) tracts in vivo. There we reviewed the existing evidence for an intrinsic nucleosome exclusion mechanism of nucleosome depletion by poly(dA:dT) tracts, and argued against this model using new analysis of published data from our group (Oberbeckmann, Niebauer, et al., 2021). For starters, *in vivo* nucleosome depletion over poly(dA:dT) tracts does not occur in all organisms. Granted, it has been observed in numerous different species (Field et al., 2008; Segal & Widom, 2009a; Tsankov et al., 2010), but is notably absent in *S. pombe* when probed via chemical mapping (Moyle-Heyrman et al., 2013). Additionally, the energetic cost of nucleosome sliding by chromatin remodelers as estimated by the physiologically energy available from ATP hydrolysis (Tran & Unden, 1998), and given an estimated step size of 1–2 bp per ATP hydrolysis (Deindl et al., 2013; Harada et al., 2016; Zhou et al., 2016) far outweighs the penalty for incorporating poly(dA:dT) tracts in nucleosomes (Lorch et al., 2014).

We hypothesised that the heavy reliance on MNase-seq for investigating nucleosome organisation may have overestimated depletion at poly(dA:dT) tracts because MNase preferentially digest AT-rich DNA (Dingwall et al., 1981; Horz & Altenburger, 1981). As such, we compared both *in vitro* and *in vivo* nucleosome organisation as mapped by MNase-seq data with equivalents generated with an MNase-independent method based on differential DNA methylation called ODM-seq (genome-wide occupancy measurements by DNA methyltransferases). This technique is capable of determining absolute nucleosome occupancy without the MNase sequence bias (Oberbeckmann et al., 2019) and allows direct comparison of nucleosome depletion extent across samples. With this approach, nucleosome depletion over poly(dA:dT) tract-enriched promoter regions *in vitro* was much weaker than *in vivo,* arguing for an active depletion mechanism (**Figure 12**, **Figure 13**). We further focused this analysis on poly(dA)/poly(dT) tracts of different lengths (**Figure 14**) and in promoter vs non-promoter regions (**Figure 15**), finding this observation to remain consistent.

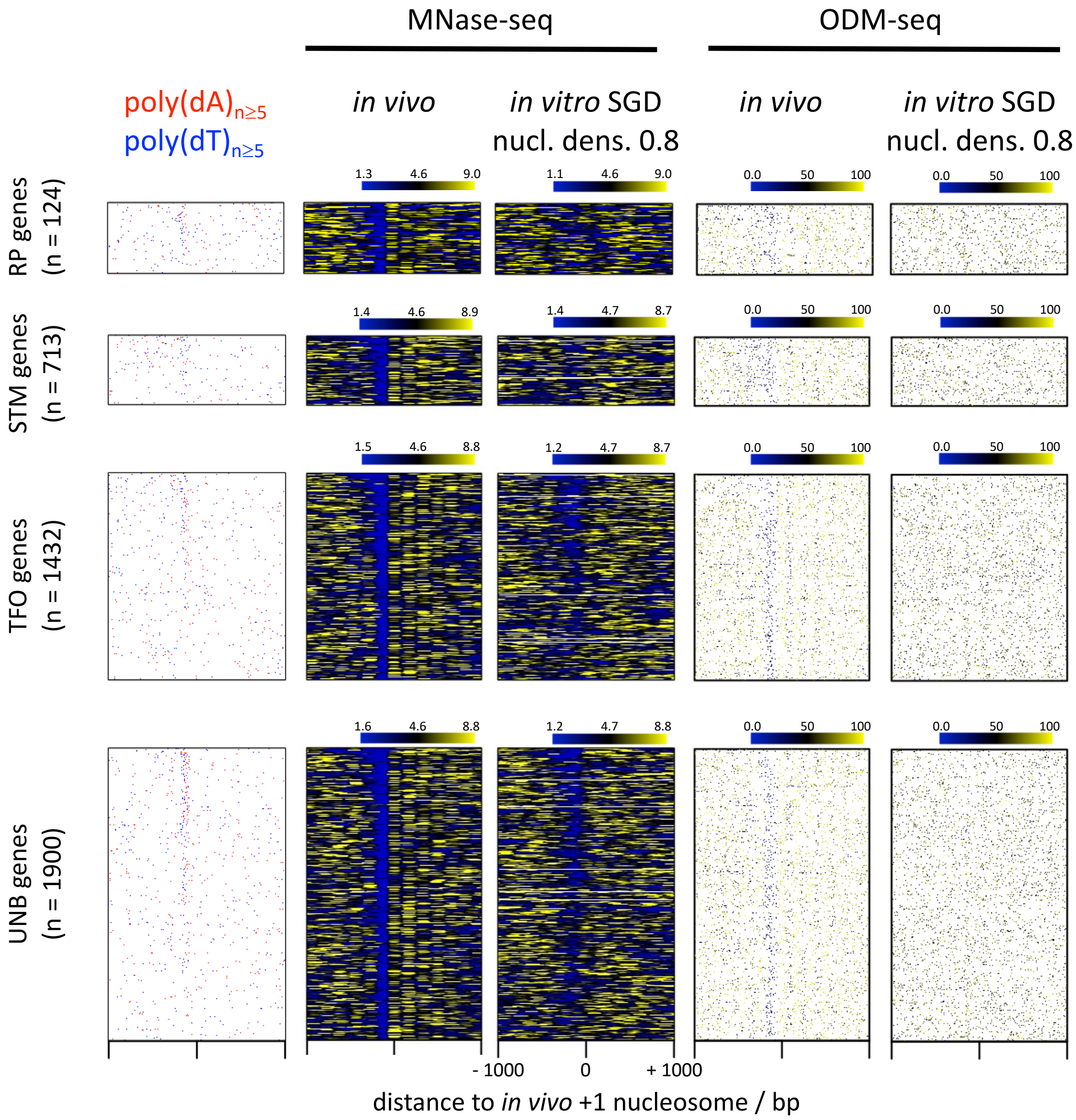

Figure 12 – Nucleosome depletion over poly(dA:dT) tracts in promoter regions is less pronounced *in vitro* than *in vivo*, especially if monitored without MNase

Correlation of poly(dA)/poly(dT) tract occurrence with low nucleosome occupancy in in vivo chromatin or in in vitro salt gradient dialysis (SGD) reconstituted chromatin monitored by MNase-seq or by DNA methylation footprinting (ODM-seq). Heatmaps of poly(dA)/poly(dT) tract occurrence on the coding strand (left panels), MNase-seq (middle 2 panels) and ODM-seq (right 2 panels) data of *in vivo* chromatin (BY4741 strain, *S. cerevisiae*) and SGD chromatin reconstituted at a ‘high’ density (‘0.8’, see Methods - 2.2.2). Panels are subdivided by specific promoter classifications (Rossi et al., 2021), namely the ribosomal protein (RP), SAGA/TUP/Mediator regulated (STM), transcription factor organised (TFO) and unbound except by preinitiation complex (UNB) groups. ODM-seq plots report absolute nucleosome occupancies, from 0 to 100%, whilst missing values (due to absence of CpG or GpC sites for the DNA methyltransferase) form a white background. Plots are aligned to *in vivo* +1 nucleosome positions, sorted by poly(dA)/poly(dT) tract density within the promoter, descending. Poly(dA)/poly(dT) tracts were called by calculating nucleotide frequency on the sense strand in a 5 bp window with 1 bp step size, then the central bp of each homopolymeric tract was coloured red (polyA) or blue (polyT). Ten, 14%, 18% and 14% of RP, STM, TFO and UNB gene promoters respectively have no poly(A)/poly(T) tracts in their promoter region. Genes were sorted by genomic coordinate, ascending from top to bottom. MNase samples from Oberbeckmann, Niebauer, et. al., (2021) - GSM4175394 (*in vivo*); GSM4175430 (*in vitro*). ODM-seq samples from Oberbeckmann, et. al., (2019) - GSE141051 (*in vivo*); GSM4193216 (*in vitro*). Figure and legends adapted from Barnes and Korber, (2021).

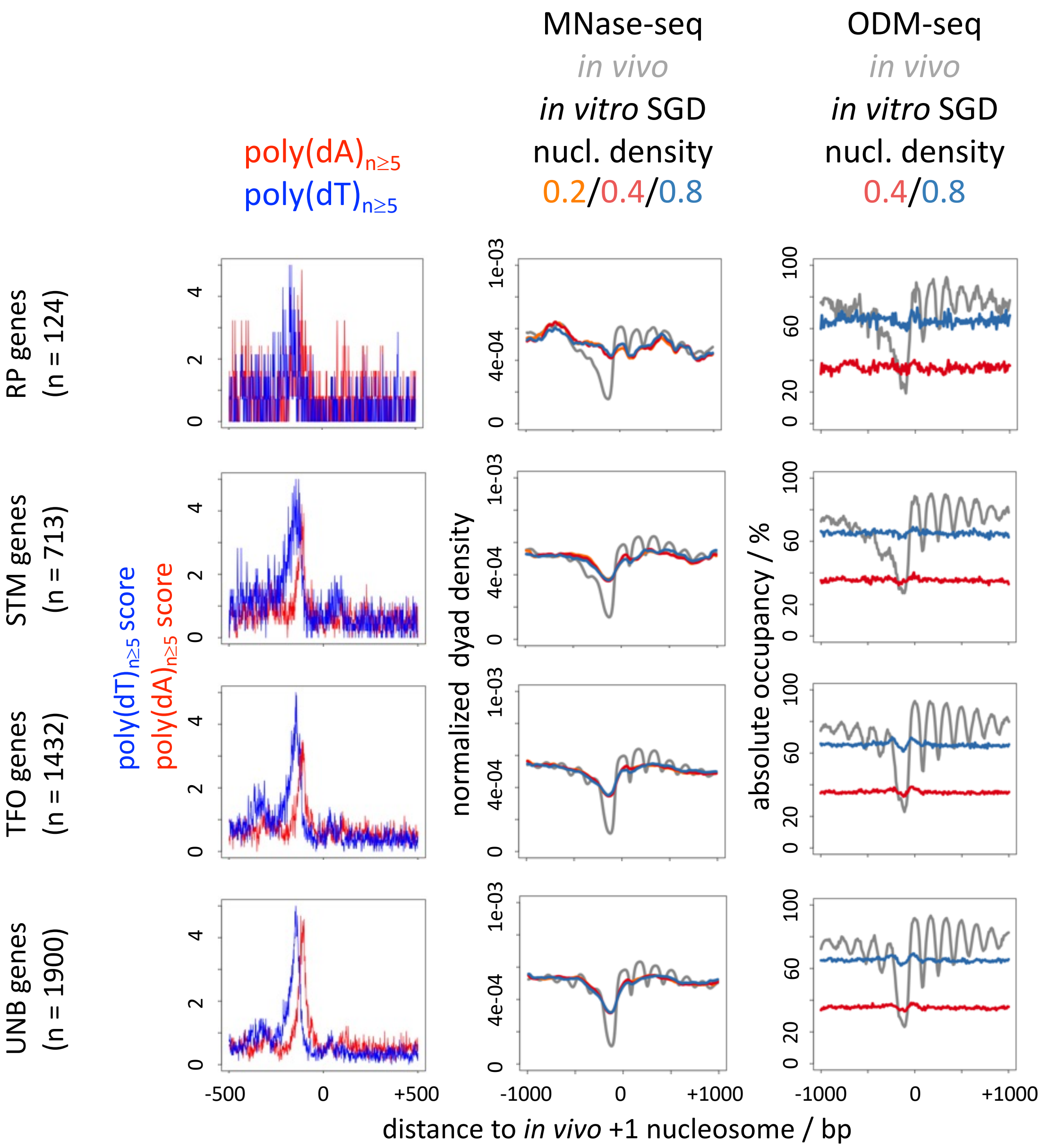

Figure 13 – Alternative visualisation of data shown in Figure 7, showing greater nucleosome depletion over promoter region poly(dA:dT) tracts *in vivo* vs *in vitro*

Composite plots of the same data and alignment points as Figure 7, with the addition of lower nucleosome density samples for MNase-seq (GSM4175428 – 0.2; GSM4175429 – 0.4) and ODM-seq (GSM4193222 – 0.4). Poly(dA)/poly(dT) tract score corresponds to the percentage of promoters in each group with the center of a 5 bp homopolymeric poly(dA)/poly(dT) tract at that respective position on the x-axis. This metric accurately represents the distribution of such tracts, but underrepresents the size of each tract, as the outermost 2 bp flanking each side are not scored. Figure and legends adapted from Barnes and Korber, (2021).

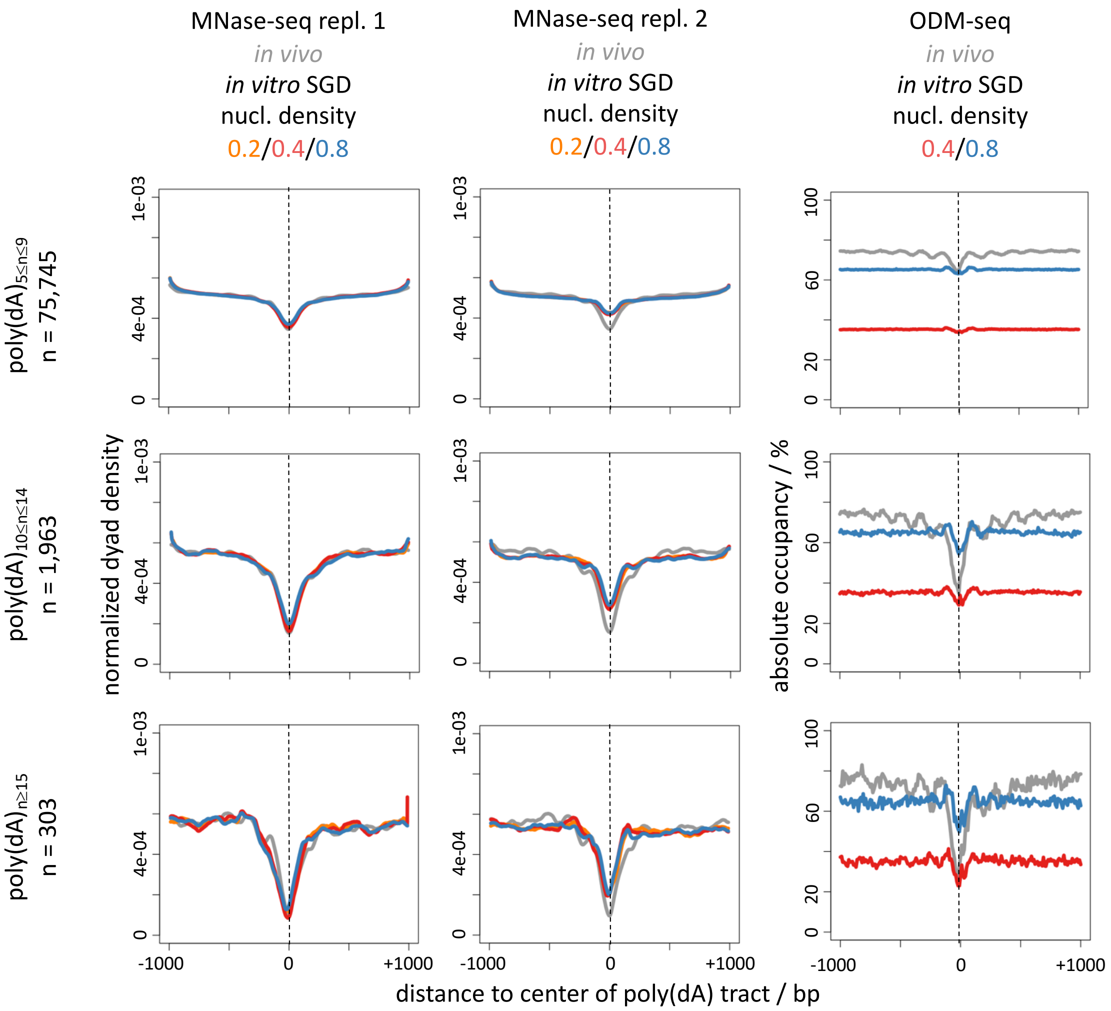

Figure 14 – Nucleosome depletion over poly(dA:dT) tracts scales with tract length and appeara similar *in vitro* vs *in vivo* with MNase-seq, but not with ODM-seq

Composite plots of the same data as in **Figure 13** (MNase-seq replicate 1 and ODM-seq), with the addition of another MNase-seq replicate (MNase-seq replicate 2 - GSM4175803 – 0.2; GSM4175804 – 0.4; GSM4175805 – 0.8). All plots were aligned to poly(dA) tracts on the *S. cerevisiae* genome and subdivided into tract length, with the tract number in each group (*n*) indicated. Strand orientation was accounted for by reversing coverage profiles for tracts on the opposite strand. Vertical dashed lines better indicate the alignment points. Figure and legends adapted from Barnes and Korber, (2021).

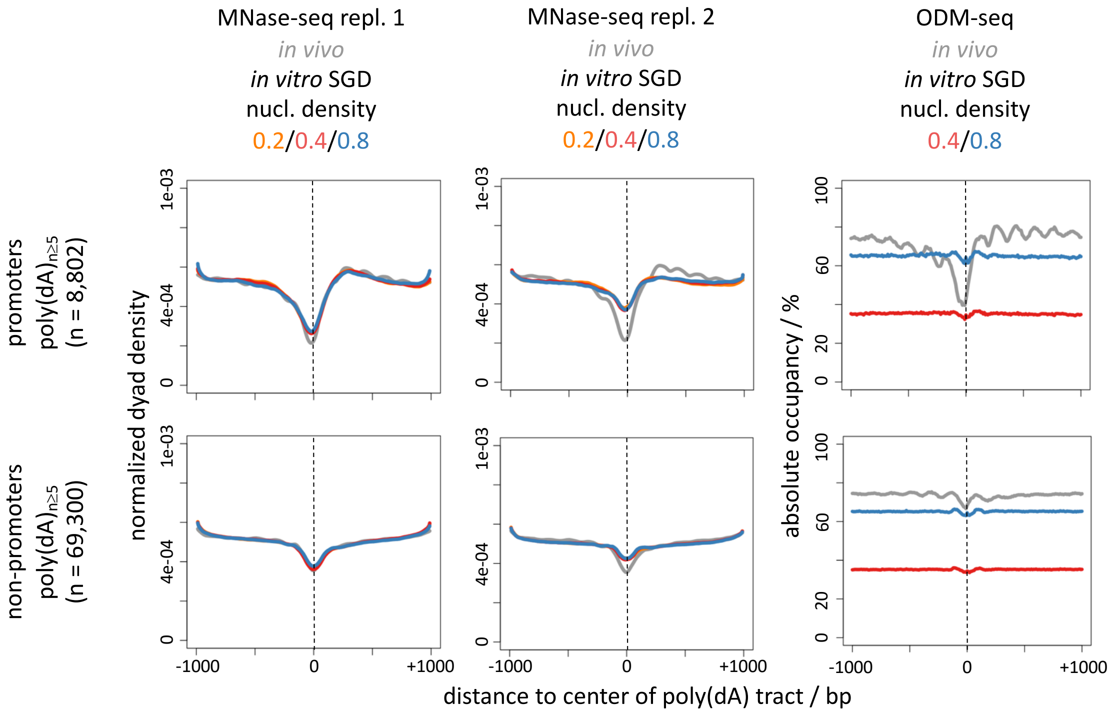

Figure 15 – Differential nucleosome depletion over poly(dA) tracts *in vivo* vs *in vitro* is more pronounced in promoter regions, vs non-promoter regions

Composite plots of data in **Figure 14**, subdivided by poly(dA) tracts within vs outside of promoter NFRs (Chereji et al., 2018). As before, number of instances (*n*) for each group is indicated, strand orientation of the tract is accounted for, and vertical dashed lines highlight the alignment points. Figure and legends adapted from Barnes and Korber, (2021).

In addition to the fact that nucleosome depletion over poly(dA:dT) tracts *in vivo* is more extensive than *in vitro* if monitored without MNase bias, the resultant NFRs are actively maintained *in vivo.* If NFRs were generated purely by the intrinsically exclusive properties of these tracts, they would likely exist without requiring maintenance. Instead, the conditional ablation of the remodeler RSC, and/or ablation of general regulatory factors (GRFs) such as Abf1, Reb1 and Rap1, fill the NFRs with nucleosomes (Badis et al., 2008; Challal et al., 2018; Ganguli et al., 2014; Hartley & Madhani, 2009; Klein-Brill et al., 2019; Kubik et al., 2019; Kubik et al., 2018; Parnell et al., 2008; Rawal et al., 2018; van Bakel et al., 2013). Thus, these factors actively maintain NFRs, which is likely the reason why these factors are essential.

Another argument for an active mechanism of nucleosome depletion at poly(dA:dT) tracts is the evolution of a strand-biased distribution of these tracts around NFR centers. We investigated the organisation of poly(dA)/poly(dT) tracts around NFR centers, in the four separate promoter classes defined by Rossi, et. al., (2021); RP (ribosomal protein genes), STM (SAGA/TUP/Mediator regulated), TFO (transcription factor organised) and UNB (unbound except by preinitiation complex). We found that many promoters have developed an arrangement of poly(dA)/poly(dT) tracts which strictly conforms to an active and directional depletion of nucleosomes by RSC, in the 5' direction of poly(dA) and 3' of poly(dT) (**Figure 16**), This organisation was particularly enriched in the UNB, then TFO groups, which were proposed to have adopted poly(dA:dT) tracts for use in NFR generation (Rossi et al., 2021).

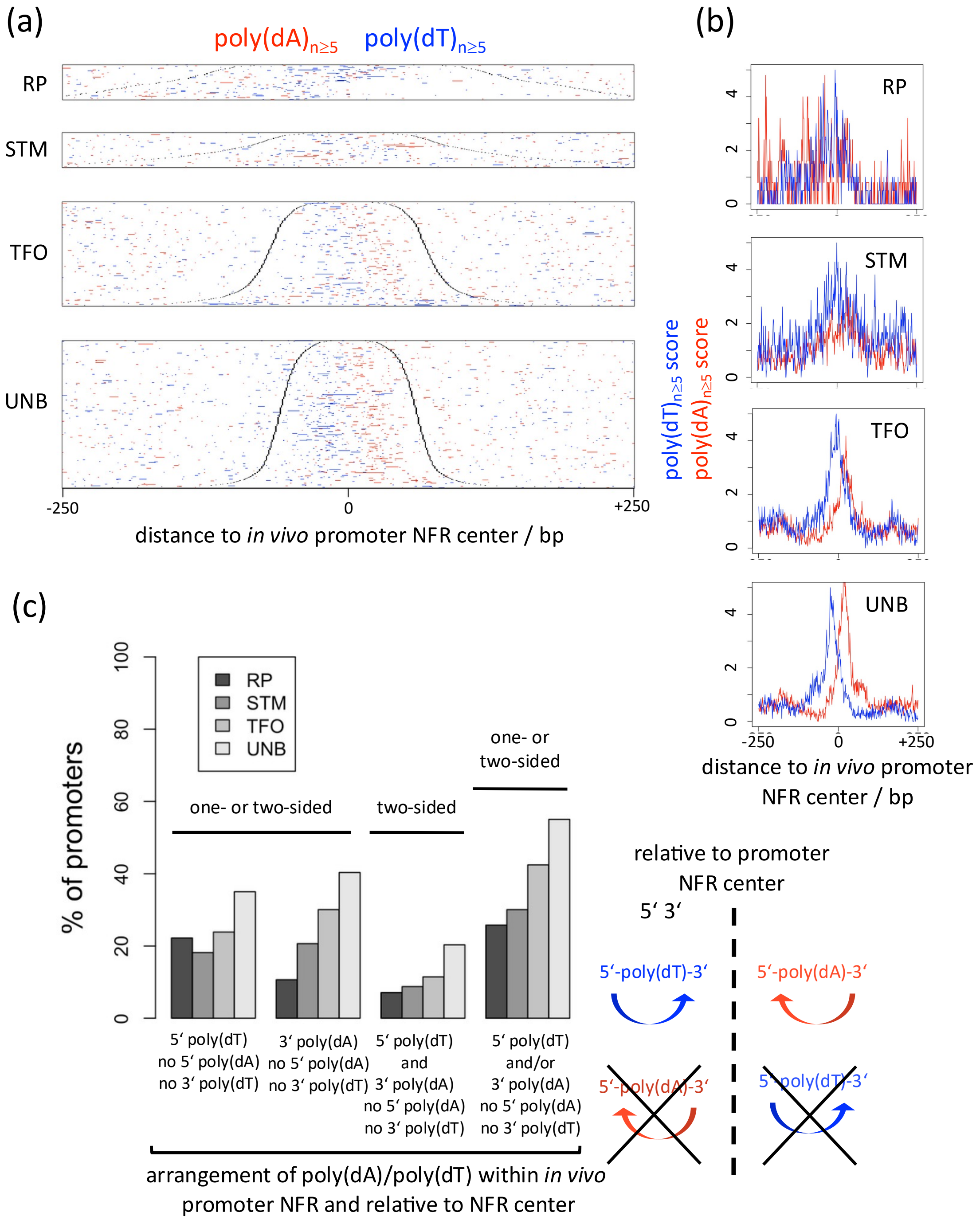

Figure 16 – *S. cerevisiae* promoters have developed a particular poly(dA)/poly(dT) tract distribution which argues for active and directional nucleosome depletion

(a) Heatmap (as in Figure 7, left panel) aligned to NFR centers and sorted by increasing NFR length. Black lines mark +1/-1 nucleosome borders. (b) Composite plots (as in Figure 8, left panel) aligned to NFR centers. (c, left) Barplot showing the percentage of promoters in each group, which contain at least one poly(dA) or poly(dT) tract and conform to the respective arrangement stated below on the x-axis, relative to the NFR center. (c, right) Schematic displaying the poly(dA)/poly(dT) tract arrangements around NFR centers (dashed lines) which conform or do not (crossed out) to the model of a RSC-mediated active and directional mechanism of nucleosome depletion at poly(dA)/poly(dT) tracts. Even just a one-sided arrangement would be sufficient to fit this model. Coloured arrows indicate directional nucleosome displacement by RSC relative to the respective tract. Figure and legends adapted from Barnes and Korber, (2021).

3.2.2 Nucleosome depletion by RSC at poly(dA:dT) tracts *in vitro*

The asymmetrical depletion of nucleosomes by RSC at poly(dA:dT) tracts was shown at a subset of promoters (Krietenstein et al., 2016). So our first question of RSC's action at such DNA elements was whether this was specific to *S. cerevisiae* promoters, or a more general mechanism. To this end, we reconstituted SGD-chromatin using an equimolar mixture of *S. cerevisiae, S. pombe* and *E. coli* genomic plasmid libraries and endogenous *D. melanogaster* embryo histone octamers, before incubation with or without the addition of purified RSC and subsequent MNase-seq analysis. Both ‘medium’ and ‘high’ assembly degrees were reconstituted (see Methods – 2.2.2), but only the results for ‘medium’ are shown here for simplicity and as effects for ‘high’ were equivalent but less pronounced in extent.

Alignment of sequencing reads to all poly(dA) tracts of at least 6 bp length (29,652) on the *S. cerevisiae* genome (**Figure 17**, left) showed the known depletion effect in SGD chromatin and revealed the much more pronounced and asymmetric depletion of nucleosomes 5’ of the tract by RSC. This is ~5x more poly(dA) tracts than found in promoter regions (5,598). Additionally, this asymmetric depletion is also observed at poly(dA) tracts on the *S. pombe* (39,437) and *E. coli* (4,951) genomes (**Figure 17**, middle and right). The *S. pombe* genome has not evolved to utilise such tracts at nucleosome depleted promoter regions *in vivo* and they are instead found enriched within nucleosomes, close to dyads (Lantermann et al., 2010; Moyle-Heyrman et al., 2013). The prokaryotic *E. coli* genome is of a lower AT-richness than the eukaryotic yeast genomes (49.2%, compared to 61.8% *S. cerevisiae* and 64% *S. pombe*), with generally shorter poly(dA) tracts which are more sparsely distributed, possibly accounting for the reduction in depletion effect, especially in SGD chromatin. Nevertheless, simply the presence of a poly(dA:dT) tract appears to be sufficient to stimulate asymmetric nucleosome depletion by RSC, regardless of genomic context.

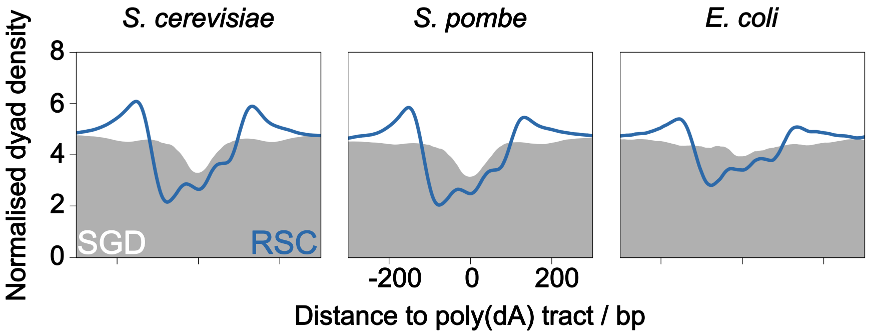

Figure 17 - RSC directionally depletes nucleosomes from poly(dA) tracts *in vitro.*

Composite plots of MNase-seq data generated from SGD chromatin reconstituted at medium (0.4) nucleosome density with an equimolar mixture of *S. cerevisiae, S. pombe* and *E. coli* genomic plasmid library DNA and without (grey background) or after (blue line) remodeling by RSC. MNase-seq reads were aligned as 50 bp extended dyads to the center of every poly(dA) tract in each genome of at least 6 bp in length (*S. cerevisiae* - 29,652; *S. pombe* - 39,437; *E. coli* - 4,951).

Window orientation is flipped for poly(dA) tracts on the minus strand. Plots show zoomed-in ± 250 bp window and a merge of triplicates (SGD - TBPool1_0.4, TBPool1_0.42, TBPool2_Univ9; RSC - TBPool1_1, TBPool1_18, TBPool2_Univ1). Normalisation was performed as in 2.2.8.

We further investigated the effect of poly(dA) tracts on remodeling by RSC by grouping them by tract length (6-10 bp, 11-15 bp and 16+ bp) and asking whether longer tracts exhibit more extensive nucleosome depletion in the presence of RSC. In fact, both conditions with and without RSC remodelling displayed greater depletion at longer tract lengths (**Figure 18**), as seen earlier (**Figure 14**).

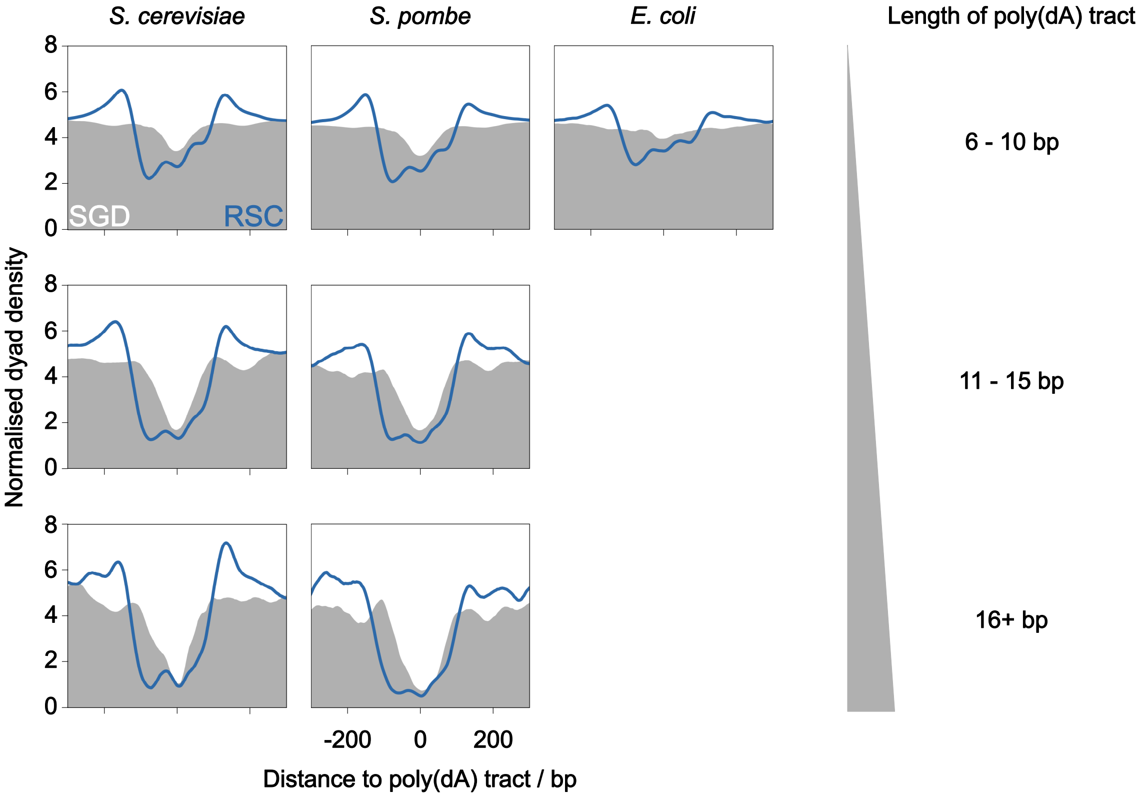

Figure 18 - Nucleosome depletion at poly(dA) tracts scales with tract length.

Composites plots as in **Figure 17**, subdivided by poly(dA) tract length. Number of poly(dA) tracts in each plot are as follows: *S. cerevisiae* – 28,051 x 6-10 bp, 1,298 x 11-15 bp, 303 x 16+ bp; *S. pombe* – 38,326 x 6-10 bp, 838 x 11-15 bp, 273 x 16+ bp; *E. coli* – 4,951 x 6-10 bp.

As a negative control, we probed RSC activity at poly(dG) tracts by aligning at every homopolymeric tract of at least 6 bp in length. In this case, RSC did not deplete nucleosomes and in fact slightly enriched nucleosome density at these sites (**Figure 19**), demonstrating RSC’s specificity for poly(dA) tracts and not just any homopolymeric tracts.

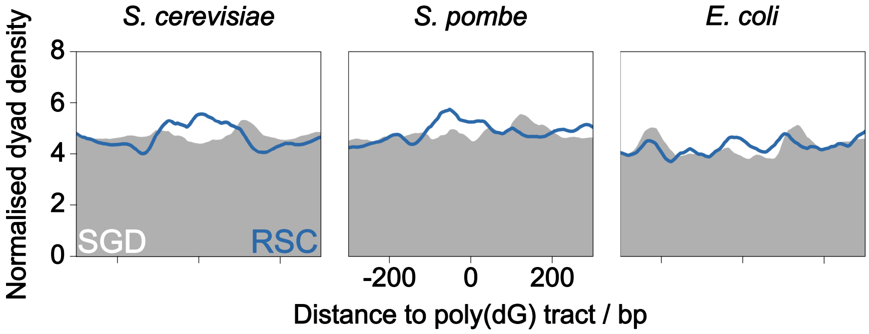

Figure 19 – RSC does not deplete nucleosomes from poly(dG) tracts *in vitro.*

Composite plots as in **Figure 17**, aligned to poly(dG) tracts of at least 6 bp length (*S. cerevisiae* - 846; *S. pombe* - 604; *E. coli* - 450).

We typically add remodelers to a final concentration of 10 nM when conducting *in vitro* remodelling reactions, but we had to test lower concentrations of RSC to ensure that we were analysing the steady state of the system at the usual 2-hour endpoint (see Methods – 2.2.5). To this end, we serially diluted RSC from 10 nM down to 0.37 nM in 3-fold steps, then performed remodelling and MNase-seq as usual with each RSC concentration, before aligning at all poly(dA) tracts (**Figure 20**, top) or poly(dA:dT) tracts grouped by length (**Figure 20**, bottom). For simplicity, only the 10 nM and 1.1 nM concentrations are shown. Even at 1.1 nM, the coverage trace is almost indistinguishable from the 10 nM condition, across all tract lengths. The trace for a RSC concentration of 0.37 nM displayed less developed NFRs over poly(dA) tracts, whilst for 3.3 nM it appeared similar to both traces for 1.1 nM and 10 nM (not shown). Hence, the system appears to reach steady state after 2 hours remodelling at a RSC concentration between 0.37 – 1.1 nM and our usual 10 nM concentration ensured steady state. Furthermore, there is no evidence of RSC preferentially remodelling any genome at the lower concentrations tested here, which could have been taken as indication for the presence of some RSC-recruiting sequence. It could be further explored with shorter remodelling times and even lower RSC concentrations if poly(dA:dT) tracts recruit vs stimulate RSC activity.

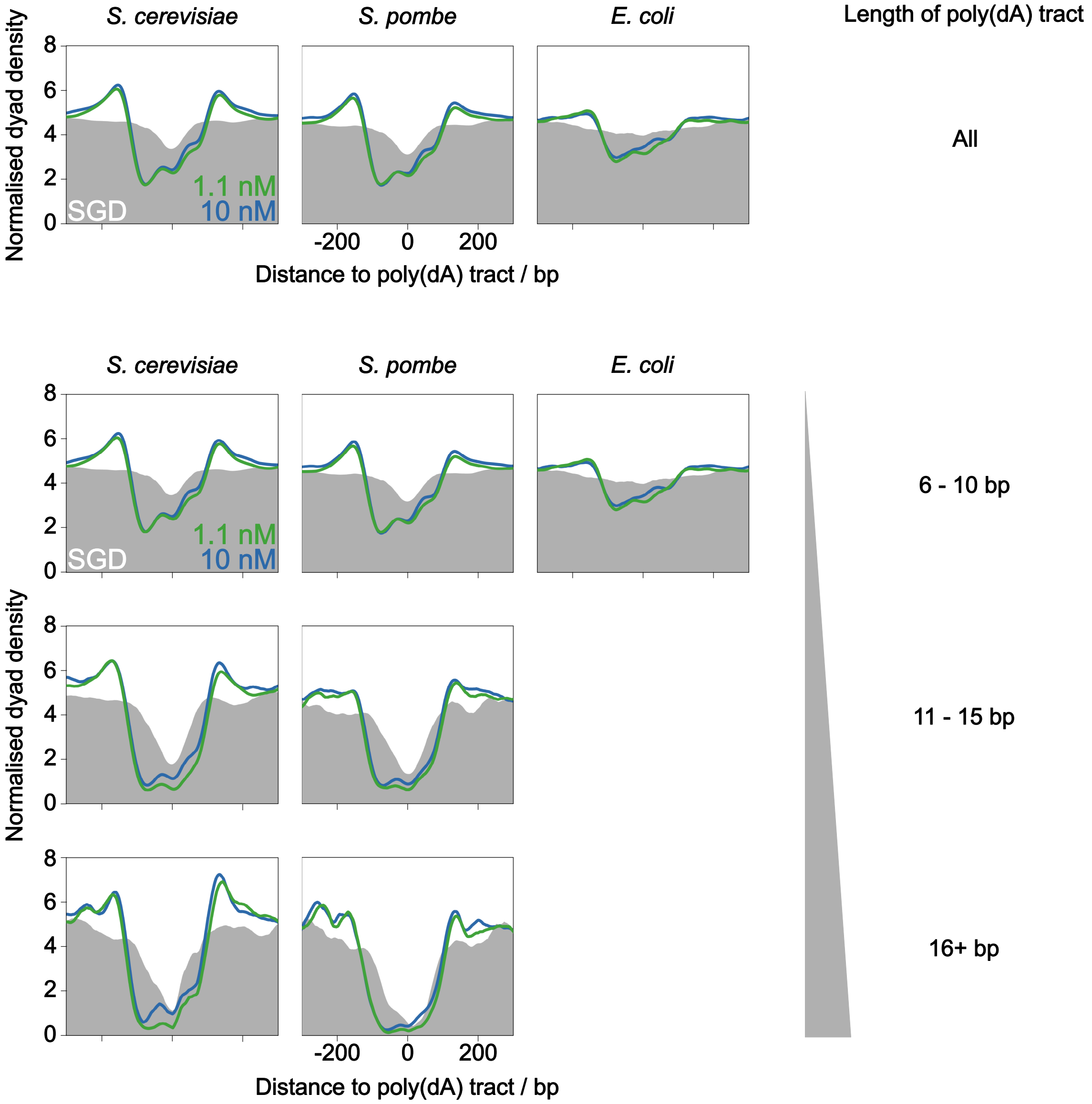

Figure 20 – Our usual RSC concentrations are sufficient to reach the system's steady state.

As **Figure 17** (top) and **Figure 18** (bottom), with the addition of MNase-seq data monitoring remodeling by a lower (1.1 nM) concentration of RSC (green). Single replicates shown (SGD - TBPool2_i5031; RSC (10 nM) - TBPool2_i5033; RSC (1.1 nM) - TBPool2_i5036). Related but not shown – RSC (3.3 nM) – TBPool2_i5034; RSC (0.37 nM) – TBPool2_i5037.

3.2.3 Remodeler-specific NDSs

At this point, the depletion of nucleosomes by RSC at poly(dA:dT) tracts is well established, despite the details still requiring further investigation. However, by strictly focusing on well-defined, contiguous homopolymeric poly(dA:dT) tracts of at least 6 bp length, we could potentially miss more complex or degenerate nucleosome depleting sequences. Unfortunately, this approach where we select genomic locations of potential interest and look at the surrounding nucleosome landscape via MNase-seq patterns, is only possible when we know where in the genome to look. To search for novel determinants of nucleosome depletion, we used a different approach, defining nucleosome free regions (NFRs) in the MNase-seq data and querying the underlying sequences for commonality. ‘Classic’ motif searches, using the MEME suite, on NFRs defined in SGD and RSC samples only yielded long, degenerate AT-rich sequences, whilst ‘discriminative’ and ‘differential enrichment’ searches, using the SGD dataset as a background for probing motifs enriched in the RSC dataset, yielded similar results, i.e., AT-rich DNA was enriched in NFRs generated by RSC, compared to SGD only (Bailey & Elkan, 1994; Bailey et al., 2015; Narlikar et al., 2007).

Next, we adapted the workflow used to analyse NPS shape profiles and asked if remodelers display any preferences for specific DNA shape/mechanics at sequences they deplete of nucleosomes (**Figure 21**). The first adaptation required was to limit the search for nucleosome depletion sequences (NDSs) to genomic regions of generally high coverage (2.2.10.1). This was necessary because NDSs were defined as regions between 100 – 350 bp long where every base-pair had a coverage lower than the mean of that chromosome. In poorly covered regions, e.g., genes with a low copy number in the plasmid library, the signal to noise ratio was lower, generating many more artefactual NDS calls. Additionally, most samples used in this study were sequenced to a total of ~5 million reads each, which is generally sufficient for looking at well-defined nucleosome positions but proved problematic for looking at depleted regions for the same reason as above. Another issue we faced was the heterogeneity in NDS size. Whilst we treated nucleosomes as covering a standardised 147 bp of DNA, our NDS pool spanned 100 – 350 bp. This needed to be reflected in the analysis, as the widening of NFRs is a key function of RSC, so we could not reduce NDSs down to well-defined centers, as with nucleosome dyads. As a result, we could not manually filter sequences for reproducible NDSs, or those unique to an experimental condition, instead we were forced to work either directly with the called NDSs or use the PCA workflow to separate groups. DNA shape analysis of NDSs without further processing (corresponding to the “Denoised” workflow for NPSs in **Figure 7**) generated non-descript shape profiles, indistinguishable between experimental condition, but the PCA workflow was able to separate groups of remodeler NDSs away from the SGD controls (**Figure 22**).

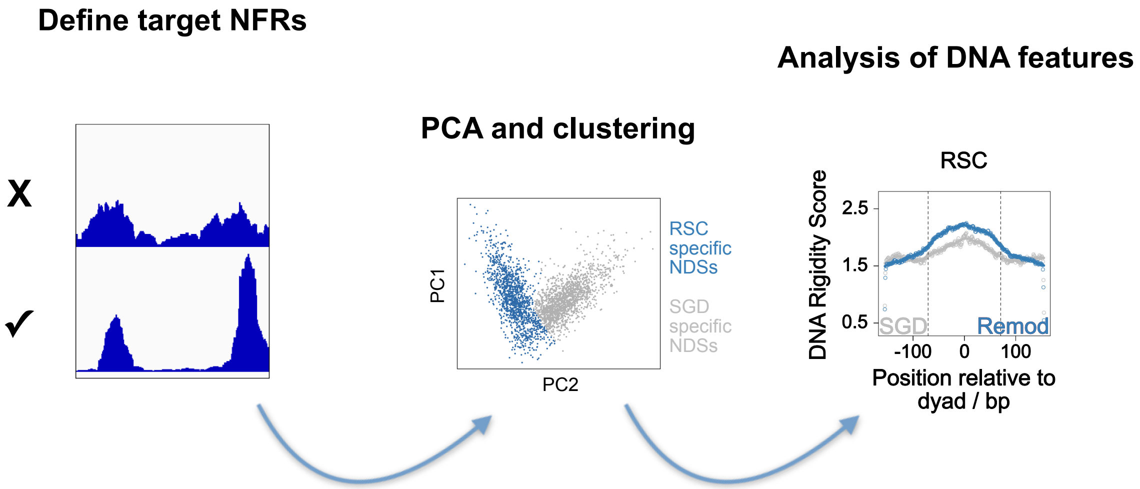

Figure 21 – Overview of bioinformatic workflow used to generate NDSs

Brief overview of the workflow used to define and analyse nucleosome depletion sequences (NDSs). Nucleosome free regions (NFRs) were detected in generally high coverage regions of the genome for each sample, from MNase-seq data. NDSs were separated into condition-specific groups by PCA and clustering, before DNA shape/mechanic analysis, as with NPSs. See accompanying text and Methods - Nucleosome depleting sequences (NDS) analysis for details.

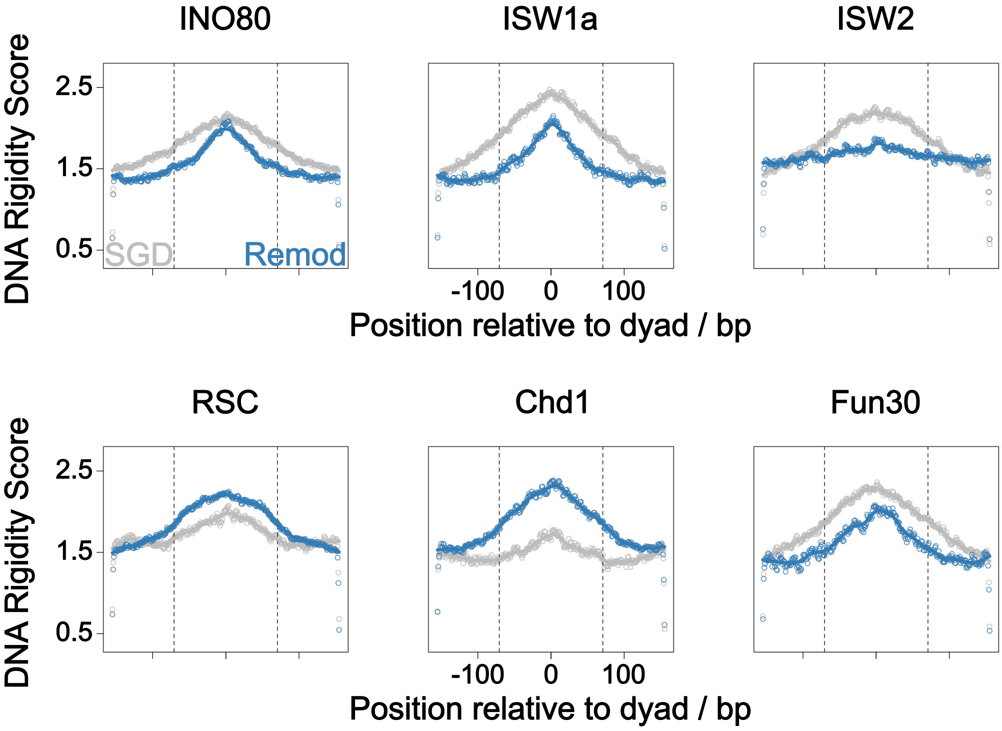

Figure 22 - Chromatin remodelers differentially process DNA sequence information into nucleosome depletion.

Rigidity score profiles of DNA sequences depleted of nucleosomes in SGD chromatin (grey) and remodelled SGD chromatin (blue). See **Figure 21** and Methods - Nucleosome depleting sequences (NDS) analysis for details on determining these sequences. Vertical dashed lines indicate the position of theoretical nucleosome borders at +/-73bp from the dyad. Number of sequences plotted in each panel: INO80 – 10,968 x SGD, 11,716 x INO80; ISW1a – 6,832 x SGD, 2,882 x ISW1a; ISW2 – 5,244 x SGD, 5,861 x ISW2; RSC – 6,649 x SGD, 13,974 x RSC; Chd1 – 3,125 x SGD, 8,618 x Chd1; Fun30 – 7,635 x SGD, 3,212 x Fun30. Samples used: INO80 panel – SGD (GSM4175544, GSM4175545, GSM4175599, GSM4175600, GSM4175670, GSM4175671), INO80 (GSM4175541, GSM4175542, GSM4175593, GSM4175594, GSM4175661, GSM4175662); RSC panel – SGD (TBPool1_04, TBPool1_042, TBPool2_Univ9), RSC (TBPool1_1, TBPool1_18, TBPool2_Univ1); ISW1a panel – SGD (GSM4175670, GSM4175671), ISW1a (GSM4175664, GSM4175665); ISW2 panel – SGD (GSM4175670, GSM4175671), ISW2 (GSM4175667, GSM4175668); Fun30 panel – SGD (GSM4175671, GSM4175672), Fun30 (GSM4175659, GSM4175660); Chd1 panel – SGD (GSM4175544, GSM4175545), Chd1 (GSM4175538, GSM4175539). All samples listed can be found at GEO accession GSE140614 or in **Table 5**.

Whilst the resulting rigidity score profiles of NDSs were less detailed than those arising from NPSs, we could still make some observations regarding remodeler-specific differences. For instance, most remodelers showed a propensity to deplete nucleosomes from rigid DNA, but only RSC and Chd1 displayed a greater preference for this than the SGD procedure (**Figure 22**, RSC and Chd1 panels). This result was expected for RSC, due to its' established use of rigid poly(dA:dT) tracts for stimulating nucleosome depletion, as outlined above (3.2.2), but it was more surprising to see for Chd1, as it's not documented to utilise poly(dA:dT) tracts for nucleosome displacement. However, this does concur with Chd1's apparent tendency to position nucleosomes over flexible DNA (**Figure 11**) and together with previous findings (Winger & Bowman, 2017) may represent a mechanism by which Chd1 disfavours translocating rigid DNA toward the dyad of a bound nucleosome. ISW2 appeared to be least discriminative toward DNA rigidity, a trend consistent with its' NPS rigidity profile, although it's unclear whether this reflects a true lack of DNA sequence preference, or a smaller window of effect than with other remodelers which is smoothed out with imperfect alignment of NPS/NDS composites.

3.3 Where has the *S. cerevisiae* genome evolved remodeler-specific nucleosome positioning sequences?

A logical step after defining sets of remodeler-specific NPSs and NDSs was to ask if evidence exists for their use *in vivo*. However, whilst working with NDSs, we realised that the lower resolution they provide (see 3.2.3 - Remodeler-specific NDSs for details) proved to be problematic for downstream applications. Without further optimisation to the NDS workflow, we opted to just work with NPSs from this point onwards.

Initially, we asked if remodeler NPSs overlap with *in vivo* dyad positions. At the same time, we asked if any pair of remodelers showed greater commonality in nucleosome positioning preference. We first approached this by calculating a Jaccard similarity coefficient for each pairwise comparison of remodeler NPS groups, plus *in vivo* dyad positions (Oberbeckmann et al., 2019). This entails calculating the base-pair intersect of two groups in a pairwise comparison (i.e., the base pairs common to both groups of NPSs) and dividing the total by the base-pair union of the two groups (i.e., the total of distinct base pairs covered by both NPS groups). This provides a number between 0 – 1, with a higher number indicating a greater similarity between the two groups. However, resulting values were quite low, with a max coefficient of 0.13. In order to increase the spread of the data to better highlight trends, we modified the similarity index to instead calculate the number of overlapping dyad positions (given that all dyads were extended to 20 bp), divided by the total number of dyads in the comparison, whilst only counting overlapped locations once. The results (**Figure 23**) indicated the largest similarities in nucleosome positioning preference between ISW1a and Fun30, INO80 and Chd1, whilst RSC displayed the lowest similarity with the rest of the remodelers.

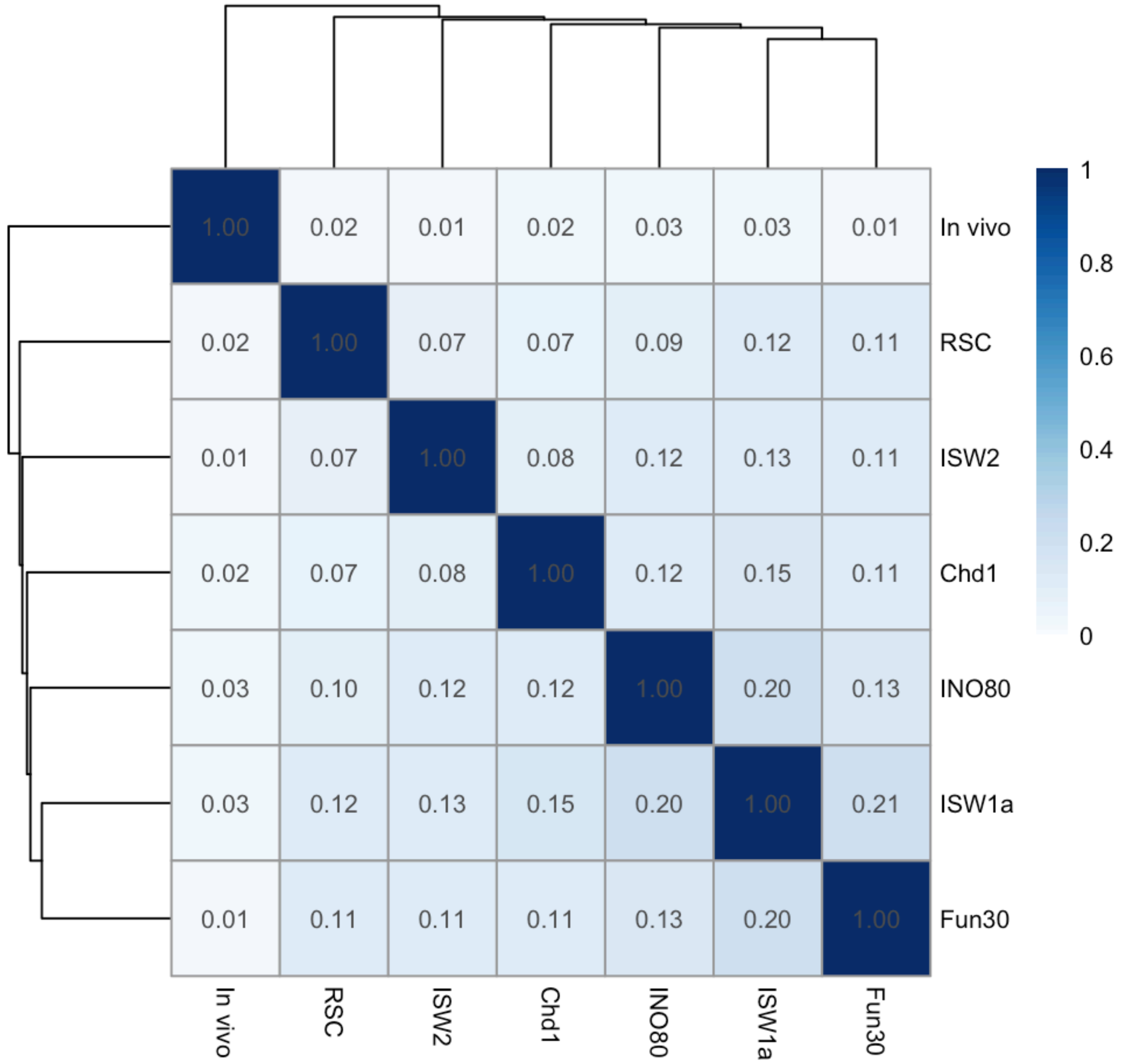

Figure 23 – Pairwise comparisons of remodeler-specific NPS and *in vivo* dyad overlaps

Heatmap showing pairwise comparisons of dyad position overlaps between each group. Dyad positions were resized to 20 bp, so an overlap constitutes dyad positions within 20 bp of each other. Numbers are reported as the ratio of overlapping NPSs divided by the size of the union between the two compared groups (i.e., overlap/total). The size of each remodeler group can be found in **Table 2**, except for the *in vivo* group (67,935).

This calculation was largely influenced by the non-overlapping fraction of dyad positions in the union between two groups, particularly when comparing a remodeler with the large number of *in vivo* dyad positions (67,935). Many of these nucleosomes are present in intragenic arrays where positioning is influenced by a remodeler 'ruler' mechanism (Oberbeckmann, Niebauer, et al., 2021) and NPSs are likely less important. Instead, we took the well-defined *in vivo* dyad positions and asked how many NPSs from each remodeler closely overlapped with these locations, to determine if any remodeler defined the *in vivo* nucleosome positions better than others. All dyad positions were extended to 20 bp, hence an overlap constitutes a nucleosome from each NPS group with *in vivo* dyad positions <20 bp apart from each other. We found similar overlap percentages of around 30% with INO80 (36.4%), ISW1a (33.5%) and Chd1 (32.8%) a bit on the higher and ISW2 (28.5%) and RSC (29.9%) on the lower side (**Table 2**).

Table 2 – Overlap of remodeler-specific NPSs with *in vivo* dyad positions. NPSs as in Figure 8, but overlapping dyads from different replicates only counted once.

Remodeler	# NPSs	# NPSs overlapping *in vivo* positions	% NPSs overlapping *in vivo* positions
INO80	6,327	2,304	36.4
RSC	4,325	1,293	29.9
ISW1a	5,701	1,910	33.5
ISW2	3,612	1,029	28.5
Fun30	3,442	1,053	30.6
Chd1	5,223	1,715	32.8

We then returned to the four promoter classes laid out by Rossi, et. al., (2021), to ask if NPSs were more prevalent at a particular promoter class, which could suggest a more dominant role for their use. We also included the distinction between uni- and bidirectional promoters for the same reason. We found that +1 nucleosome positions at RP gene promoters less frequently overlapped with remodeler NPSs than those in the other Rossi promoter classes (**Figure 24** & **Table 3**), but there was no indication of a bias toward NPS use between the other Rossi promoters (11.3% RP vs 18.6% STM, 17.7% TFO and 17% UNB). NPSs may occur and be used slightly more at bidirectional vs unidirectional promoters (19% vs 15.2%). Interestingly, the overlap between *in vivo* +1 positions and INO80 NPSs accounted for the majority of remodeler NPS overlaps for every promoter class, suggesting that INO80's DNA sequence preference for nucleosome positioning is dominant over other remodeler's preferences at +1 positions *in vivo* (**Table 3**).

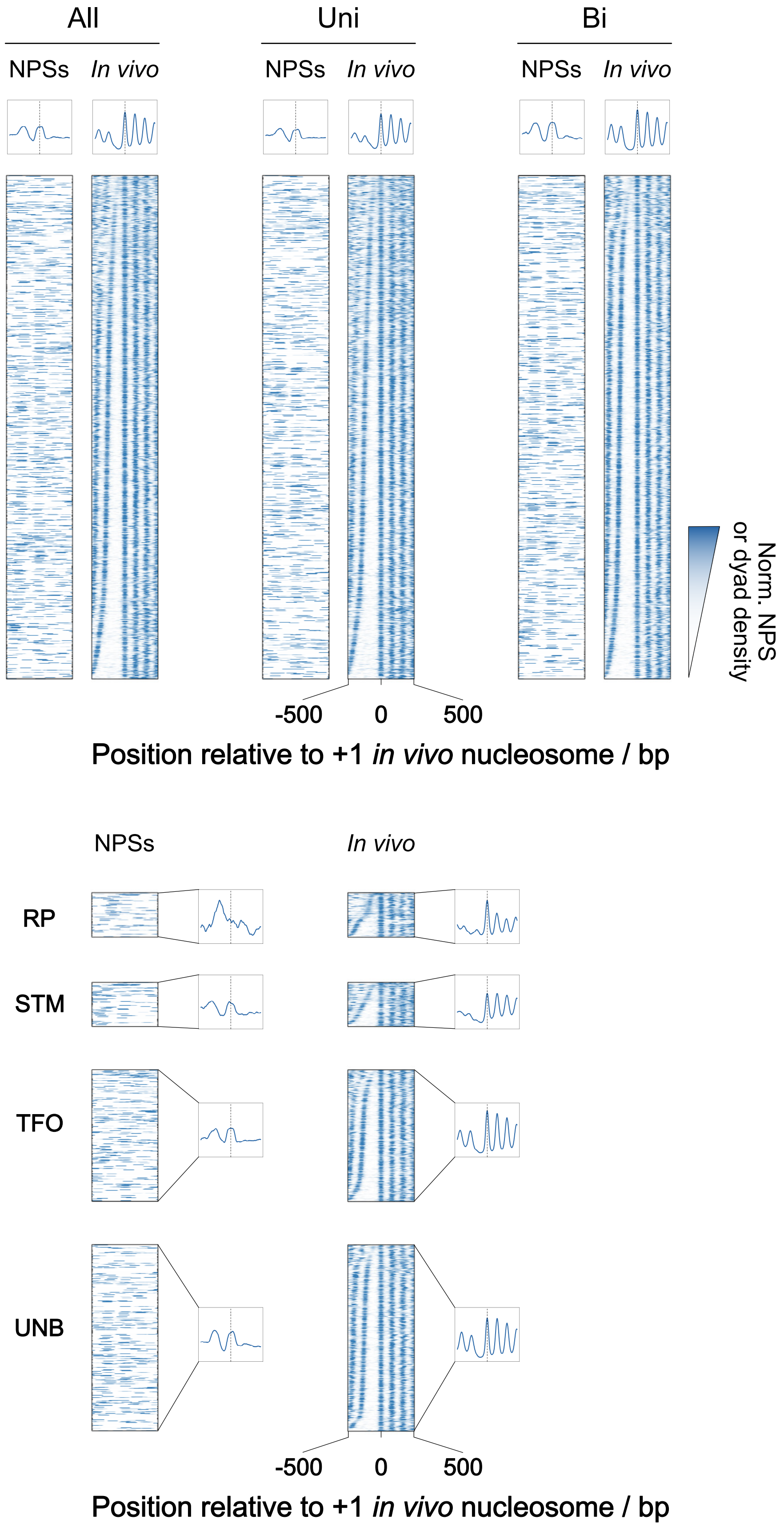

Figure 24 – NPS distributions and *in vivo* MNase-seq coverage at different promoter classes

Heatmaps and composite plots of all remodeler NPSs and *in vivo* MNase-seq coverage data (GSM4175394) aligned to +1 *in vivo* dyad positions. Promoters were further subcategorised by all promoters (4,818), unidirectional (2,905), bidirectional (1,913) or the Rossi et. al., (2021) subcategories of RP (105), STM (650), TFO (1,382) or UNB (1,831). Heatmaps were sorted from top to bottom by ascending NFR width.

Table 3 – Percentage of +1 *in vivo* nucleosome dyads at each promoter class within 20 bp of an NPS dyad for each remodeler

	INO80	**RSC**	**ISW1a**	**ISW2**	**Fun30**	**Chd1**	**All**
RP	7.5	3.8	1.9	0	0.9	0.9	11.3
STM	9.8	4.1	5.1	5.4	4.1	5	18.6
TFO	11.4	4.2	5.6	3.9	2.9	3.6	17.7
UNB	11.3	3	5	3.2	1.9	4.4	17
Uni	8.1	2.9	4.9	3.4	2.2	3.6	15.2
Bi	13.3	4.4	5.2	4.2	2.9	4.5	19
All	10.2	3.5	5	3.7	2.5	4	16.7

One unexpected outcome of this analysis was the high number of *in vivo* +1 nucleosome positions with no remodeler NPS nearby (**Figure 24** & **Table 3**). We did not necessarily expect NPSs to precisely define the majority of +1 positions, especially considering the use of GRFs to fine-tune nucleosome positioning *in vivo,* but the >80% of all promoters with no NPS present at the +1 position was a surprise, because a significant amount of promoters don't use GRFs for nucleosome organisation (see Rossi UNB class, or **Figure 28** promoters with GRF sites). We looked at the *in vivo* coverage at the same promoter subcategories and confirmed that the majority of +1 nucleosome positions were enriched at each class (**Figure 24**). However, the peak calling we used to detect NPSs *in vitro* relies on identifying regions above a coverage threshold. This threshold is somewhat arbitrarily set (at 99%), although kept constant in this study. Peaks are called one chromosome at a time, meaning this threshold accounts for differences in coverage between chromosomes. However, the DNA substrate we use in our reconstitution system is plasmid based, with heterogeneity in gene copy number and plasmid sequencing, meaning large absolute coverage differences occur on the scale of each ~10 kb plasmid insert, rather than per chromosome. As a result, +1 nucleosome peaks may readily fall below the threshold for detection if the local coverage was low enough. However, this is a necessary sacrifice, as lowering the threshold dramatically increases the number of peaks called, giving false positives from high coverage regions and reducing specificity of NPSs, which is essential for revealing the DNA shape/mechanic profiles. For example, peak detection on chrI of the *in vivo* sample with a threshold of 99% generates 73 peaks, whilst a threshold of 90% yields 448 peaks.

Collectively, our attempts to quantify the extent of correlation between remodeler-specific NPSs and *in vivo* dyad positions can only yield relative trends but is not conclusive so far in absolute terms and will required further development of the bioinformatics approach.

3.4 The indirect role of DNA sequence on nucleosome organisation

3.4.1 RSC cooperation with GRFs *in vitro*

It has previously been shown that chromatin remodelers may cooperate with a small class of sequence-specific DNA binding proteins known as general regulatory factors (GRFs) in affecting local nucleosome organisation (Hartley & Madhani, 2009; Krietenstein et al., 2016; Kubik et al., 2018; Oberbeckmann, Krietenstein, et al., 2021; Oberbeckmann, Niebauer, et al., 2021). Specifically, Oberbeckmann, Niebauer, et al. (2021) investigated the cooperation between the remodelers INO80, ISW1a, ISW2 and Chd1, and the GRF Reb1, finding that they were all capable of generating regular and phased arrays relative to bound Reb1 sites. However, the interaction/cooperation between RSC and GRFs is more poorly understood. It is unclear whether GRFs recruit RSC to promoters or bind to available DNA after RSC has depleted the region from nucleosomes or if RSC displaces GRFs from DNA, at least in some cases, as remodelers of the SWI/SNF-family, to which RSC belongs, were shown to displace transcription factors from their sites (Li et al., 2015). Additionally, the combination of GRF binding and poly(dA:dT) tract stimulation on RSC has yet to be explored. For instance, how does GRF binding in the vicinity of a poly(dA:dT) tract influence the asymmetrical nucleosome depletion observed by RSC? Do GRFs themselves modulate RSC activity and do they also confer directionality? Kubik et al. (2018) investigated the relationship between RSC, GRFs and stimulatory sequence organisation at promoters *in vivo*, but the complexity of the *in vivo* environment limited the potential for mechanistic insight, e.g., due to redundancy of remodeler action, and effects of other processes like transcription.

In order to address these questions in a biochemically more defined way with our *in vitro* system, we added to SGD-chromatin different combinations of RSC and the GRFs Abf1, Rap1 and Reb1, or the transcription factor (TF) Pho4, and monitored resulting nucleosome organization by MNase-seq as before. We then aligned reads at the binding site of each respective GRF/TF as determined by the best available position weight matrix (PWM; ScerTF (Spivak & Stormo, 2012); Abf1 (MacIsaac et al., 2006); Rap1 and Pho4 (Morozov & Siggia, 2007); Reb1 (Badis et al., 2008)). We only looked at unique binding sites without another of the same type within 300 bp. These sites were then further subdivided by the presence or absence of a poly(dA:dT) tract of at least 6 bp length within 50 bp.

This analysis revealed that adding a GRF to a sample containing RSC led to the formation of wider and deeper NFRs around the respective GRF binding site than accomplished by RSC alone, in all cases (**Figure 25**), This relative enhancement was even more pronounced for GRF sites without flanking poly(dA:dT) tracts (**Figure 25**, lower panels) as RSC alone had hardly an effect in terms of NFR generation at these locations (**Figure 26**, grey (SGD) vs **Figure 25**, grey (SGD + RSC)). This shows that GRF binding by itself is sufficient to guide NFR formation by RSC activity. However, we saw no evidence that GRFs imparted directionality on the depletion of nucleosomes in the same way that poly(dA:dT) tracts do. Despite also being a DNA sequence specific binding factor, Pho4 was not sufficient to stimulate RSC-dependent nucleosome depletion in its vicinity, but rather led to nucleosomes being stacked close to rather than moved away from the Pho4 binding site, as with the GRFs. This is consistent with reports that Pho4 has a much weaker impact on nucleosome positioning by remodelers than Reb1 (Ghassabi Kondalaji & Bowman, 2022).

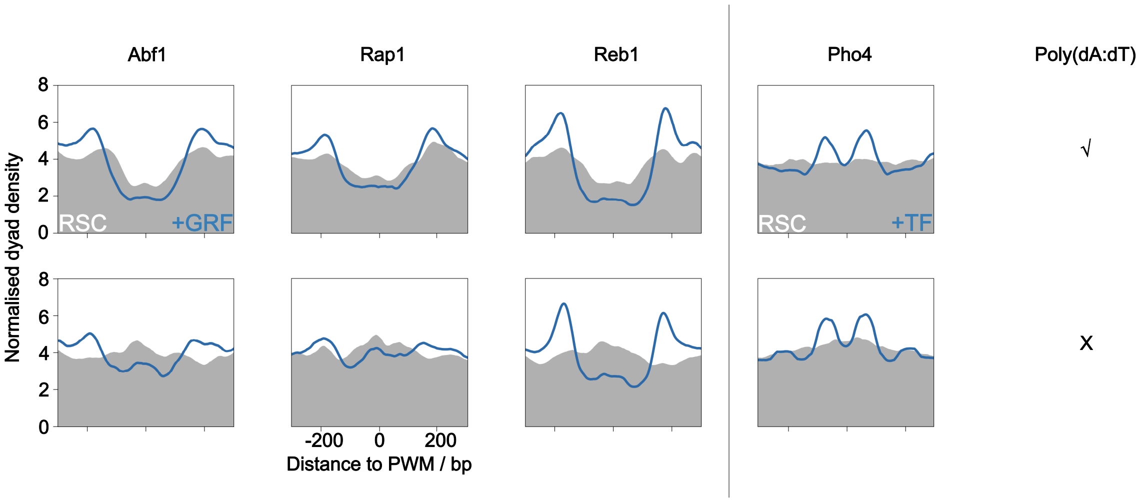

Figure 25 - GRFs alone guide NDR formation by RSC but do not in a directional way.

Composites plots of MNase-seq data generated from RSC-remodelled SGD chromatin, with or without the addition of a GRF/general regulatory factor (Abf1, Rap1, Reb1, left of vertical line) or a TF/transcription factor (Pho4, right of vertical line). Plots were generated as in **Figure 17**, but aligned to the center of each binding factor's PWM and further subdivided by the presence (top) or absence (bottom) of at least one poly(dA:dT) tract > 5 bp in length within ± 50bp of the alignment center. The number of sites plotted in each panel are as follows: Abf1 plus poly(dA:dT) – 473, minus poly(dA:dT) – 429; Rap1 plus poly(dA:dT) – 309, minus poly(dA:dT) - 410; Reb1 plus poly(dA:dT) – 449, minus poly(dA:dT) - 324; Pho4 plus poly(dA:dT) – 169, minus poly(dA:dT) – 301. Abf1 and Reb1 plots are a merge of triplicates, Rap1 is merged duplicates and Pho4 plots use a single replicate. Samples used in the +GRF panels (left) are as follows: RSC – as in **Figure 17**, with TBPool2_Univ1 omitted for Rap1 comparison; RSC + Abf1 – TBPool_5, TBPool_22, TBPool2_Univ6; RSC + Rap1 – TBPool1_6, TBPool1_23; RSC + Reb1 – TBPool1_7, TBPool_24, TBPool2_Univ7. Samples used in the Pho4 comparison (right) are as follows: RSC - RSC_2_SE; RSC + Pho4 - RSCPho4_2_SE.

In order to verify that the effects on nucleosome depletion seen in **Figure 25** were the result of RSC's action in the presence of the GRF, rather than of the GRF binding itself and/or any impact this may have had on MNase digestion, we also generated samples with GRFs in the absence of RSC remodelling and repeated this analysis. As seen in **Figure 26**, the addition of either a GRF or Pho4 in the absence of ATP-dependent chromatin remodelling had negligible effect on the chromatin landscape, i.e., neither GRFs nor Pho4 were sufficient to cause nucleosome depletion at their binding sites *in vitro*. While this negative control is important to have, its outcome is quite expected as nucleosomes are mostly unable to move under our experimental conditions without the help of ATP-dependent remodelers (Drew, 1991; Korolev et al., 2007; Shrader & Crothers, 1989; Thastrom et al., 2004).

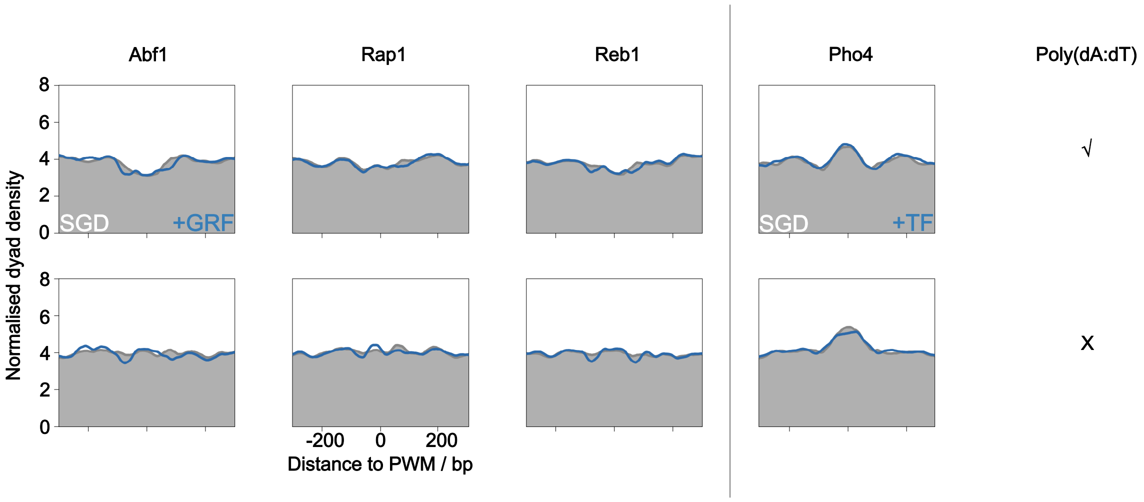

Figure 26 - GRFs alone do not cause nucleosome depletion at GRF PWMs.

Composite plots as in **Figure 25**, but all samples are without the addition of RSC. Samples used in the +GRF panels (left of vertical line) are as follows: SGD – as in **Figure 17**, with TBPool2_Univ9 omitted for Rap1 comparison; SGD + Abf1 – TBPool1_2, TBPool1_17, TBPool2_Univ1; SGD + Rap1 – TBPool1_3, TBPool1_19; SGD + Reb1 – TBPool1_4, TBPool1_20, TBPool2_Univ4. Samples used in the Pho4 comparison (right of vertical line) are as follows: SGD - SGD_1, SGD_2; SGD + Pho4 - SWISNFPho4_2 (note: SWISNF was added to this sample, but later confirmed to be inactive, so interpreted as an SGD + Pho4 sample).

During our study, Kubik et. al., (2018) also investigated the interplay between RSC and GRFs, though in the more complex and convoluted *in vivo* system, with the use of various conditional ablations via the anchor-away method (Haruki et al., 2008). The authors were able to identify five distinct classes of sites for each GRF (Abf1, Reb1 and Rap1), depending on whether local nucleosome occupancy increased significantly upon ablation of either RSC or the respective GRF (class I), only upon GRF ablation (class II), only upon RSC ablation (class III), only upon combined ablation of both factors (class IV), or not in any case (class V) (**Table 4**), We investigated these same site classes (respective annotations kindly provided by Slawomir Kubik with the help of David Shore) using our *in vitro* data. We asked if the *in vivo* observations could be explained by the isolated action of RSC +/- GRFs in our *in vitro* system, i.e., if classes which respond to ablation of RSC alone *in vivo* (I and III) would show NFR formation *in vitro* already just in the presence of RSC, whilst classes seemingly requiring the cooperation of a remodeler and the GRF (classes II and IV) would present with NFR formation primarily upon addition of both factors. Indeed, we observed nucleosome depletion by RSC alone in classes I and III (**Figure 27**), conforming with the *in vivo* situation. Unexpectedly, we made the same observation at class IV, where RSC ablation alone had little effect on nucleosome occupancy *in vivo*. Class II displayed nucleosome depletion only in the presence of both RSC and GRF *in vitro*, whilst class V showed no significant changes regardless of added factors, consistent with *in vivo* results. Collectively (Table 3), the combined action of RSC and GRFs is both necessary, as shown *in vivo* by Kubik et al., and sufficient, as shown by us *in vitro*, for NFR generation at all GRF sites of classes I-IV. However, the uncoupled action of RSC and GRFs in some cases (classes III and IV) shows differential effects *in vivo* vs. *in vitro*, probably as other DNA binding factors could compensate during GRF ablation (classes III and IV) and other remodelers could compensate during RSC ablation (class IV).

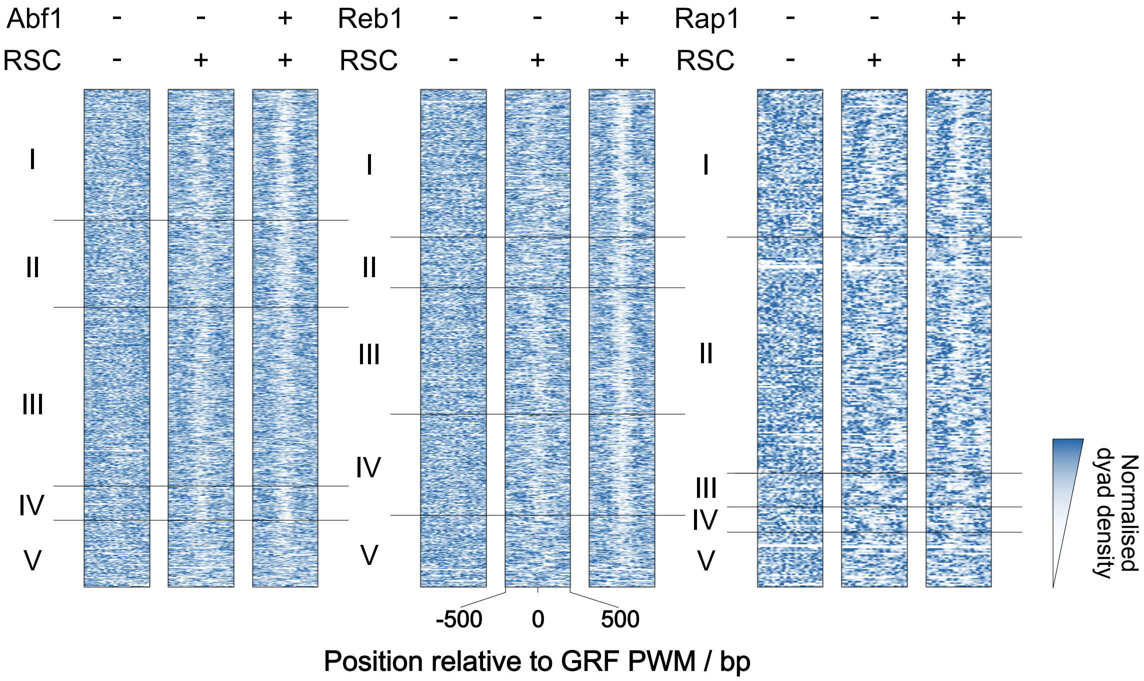

Figure 27 – Nucleosome depletion at different classes of GRF sites in response to RSC ± GRF addition *in vitro*

Heatmaps of MNase-seq data as in **Figure 25** and **Figure 26** (SGD only) and indicated above the heatmaps, aligned to the respective GRF PWMs and subdivided by responses to RSC/GRF ablation *in vivo* (Kubik et al., 2018). Number of sites in each GRF class – Abf1 (875 x total, 239 x class **I**, 158 x class **II**, 301 x class **III**, 63 x class **IV**, 114 x class **V**); Reb1 (814 x total, 247 x class **I**, 88 x class **II**, 202 x class **III**, 173 x class **IV**, 108 x class **V**); Rap1 (346 x total, 101 x class **I**, 163 x class **II**, 24 x class **III**, 17 x class **IV**, 41 x class **V**). Further information on classification of classes and comparison to *in vivo* observations can be found in **Table 4.**

Table 4 – Response of Kubik et. al., (2018) GRF site classes to factor addition *in vitro* vs factor ablation *in vivo.* '+' indicates response to the stimulus (NFR formation *in vitro* vs NFR filling *in vivo*), whilst '-' indicates no response.

Class	RSC *in vitro*	RSC + GRF *in vitro*	RSC ablation *in vivo*	GRF ablation *in vivo*	RSC + GRF ablation *in vivo*
I	+	+	+	+	+
II	-	+	- (other remodelers compensate)	+	+
III	+	+	+	- (other DNA binders or poly(dA:dT) compensate)	+
IV	+	+	- (other remodelers compensate)	- (other DNA binders or poly(dA:dT) compensate)	+
V	-	-	-	-	-

To further probe how DNA sequence elements that guide nucleosome organization by remodelers directly (poly(dA)/poly(dT) tracts, NPSs) or indirectly (GRF sites) as identified in our *in vitro* reconstitution system correlate with the *in vivo* nucleosome organization, we mapped the organisation of these elements around NFRs. As directionality of remodeler action, for example nucleosome depletion by RSC (**Figure 17**) was an intriguing feature, we limited our analysis to unidirectional promoters to better highlight patterns relative to the direction of transcription. When simply viewing all unidirectional promoters (**Figure 28**, left panel), we recapitulated the earlier observations of a strand-biased distribution of poly(dT) tracts upstream and poly(dA) downstream of the NFR center by us (Barnes & Korber, 2021) and others (de Boer & Hughes, 2014; Wu & Li, 2010). Additionally, we saw an enrichment of GRF sites upstream of the NFR center, in concordance with nucleosome occupancy rising between the GRF site and TSS upon RSC ablation (Kubik et al., 2018). Furthermore, we saw a striking similarity between the position of NPS enrichment and *in vivo* coverage trace. Note that NPSs were derived from *in vitro* data of all six remodelers in this study (INO80, RSC, ISW1a, ISW2, Fun30 and Chd1), in the absence of GRFs. As such, the NPS trace was independently obtained and need not mirror the *in vivo* trace, which is influenced by the action of all remodelers in the presence of GRFs.

We further subdivided the promoters to explore the contribution of GRF site and poly(dA)/poly(dT) tract placement to the overall organisation. At promoters containing at least one GRF site and poly(dA) or poly(dT) tract, we observed a similar organisation – with poly(dA) tracts enriched closest to the TSS, poly(dT) tracts enriched upstream, over the NFR center, and GRF sites enriched most distally. Again, NPSs were enriched at the same location as the *in vivo* ±1 nucleosome positions. This argues that such NFRs depend on both their GRFs as well as their poly(dA)/(dT) tracts for organizing the NFR center and the flanking nucleoosme positions. In contrast, at instances with at least one poly(dA:dT) tract but no GRF site, the poly(dA)/poly(dT) tract placement at these NFRs reflects what we saw at UNB promoters (**Figure 16**). This argues that such NFRs mainly depend on the relative location of poly(dA)/(dT) tracts for determination of their center. However, we also observed a shift in NPS enrichment downstream. Conversely, when we looked at promoters with at least one GRF binding site but no poly(dA:dT) tract, we again saw GRF site enrichment upstream of the NFR center, which seems to be the preferred arrangement for generation of NFRs, but this time NPS peaks were shifted toward the NFR center from both directions. Taken together, this suggests that NPSs, on average, mainly contribute to positioning of NFR-flanking +1/-1 nucleosomes if the NFR is generated by cooperation of GRFs and poly(dA:dT) tracts, but that other mechanisms fine-tune the +1/-1 nucleosomes if only one of these elements partakes in NFR formation. Finally, unidirectional promoters without a GRF site or poly(dA:dT) tract displayed poorly developed NFRs and nondescript localisation of NPSs, which may argue for wholly different and yet to be identified mechanisms of NFR formation and nucleosome positioning at such regions.

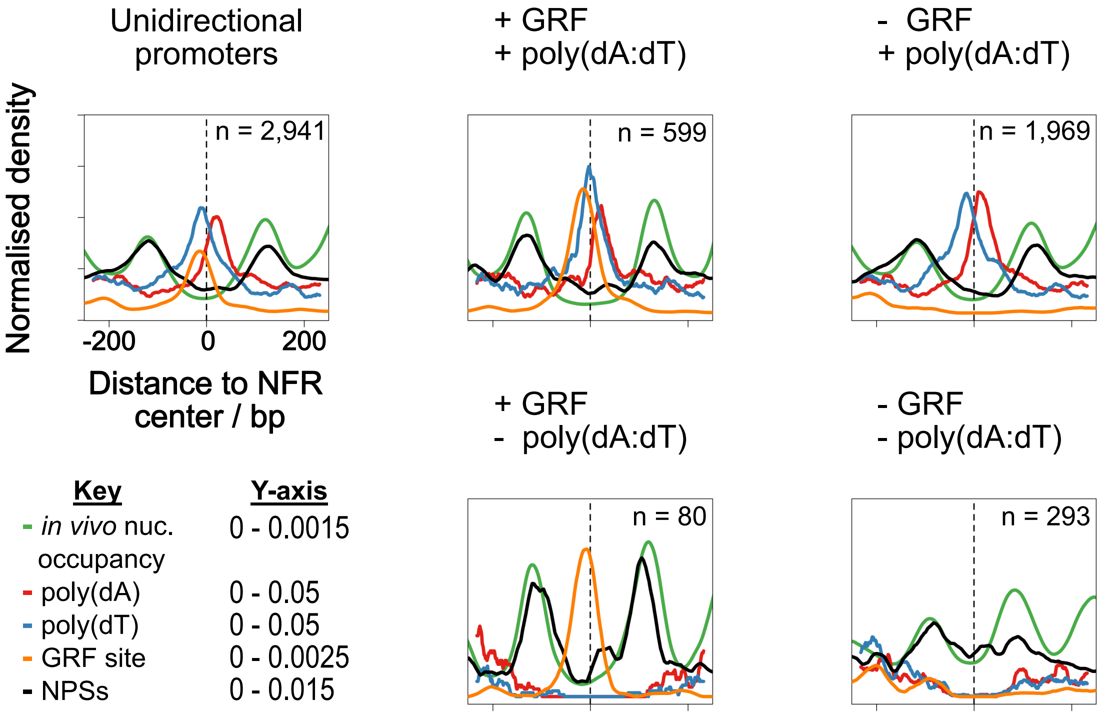

Figure 28 – Distribution of DNA sequence elements contributing to nucleosome organisation around *in vivo* NFRs

Composite plots displaying the organisation of nucleosomes and DNA sequence elements involved in guiding nucleosome positioning by remodelers around promoter NFR centers, defined as the midpoint between +1 and -1 *in vivo* nucleosome coordinates (Oberbeckmann, Krietenstein, et al., 2021). To explore potential directionality of nucleosome organizing DNA elements with respect to transcription, only unidirectional promoters were analysed, defined by the absence of divergent transcripts (Xu et al., 2009). *In vivo* (GSM4175394), GRF (Abf1, Reb1, Rap1) site and NPS traces were generated by taking MNase-seq reads, all Abf1/Rap1/Reb1 PWMs and all 'De-noised' NPSs for all six remodelers in this study (INO80, RSC, ISW1a, ISW2, Fun30 and Chd1), respectively, resizing to 50 bp and aligning/normalising as detailed in Methods (2.2.8). Poly(dA)/poly(dT) tract traces were generated as in **Figure 13**, then smoothed with a 25 bp rolling mean of 1 bp step size. NFRs were then divided into those with at least one GRF site and a poly(dA) or poly(dT) tract, a GRF site but no poly(dA) or poly(dT) tract, no GRF site but with a poly(dA) or poly(dT) tract, or without a GRF site or poly(dA)/poly(dT) tract. Number of instances (n) for each class are indicated on the respective panel. Individual y-axes values for each trace, along with respective colours are indicated (bottom left). Vertical dashed lines highlight the NFR center alignment point.

4. Discussion

In this study, we explored the contribution of DNA shape/mechanics, homopolymeric poly(dA:dT) tracts and GRFs to nucleosome organisation, as employed via readout by ATP-dependent chromatin remodelers. We discovered that the chromatin remodelers INO80, RSC, ISW1a, ISW2, Fun30 and Chd1 differentially process DNA sequence into nucleosome positioning. We further substantiated that poly(dA:dT) tracts in the *S. cerevisiae* genome influence nucleosome organisation by stimulating active and directional depletion of nucleosomes by RSC, far outweighing their intrinsic propensity to exclude nucleosomes. We found that RSC also cooperates with Abf1, Reb1 and Rap1 to generate NFRs, even in the absence of stimulation by poly(dA:dT).

4.1 Nucleosome positioning by remodeler-specific reading of DNA sequence

4.1.1 Remodeler NPSs

Following on from the work of Oberbeckmann et. al., (2021), who identified DNA shape/mechanics preferences for nucleosome positioning by INO80 as compared to SGD, termed NPSs, we identified analogous NPSs for the remodelers RSC, ISW1a, ISW2, Fun30 and Chd1, whilst recapturing INO80's NPSs. We demonstrated that detection and shape/mechanic profiles of NPSs are robust and reproducible. The key features of remodeler-DNA readout preferences could be identified with less precise position information (single end sequencing mode vs paired end), at higher chromatin density (0.8 vs 0.2/0.4), with two different modes of data processing (filtering vs PCA), and even without further processing of detected peaks ('denoised' peaks). The ease of NPS detection now presents an exciting opportunity to further compare chromatin remodelers in this regard as we can apply the same workflow with confidence to establish the sequence-dependent positioning preference of yeast SWI/SNF, ISW1b or orthologs from other species like *H. sapiens*.

Classically, the role of DNA shape in protein-DNA interactions has largely been studied in the context of static binding of transcription or general regulatory factors to consensus sequences (Chiu et al., 2020; Levo et al., 2015; Mathelier et al., 2016; Rossi et al., 2018; Yang et al., 2017; Zentner et al., 2015). Studies such as here and its precursor (Oberbeckmann, Krietenstein, et al., 2021) demonstrate an effective application to a more complex system, where large, multi-subunit complexes do not just bind to, but also track along the DNA strand in a directional manner. While tracking, they interpret DNA shape/mechanic information as this modulates their ATP-dependent DNA translocation activity. Aside from chromatin remodelers, helicases and polymerases also track along DNA, which may suggest that they respond to DNA shape/mechanics, too. Indeed, it has been suggested that RNA polymerase I (Pol I) is capable of reading DNA 'bendability' at promoters (Engel et al., 2017), providing a common mechanism for transcription initiation at Pol I target sites despite poor sequence conservation (Moss et al., 2007). Similar DNA shape recognition at promoters has also been reported for RNA polymerase II (Dienemann et al., 2019). Thus, we propose that the readout of DNA shape/mechanics constitutes an important feature of DNA translocases in general and an instructive step in determining chromatin organisation in particular, beyond DNA readout via GRF binding site recognition.

4.1.2 NPS – structure discussion

We observed that distinct characteristics of remodeler NPS shape/mechanics profiles map to key protein-DNA interactions as resolved by high resolution cryo-electron microscopy (Brahma et al., 2018; Knoll et al., 2018; Nodelman et al., 2022; Wagner et al., 2020). In the case of RSC, this comparison suggested a model by which reading of rigid extra-nucleosomal DNA via the DIM, and flexibile intra-nucleosomal DNA at SHL-6 and SHL+2 via Sth1, was propagated into nucleosome sliding toward a position with more moderate rigidity/flexibility characteristics. The known preference of RSC for remodeling nucleosomes containing poly(dA:dT) tracts suggests a role for the AT-hook of Rsc2 in this mechanism, especially combined with its' position in the DIM and its' essential nature (Cairns et al., 1999; Krietenstein et al., 2016; Lorch et al., 2014; Wagner et al., 2020). However, this interaction has still not been 'caught in the act' and directly demonstrated to be significant, likely because its essential nature hinders *in vivo* mutagenesis studies, and the DIM has proven difficult to resolve in cryo-EM structures, due to its flexibility and hetereogeneity in such structures. Nevertheless, the AT-hook motif is known to bind to the minor groove of AT-rich DNA (Aravind & Landsman, 1998; Reeves & Nissen, 1990; Singh et al., 2006), which are inherently rigid sequences. Notably, these sequences are not necessarily homopolymeric, i.e., generally AT-rich DNA is sufficient for AT-hook binding. When studying RSC via MNase-seq, we often confined analyses to homopolymeric poly(dA)/poly(dT) tracts, e.g., AAAAA or TTTTT, as they're much easier to define, search for and work with bioinformatically. However, the points laid out in this section argue that the structural characteristics poly(dA:dT) tracts confer to the DNA sequence (high rigidity, low MGW, high HelT, low ProT, low Roll and low EP) are what is read and enacted upon by RSC, rather than a specific consensus sequence. In future experiments, this could be verified by purifying recombinant versions of RSC with a mutated AT-hook, generating NPSs as in this study and assessing the impact on the resultant shape/mechanic profiles. For instance, maybe RSC targeting could be altered *in vitro* by replacing the AT-hook of Rsc2 with another DNA binding motif, such as a Basic-region leucine zipper (bZIP), which binds to the major groove of DNA at the consensus sequence ACGT (E et al., 2014; Landschulz et al., 1988; Nijhawan et al., 2008).

The proposed interpretations of NPS shape profiles offered here and in Results - 3.1 may seem to suggest that NPSs represent a static endpoint, where nucleosomes are no longer moved as the underlying sequence acts as a poor substrate for remodeling a so-called 'kinetic release' model (Manelyte et al., 2014; Rippe et al., 2007). However, we do not discount the possibility that these sequences may represent a point of dynamic equilibrium, where nucleosome sliding continues to occur but with a sliding direction bias always pointing towards this point (Oberbeckmann, Niebauer, et al., 2021). In favor of the latter model are observations that remodelers do remodel mononucleosomes, as monitored by generating restriction enzyme accessibility in an ATP-dependent way, even though the mononucleosomes are not moved away from their starting positions ((Zhou et al., 2018), see Fig. 1G). It remains to be clarified if the NPSs reflect effects of DNA shape/mechanics on remodeler binding/targeting, catalytic efficiency, i.e., coupling of ATP hydrolysis energy to DNA translocation, remodeling direction bias, e.g., preferences for binding or translocation direction, or other regulation modes on the mechanistic level.

4.1.3 Interpreting NPSs

Detecting and working with NPSs using our *in vitro* reconstitution system was not without difficulties, as technical limitations detailed in Results - 3.3 all but guarantee that we miss many relevant sequences due to heterogeneity of MNase-seq coverage across the plasmid library. This may be ameliorated in the future by normalizing for local coverage according to the tile borders of the plasmid library inserts. Probably due to missing many NPS instances across the genome, the degree of overlap between NPS and *in vivo* dyad positions appeared to be quite low (**Table 2**). Nonetheless, those NPSs were determined *in vitro* at much lower chromatin densities (0.2 & 0.4 or just 0.4 assembly degrees – see Methods - 2.2.2) than *in vivo,* in the absence of additional factors which influence nucleosome positioning, such as GRFs or other remodelers. As such, NPSs are indicative of an individual remodeler's preference for nucleosome positioning, but *in vivo* this is modulated by phasing to GRFs, spacing nucleosomes relative to each other and competition between remodelers to impart their own unique positioning preference (Oberbeckmann, Niebauer, et al., 2021). Besides the now well-documented case of +1 nucleosome positioning by INO80 (Krietenstein et al., 2016; Oberbeckmann, Krietenstein, et al., 2021), it remains to be analyzed in which other cases remodeler-specific NPSs are employed *in vivo*. Such analyses were started in this work and will require follow-up efforts. One difficulty here is to define what "employment *in vivo*" shall mean. For each remodeler-type investigated, about 30% of NPSs overlap (within a 20 bp window) with an *in vivo* nucleosome position of wild type yeast growing logarithmically in full media. Does this mean that these nucleosomes were indeed positioned by the respective remodeler? Or are these coincidences by chance? Given the average nucleosome repeat length in yeast of 165 bp (Thomas & Furber, 1976), a random distribution of remodeler NPSs has a chance of 20/165 = 12% to overlap with *in vivo* nucleosome positions by chance. As the actual overlap frequency is about twofold higher and as the actual number of NPSs in the genome may be underestimated (see above), this argues against a chance coincidence. Further, any nucleosome position *in vivo* may reflect not only the preference of one remodeler type but may also result from a competition between several types, i.e., integrate over several NPS profiles. Therefore, even a position that does not coincide with any remodeler's sequence preferences may still result from an "empolyment of NPSs". Nonetheless, by using heterologous genomic DNA from *S. pombe* or *E. coli*, it was shown (Oberbeckmann, Niebauer, et al., 2021) that remodelers position nucleosome in regular arrays relative to barriers by a phasing and spacing mechanism that involves remodelers' ruler elements but not necessarily the sequence underlying nucleosomes in the arrays. Therefore, it is even expected that a large fraction of nucleosome positions are not generated via remodeler NPSs in vivo. Finally, nucleosome positions, especially in promoter regions, may respond to growth conditions (Boeger et al., 2003; Jiang & Pugh, 2009; Shivaswamy & Iyer, 2008). As such, some nucleosome positions may correspond to a remodeler NPS only under certain conditions different from the log phase full media conditions analyzed so far.

Collectively, at least the *S. cerevisiae* genome sequence appears to have evolved DNA sequence cues that are read out by specific remodelers and turned into nucleosome positioning. To which extent and under which circumstances and to which effect this happens remains to be clarified.

4.2 The role of poly(dA:dT) tracts in nucleosome depletion

In the course of this study and accompanying paper (Barnes & Korber, 2021), we presented evidence that the nucleosome depletion observed at poly(dA:dT) tracts is driven primarily through the action of RSC, rather than through an intrinsic exclusion mechanism inherent to such tracts. This has been a topic of debate for many years, as many studies have reported poly(dA:dT) tracts to intrinsically disfavour nucleosome formation (Chereji & Clark, 2018; Field et al., 2008; Iyer & Struhl, 1995; Kunkel & Martinson, 1981; Prunell, 1982; Satchwell et al., 1986; Segal & Widom, 2009a; Yuan et al., 2005). As a result, this was commonly believed to be the driving force behind NFR formation *in vivo*, until RSC was directly shown to be responsible for depleting nucleosomes from dA/dT-rich DNA *in vitro* (Lorch et al., 2014). Doubts remained about the physiological relevance of these findings, which used mononucleosomal substrates, until a genome-wide reconstitution assay (Krietenstein et al., 2016) allowed to detect that RSC formed NFRs at *S. cerevisiae* promoter poly(dA:dT) tracts in a directional manner that fit the evolved asymmetry of poly(dA) versus poly(dT) distribution in NFRs *in vivo* (Barnes & Korber, 2021). Here, we report that RSC depletion at poly(dA:dT) tracts occurs irrespective of genome context, although we do not discount the possibility of additional contributions to NFR formation at promoters, such as binding factor competition (Ozonov & van Nimwegen, 2013), *in vivo*. Indeed, GRFs contribute, too (see below 4.3).

A major outstanding question arising from the work by Lorch et. al., (2014) is that of the distinction between nucleosome sliding and eviction by RSC. In this study, nucleosome disassembly was assessed by the appearance of free DNA as mononucleosomes were incubated with RSC, ATP and a histone chaperone, Nap1. It has been suggested that RSC is able to evict such nucleosomes by disrupting multiple DNA-histone contact simultaneously through efficient coupling of ATP hydrolysis to DNA translocation, leading to a forceful ejection of H2A-H2B dimers and subsequent destabilisation of the nucleosome (Clapier et al., 2017). Indeed, Lorch et. al., (2014) observed hexasomal species in their disassembly assay, representing intermediate nucleosomes with H2A-H2B dimers ejected. Additionally, RSC has been ‘caught in the act’ disassembling promoter nucleosomes, accounting for what were previously referred to as ‘fragile nucleosomes’ (Brahma & Henikoff, 2019). On the other hand, RSC has also been proposed to evict neighbouring nucleosomes, by sliding its bound target toward an adjacent nucleosome and ‘spooling’ the DNA off the histone octamer (Clapier et al., 2017). This has been supported with the use of dinucleosomal substrates (Engeholm et al., 2009; Prasad et al., 2016). However, it’s still unresolved to what degree either mechanism of nucleosome eviction by RSC occurs *in vivo*, and how the decision between sliding and eviction may be regulated. It’s been suggested that intra-molecular interactions between regulatory domains of Sth1 (Post-HSA and Protusion 1), as well as the interacting ARP module (Arp7, Arp9 and Rtt102) act to modify ATPase activity and coupling to DNA translocation (Clapier et al., 2016), though this has yet to be verified in a genomic context, and the contribution of poly(dA:dT) tracts to this decision making is unknown.

We attempted to address the question of sliding vs eviction by RSC in our genome-wide *in vitro* reconstitution assay, but it became clear that the biases of MNase digestion were detrimental for a quantitative analysis. With no way to quantify and correct for the biased digestion of dA/dT-rich DNA, along with the usual difficulty in controlling digestion degree across independent replicates, it was not feasible to quantify the fraction of nucleosomes which had been repositioned vs ejected by RSC. Additionally, MNase-seq does not score the non-nucleosomal DNA, so regions where RSC removes a nucleosome are digested and an absolute measure of RSC’s impact cannot be determined, only a relative comparison with the assumption that systematic biases in MNase digestion, library preparation and sequencing affect all replicates equally. However, a new sequencing technology based on DNA methylation footprinting (ODM-seq) permits the determination of absolutely occupancy genome-wide (Oberbeckmann et al., 2019). This method could be combined with H3Q85C chemical mapping (Chereji et al., 2018), capable of base-pair resolution of nucleosome positioning, without complications from other DNA binding factors protecting against MNase digestion. In this way, the precise genome-wide position and absolute occupancy of nucleosomes could be measured simultaneously in response to RSC remodelling. Presumably, heterogeneity in sliding vs eviction would occur across RSC target sites, and the underlying DNA sequence could be probed to determine its effect on modulating RSC’s output. This proposed experiment would also provide a more precise method of determining remodeler NPSs and NDSs and allow for quantification of their strengths, i.e., which NPSs/NDSs mostly strongly determine nucleosome occupancy, and which features underly nucleosomes of highest occupancy or NFRs of lowest occupancy under different conditions *in vitro.*

4.3 The role of GRFs in nucleosome organisation by RSC

4.3.1 NFR generation but no array formation

In this study, we found evidence that GRFs cooperate with RSC to enhance NFR generation at GRF binding sites, *in vitro.* Nucleosome depletion at these sites was not dependent on the presence of poly(dA:dT) tracts, though they did enhance NFR formation in addition. We found no evidence of a directional bias in occupancy change relative to the orientation of the GRF binding site, as is seen with poly(dA:dT) tracts. Notably, whilst RSC remodelling at GRF sites did somewhat produce peaks up- and downstream, albeit broad, no regularly spaced arrays were generated, in contrast to the response observed with INO80, ISW1a, ISW2 and Chd1 in connection with GRFs (Krietenstein et al., 2016; Oberbeckmann, Niebauer, et al., 2021). These remodelers phased arrays relative to the GRF barrier and introduced regular spacing via a proposed ‘ruler’ mechanism (Oberbeckmann, Niebauer, et al., 2021; Yamada et al., 2011). This disparity between remodeler responses to GRFs demonstrates that chromatin remodelers act as information processing hubs, which ‘read’ common signals such as DNA sequence mechanics and bound GRFs, but differentially interpret the stimuli to affect nucleosome organisation based on their own intrinsic preferences and mechanisms.

We compared the effect of RSC remodeling, with or without the addition of GRFs, to five distinct GRF site classes as defined by the outcome of their ablation *in vivo* (Kubik et al., 2018), finding that many of the results could be recapitulated *in vitro* (**Figure 27**, **Table 4**). Notably, we observed NFR generation by RSC alone in class IV, whilst neither RSC nor GRF ablation alone had a significant impact on nucleosome occupancy at these sites *in vivo.* This suggests that other remodelers cooperate with the respective GRF at these sites to accomplish a similar result to what RSC achieves alone by directly reading DNA mechanics. The authors theorise that GRF redundancy may explain the lack of nucleosome occupancy change upon GRF ablation at these sites, and we do not discount this possibility, but our results suggest they are not strictly necessary at these locations. Additionally, we recapitulated the finding that GRFs are not as influential at classes III and V, since RSC was either capable of nucleosome depletion without a GRF, or not capable even with one, respectively. This poses the question of what determines which GRF sites are functional. Kubik et. al., (2018) suggest that lower information content of the binding motifs and reduced GRF binding as measured by ChIP (Kasinathan et al., 2014; Knight et al., 2014) are responsible. However, ChIP signal intensities were still far above background and its unclear whether GRFs possess lower affinity for these sites, or if other aspects such as factor binding competition are important here. Indeed, protein-DNA interactions are influenced by the shape properties of the DNA at the binding site (Mathelier et al., 2016; Yang et al., 2017) and flanking (Suter, 2020), local chromatin organisation (Mirny, 2010), and cooperativity and competition between factors (Eggers & Becker, 2021; Morgunova & Taipale, 2017). Complicating matters further, binding sites can be defined in numerous ways. For instance, six different PWMs for Abf1 are readily available for use on ScerTF, a curated database for *S. cerevisiae* transcription factor PWMs, which although similar each have different thresholds for defining a binding site (Spivak & Stormo, 2012). Alternatively, binding sites defined *in vivo* via ChIP-exo, or *in vitro* via PB-exo could be used (Rossi et al., 2018), or by a technique called SLIM-ChIP (Gutin et al., 2018). We suggest a twofold mechanistic approach to define “functional GRF sites”. *In vitro*, all sites that show a response to GRF addition in our genome-wide remodeling assay using purified remodelers like RSC are sufficient to be functional. *In vivo*, all sites that show a response to GRF ablation are necessary for function. Only the combination of the *in vitro* and the *in vivo* approach allows the delineation of both a necessary and a sufficient contribution.

Indeed, our study of *in vitro* data here contributes to dissect the mechanism of individual remodelers in terms of what they are able to do. Complementarily, the analyses of *in vivo* data shows where these remodeler activities are employed and to which effect. We envision that further studies following this two-pronged approach will lead to a fuller understanding of the role of remodelers in shaping chromatin organization in the nucleus.

Bibliography

Albert, I., Mavrich, T. N., Tomsho, L. P., Qi, J., Zanton, S. J., Schuster, S. C., & Pugh, B. F. (2007). Translational and rotational settings of H2A.Z nucleosomes across the Saccharomyces cerevisiae genome. *Nature*, *446*(7135), 572-576. https://doi.org/10.1038/nature05632

Ame, J. C., Spenlehauer, C., & de Murcia, G. (2004). The PARP superfamily. *Bioessays*, *26*(8), 882-893. https://doi.org/10.1002/bies.20085

Aravind, L., & Landsman, D. (1998). AT-hook motifs identified in a wide variety of DNA-binding proteins. *Nucleic Acids Res*, *26*(19), 4413-4421. https://doi.org/10.1093/nar/26.19.4413

Arents, G., Burlingame, R. W., Wang, B. C., Love, W. E., & Moudrianakis, E. N. (1991). The nucleosomal core histone octamer at 3.1 A resolution: a tripartite protein assembly and a left-handed superhelix. *Proc Natl Acad Sci U S A*, *88*(22), 10148-10152. https://doi.org/10.1073/pnas.88.22.10148

Azmi, I. F., Watanabe, S., Maloney, M. F., Kang, S., Belsky, J. A., MacAlpine, D. M., Peterson, C. L., & Bell, S. P. (2017). Nucleosomes influence multiple steps during replication initiation. *Elife*, *6*. https://doi.org/10.7554/eLife.22512

Badis, G., Chan, E. T., van Bakel, H., Pena-Castillo, L., Tillo, D., Tsui, K., Carlson, C. D., Gossett, A. J., Hasinoff, M. J., Warren, C. L., Gebbia, M., Talukder, S., Yang, A., Mnaimneh, S., Terterov, D., Coburn, D., Li Yeo, A., Yeo, Z. X., Clarke, N. D., . . . Hughes, T. R. (2008). A library of yeast transcription factor motifs reveals a widespread function for Rsc3 in targeting nucleosome exclusion at promoters. *Mol Cell*, *32*(6), 878-887. https://doi.org/10.1016/j.molcel.2008.11.020

Bai, L., Ondracka, A., & Cross, F. R. (2011). Multiple sequence-specific factors generate the nucleosome-depleted region on CLN2 promoter. *Mol Cell*, *42*(4), 465-476. https://doi.org/10.1016/j.molcel.2011.03.028

Bailey, T. L., & Elkan, C. (1994). Fitting a mixture model by expectation maximization to discover motifs in biopolymers. *Proc Int Conf Intell Syst Mol Biol*, *2*, 28-36. https://www.ncbi.nlm.nih.gov/pubmed/7584402

Bailey, T. L., Johnson, J., Grant, C. E., & Noble, W. S. (2015). The MEME Suite. *Nucleic Acids Res*, *43*(W1), W39-49. https://doi.org/10.1093/nar/gkv416

Bao, Y., & Shen, X. (2011). SnapShot: Chromatin remodeling: INO80 and SWR1. *Cell*, *144*(1), 158-158 e152. https://doi.org/10.1016/j.cell.2010.12.024

Barnes, T., & Korber, P. (2021). The Active Mechanism of Nucleosome Depletion by Poly(dA:dT) Tracts In Vivo. *Int J Mol Sci*, *22*(15). https://doi.org/10.3390/ijms22158233

Barski, A., Cuddapah, S., Cui, K., Roh, T. Y., Schones, D. E., Wang, Z., Wei, G., Chepelev, I., & Zhao, K. (2007). High-resolution profiling of histone methylations in the human genome. *Cell*, *129*(4), 823-837. https://doi.org/10.1016/j.cell.2007.05.009

Bednar, J., Horowitz, R. A., Grigoryev, S. A., Carruthers, L. M., Hansen, J. C., Koster, A. J., & Woodcock, C. L. (1998). Nucleosomes, linker DNA, and linker histone form a unique structural motif that directs the higher-order folding and compaction of chromatin. *Proc Natl Acad Sci U S A*, *95*(24), 14173-14178. https://doi.org/10.1073/pnas.95.24.14173

Berger, S. L. (2002). Histone modifications in transcriptional regulation. *Curr Opin Genet Dev*, *12*(2), 142-148. https://doi.org/10.1016/s0959-437x(02)00279-4

Bintu, L., Ishibashi, T., Dangkulwanich, M., Wu, Y. Y., Lubkowska, L., Kashlev, M., & Bustamante, C. (2012). Nucleosomal elements that control the topography of the barrier to transcription. *Cell*, *151*(4), 738-749. https://doi.org/10.1016/j.cell.2012.10.009

Boeger, H., Griesenbeck, J., & Kornberg, R. D. (2008). Nucleosome retention and the stochastic nature of promoter chromatin remodeling for transcription. *Cell*, *133*(4), 716-726. https://doi.org/10.1016/j.cell.2008.02.051

Boeger, H., Griesenbeck, J., Strattan, J. S., & Kornberg, R. D. (2003). Nucleosomes unfold completely at a transcriptionally active promoter. *Mol Cell*, *11*(6), 1587-1598. https://doi.org/10.1016/s1097-2765(03)00231-4

Brahma, S., & Henikoff, S. (2019). RSC-Associated Subnucleosomes Define MNase-Sensitive Promoters in Yeast. *Mol Cell*, *73*(2), 238-249 e233. https://doi.org/10.1016/j.molcel.2018.10.046

Brahma, S., Ngubo, M., Paul, S., Udugama, M., & Bartholomew, B. (2018). The Arp8 and Arp4 module acts as a DNA sensor controlling INO80 chromatin remodeling. *Nat Commun*, *9*(1), 3309. https://doi.org/10.1038/s41467-018-05710-7

Brogaard, K., Xi, L., Wang, J. P., & Widom, J. (2012). A map of nucleosome positions in yeast at base-pair resolution. *Nature*, *486*(7404), 496-501. https://doi.org/10.1038/nature11142

Bryant, J. M., Govin, J., Zhang, L., Donahue, G., Pugh, B. F., & Berger, S. L. (2012). The linker histone plays a dual role during gametogenesis in Saccharomyces cerevisiae. *Mol Cell Biol*, *32*(14), 2771-2783. https://doi.org/10.1128/MCB.00282-12

Cairns, B. R., Kim, Y. J., Sayre, M. H., Laurent, B. C., & Kornberg, R. D. (1994). A multisubunit complex containing the SWI1/ADR6, SWI2/SNF2, SWI3, SNF5, and SNF6 gene products isolated from yeast. *Proc Natl Acad Sci U S A*, *91*(5), 1950-1954. https://doi.org/10.1073/pnas.91.5.1950

Cairns, B. R., Lorch, Y., Li, Y., Zhang, M., Lacomis, L., Erdjument-Bromage, H., Tempst, P., Du, J., Laurent, B., & Kornberg, R. D. (1996). RSC, an essential, abundant chromatin-remodeling complex. *Cell*, *87*(7), 1249-1260. https://doi.org/10.1016/s0092-8674(00)81820-6

Cairns, B. R., Schlichter, A., Erdjument-Bromage, H., Tempst, P., Kornberg, R. D., & Winston, F. (1999). Two functionally distinct forms of the RSC nucleosome-remodeling complex, containing essential AT hook, BAH, and bromodomains. *Mol Cell*, *4*(5), 715-723. https://doi.org/10.1016/s1097-2765(00)80382-2

Challal, D., Barucco, M., Kubik, S., Feuerbach, F., Candelli, T., Geoffroy, H., Benaksas, C., Shore, D., & Libri, D. (2018). General Regulatory Factors Control the Fidelity of Transcription by Restricting Non-coding and Ectopic Initiation. *Mol Cell*, *72*(6), 955-969 e957. https://doi.org/10.1016/j.molcel.2018.11.037

Chen, Z., Gabizon, R., Brown, A. I., Lee, A., Song, A., Diaz-Celis, C., Kaplan, C. D., Koslover, E. F., Yao, T., & Bustamante, C. (2019). High-resolution and high-accuracy topographic and transcriptional maps of the nucleosome barrier. *Elife*, *8*. https://doi.org/10.7554/eLife.48281

Chereji, R. V., & Clark, D. J. (2018). Major Determinants of Nucleosome Positioning. *Biophys J*, *114*(10), 2279-2289. https://doi.org/10.1016/j.bpj.2018.03.015

Chereji, R. V., Ramachandran, S., Bryson, T. D., & Henikoff, S. (2018). Precise genome-wide mapping of single nucleosomes and linkers in vivo. *Genome Biol*, *19*(1), 19. https://doi.org/10.1186/s13059-018-1398-0

Chiu, T. P., Comoglio, F., Zhou, T., Yang, L., Paro, R., & Rohs, R. (2016). DNAshapeR: an R/Bioconductor package for DNA shape prediction and feature encoding. *Bioinformatics*, *32*(8), 1211-1213. https://doi.org/10.1093/bioinformatics/btv735

Chiu, T. P., Xin, B., Markarian, N., Wang, Y., & Rohs, R. (2020). TFBSshape: an expanded motif database for DNA shape features of transcription factor binding sites. *Nucleic Acids Res*, *48*(D1), D246-D255. https://doi.org/10.1093/nar/gkz970

Churchman, L. S., & Weissman, J. S. (2011). Nascent transcript sequencing visualizes transcription at nucleotide resolution. *Nature*, *469*(7330), 368-373. https://doi.org/10.1038/nature09652

Clapier, C. R., Iwasa, J., Cairns, B. R., & Peterson, C. L. (2017). Mechanisms of action and regulation of ATP-dependent chromatin-remodelling complexes. *Nat Rev Mol Cell Biol*, *18*(7), 407-422. https://doi.org/10.1038/nrm.2017.26

Clapier, C. R., Kasten, M. M., Parnell, T. J., Viswanathan, R., Szerlong, H., Sirinakis, G., Zhang, Y., & Cairns, B. R. (2016). Regulation of DNA Translocation Efficiency within the Chromatin Remodeler RSC/Sth1 Potentiates Nucleosome Sliding and Ejection. *Mol Cell*, *62*(3), 453-461. https://doi.org/10.1016/j.molcel.2016.03.032

Clark, D. J., & Kimura, T. (1990). Electrostatic mechanism of chromatin folding. *J Mol Biol*, *211*(4), 883-896. https://doi.org/10.1016/0022-2836(90)90081-V

Davey, C. A., Sargent, D. F., Luger, K., Maeder, A. W., & Richmond, T. J. (2002). Solvent mediated interactions in the structure of the nucleosome core particle at 1.9 a resolution. *J Mol Biol*, *319*(5), 1097-1113. https://doi.org/10.1016/S0022-2836(02)00386-8

de Boer, C. G., & Hughes, T. R. (2014). Poly-dA:dT tracts form an in vivo nucleosomal turnstile. *PLoS One*, *9*(10), e110479. https://doi.org/10.1371/journal.pone.0110479

Deindl, S., Hwang, W. L., Hota, S. K., Blosser, T. R., Prasad, P., Bartholomew, B., & Zhuang, X. (2013). ISWI remodelers slide nucleosomes with coordinated multi-base-pair entry steps and single-base-pair exit steps. *Cell*, *152*(3), 442-452. https://doi.org/10.1016/j.cell.2012.12.040

Di Cerbo, V., Mohn, F., Ryan, D. P., Montellier, E., Kacem, S., Tropberger, P., Kallis, E., Holzner, M., Hoerner, L., Feldmann, A., Richter, F. M., Bannister, A. J., Mittler, G., Michaelis, J., Khochbin, S., Feil, R., Schuebeler, D., Owen-Hughes, T., Daujat, S., & Schneider, R. (2014). Acetylation of histone H3 at lysine 64 regulates nucleosome dynamics and facilitates transcription. *Elife*, *3*, e01632. https://doi.org/10.7554/eLife.01632

Dienemann, C., Schwalb, B., Schilbach, S., & Cramer, P. (2019). Promoter Distortion and Opening in the RNA Polymerase II Cleft. *Mol Cell*, *73*(1), 97-106 e104. https://doi.org/10.1016/j.molcel.2018.10.014

Dingwall, C., Lomonossoff, G. P., & Laskey, R. A. (1981). High sequence specificity of micrococcal nuclease. *Nucleic Acids Res*, *9*(12), 2659-2673. https://doi.org/10.1093/nar/9.12.2659

Drew, H. R. (1991). Can one measure the free energy of binding of the histone octamer to different DNA sequences by salt-dependent reconstitution? *J Mol Biol*, *219*(3), 391-392. https://doi.org/10.1016/0022-2836(91)90179-a

E, Z. G., Zhang, Y. P., Zhou, J. H., & Wang, L. (2014). Mini review roles of the bZIP gene family in rice. *Genet Mol Res*, *13*(2), 3025-3036. https://doi.org/10.4238/2014.April.16.11

Echigoya, K., Koyama, M., Negishi, L., Takizawa, Y., Mizukami, Y., Shimabayashi, H., Kuroda, A., & Kurumizaka, H. (2020). Nucleosome binding by the pioneer transcription factor OCT4. *Sci Rep*, *10*(1), 11832. https://doi.org/10.1038/s41598-020-68850-1

Eggers, N., & Becker, P. B. (2021). Cell-free genomics reveal intrinsic, cooperative and competitive determinants of chromatin interactions. *Nucleic Acids Res*, *49*(13), 7602-7617. https://doi.org/10.1093/nar/gkab558

Eltsov, M., Maclellan, K. M., Maeshima, K., Frangakis, A. S., & Dubochet, J. (2008). Analysis of cryo-electron microscopy images does not support the existence of 30-nm chromatin fibers in mitotic chromosomes in situ. *Proc Natl Acad Sci U S A*, *105*(50), 19732-19737. https://doi.org/10.1073/pnas.0810057105

Engeholm, M., de Jager, M., Flaus, A., Brenk, R., van Noort, J., & Owen-Hughes, T. (2009). Nucleosomes can invade DNA territories occupied by their neighbors. *Nat Struct Mol Biol*, *16*(2), 151-158. https://doi.org/10.1038/nsmb.1551

Engel, C., Gubbey, T., Neyer, S., Sainsbury, S., Oberthuer, C., Baejen, C., Bernecky, C., & Cramer, P. (2017). Structural Basis of RNA Polymerase I Transcription Initiation. *Cell*, *169*(1), 120-131 e122. https://doi.org/10.1016/j.cell.2017.03.003

Eustermann, S., Schall, K., Kostrewa, D., Lakomek, K., Strauss, M., Moldt, M., & Hopfner, K. P. (2018). Structural basis for ATP-dependent chromatin remodelling by the INO80 complex. *Nature*, *556*(7701), 386-390. https://doi.org/10.1038/s41586-018-0029-y

Farnung, L., Ochmann, M., Engeholm, M., & Cramer, P. (2021). Structural basis of nucleosome transcription mediated by Chd1 and FACT. *Nat Struct Mol Biol*, *28*(4), 382-387. https://doi.org/10.1038/s41594-021-00578-6

Farnung, L., Vos, S. M., & Cramer, P. (2018). Structure of transcribing RNA polymerase II-nucleosome complex. *Nat Commun*, *9*(1), 5432. https://doi.org/10.1038/s41467-018-07870-y

Field, Y., Kaplan, N., Fondufe-Mittendorf, Y., Moore, I. K., Sharon, E., Lubling, Y., Widom, J., & Segal, E. (2008). Distinct modes of regulation by chromatin encoded through nucleosome positioning signals. *PLoS Comput Biol*, *4*(11), e1000216. https://doi.org/10.1371/journal.pcbi.1000216

Finch, J. T., & Klug, A. (1976). Solenoidal model for superstructure in chromatin. *Proc Natl Acad Sci U S A*, *73*(6), 1897-1901. https://doi.org/10.1073/pnas.73.6.1897

Flaus, A., Martin, D. M., Barton, G. J., & Owen-Hughes, T. (2006). Identification of multiple distinct Snf2 subfamilies with conserved structural motifs. *Nucleic Acids Res*, *34*(10), 2887-2905. https://doi.org/10.1093/nar/gkl295

Flores, O., & Orozco, M. (2011). nucleR: a package for non-parametric nucleosome positioning. *Bioinformatics*, *27*(15), 2149-2150. https://doi.org/10.1093/bioinformatics/btr345

Forne, I., Ludwigsen, J., Imhof, A., Becker, P. B., & Mueller-Planitz, F. (2012). Probing the conformation of the ISWI ATPase domain with genetically encoded photoreactive crosslinkers and mass spectrometry. *Mol Cell Proteomics*, *11*(4), M111 012088. https://doi.org/10.1074/mcp.M111.012088

Gamarra, N., & Narlikar, G. J. (2021). Collaboration through chromatin: motors of transcription and chromatin structure. *J Mol Biol*, *433*(14), 166876. https://doi.org/10.1016/j.jmb.2021.166876

Gangaraju, V. K., & Bartholomew, B. (2007a). Dependency of ISW1a chromatin remodeling on extranucleosomal DNA. *Mol Cell Biol*, *27*(8), 3217-3225. https://doi.org/10.1128/MCB.01731-06

Gangaraju, V. K., & Bartholomew, B. (2007b). Mechanisms of ATP dependent chromatin remodeling. *Mutat Res*, *618*(1-2), 3-17. https://doi.org/10.1016/j.mrfmmm.2006.08.015

Ganguli, D., Chereji, R. V., Iben, J. R., Cole, H. A., & Clark, D. J. (2014). RSC-dependent constructive and destructive interference between opposing arrays of phased nucleosomes in yeast. *Genome Res*, *24*(10), 1637-1649. https://doi.org/10.1101/gr.177014.114

Garcia-Saez, I., Menoni, H., Boopathi, R., Shukla, M. S., Soueidan, L., Noirclerc-Savoye, M., Le Roy, A., Skoufias, D. A., Bednar, J., Hamiche, A., Angelov, D., Petosa, C., & Dimitrov, S. (2018). Structure of an H1-Bound 6-Nucleosome Array Reveals an Untwisted Two-Start Chromatin Fiber Conformation. *Mol Cell*, *72*(5), 902-915 e907. https://doi.org/10.1016/j.molcel.2018.09.027

Ghaemmaghami, S., Huh, W. K., Bower, K., Howson, R. W., Belle, A., Dephoure, N., O'Shea, E. K., & Weissman, J. S. (2003). Global analysis of protein expression in yeast. *Nature*, *425*(6959), 737-741. https://doi.org/10.1038/nature02046

Ghassabi Kondalaji, S., & Bowman, G. D. (2022). Reb1, Cbf1, and Pho4 Bias Histone Sliding and Deposition Away from Their Binding Sites. *Mol Cell Biol*, *42*(2), e0047221. https://doi.org/10.1128/MCB.00472-21

Gibson, B. A., Doolittle, L. K., Schneider, M. W. G., Jensen, L. E., Gamarra, N., Henry, L., Gerlich, D. W., Redding, S., & Rosen, M. K. (2019). Organization of Chromatin by Intrinsic and Regulated Phase Separation. *Cell*, *179*(2), 470-484 e421. https://doi.org/10.1016/j.cell.2019.08.037

Gonzalez, S., Garcia, A., Vazquez, E., Serrano, R., Sanchez, M., Quintales, L., & Antequera, F. (2016). Nucleosomal signatures impose nucleosome positioning in coding and noncoding sequences in the genome. *Genome Res*, *26*(11), 1532-1543. https://doi.org/10.1101/gr.207241.116

Gutin, J., Sadeh, R., Bodenheimer, N., Joseph-Strauss, D., Klein-Brill, A., Alajem, A., Ram, O., & Friedman, N. (2018). Fine-Resolution Mapping of TF Binding and Chromatin Interactions. *Cell Rep*, *22*(10), 2797-2807. https://doi.org/10.1016/j.celrep.2018.02.052

Hall, M. A., Shundrovsky, A., Bai, L., Fulbright, R. M., Lis, J. T., & Wang, M. D. (2009). High-resolution dynamic mapping of histone-DNA interactions in a nucleosome. *Nat Struct Mol Biol*, *16*(2), 124-129. https://doi.org/10.1038/nsmb.1526

Hansen, J. C., Connolly, M., McDonald, C. J., Pan, A., Pryamkova, A., Ray, K., Seidel, E., Tamura, S., Rogge, R., & Maeshima, K. (2018). The 10-nm chromatin fiber and its relationship to interphase chromosome organization. *Biochem Soc Trans*, *46*(1), 67-76. https://doi.org/10.1042/BST20170101

Harada, B. T., Hwang, W. L., Deindl, S., Chatterjee, N., Bartholomew, B., & Zhuang, X. (2016). Stepwise nucleosome translocation by RSC remodeling complexes. *Elife*, *5*. https://doi.org/10.7554/eLife.10051

Hartley, P. D., & Madhani, H. D. (2009). Mechanisms that specify promoter nucleosome location and identity. *Cell*, *137*(3), 445-458. https://doi.org/10.1016/j.cell.2009.02.043

Haruki, H., Nishikawa, J., & Laemmli, U. K. (2008). The anchor-away technique: rapid, conditional establishment of yeast mutant phenotypes. *Mol Cell*, *31*(6), 925-932. https://doi.org/10.1016/j.molcel.2008.07.020

Heins, J. N., Suriano, J. R., Taniuchi, H., & Anfinsen, C. B. (1967). Characterization of a nuclease produced by Staphylococcus aureus. *J Biol Chem*, *242*(5), 1016-1020. https://www.ncbi.nlm.nih.gov/pubmed/6020427

Henikoff, J. G., Belsky, J. A., Krassovsky, K., MacAlpine, D. M., & Henikoff, S. (2011). Epigenome characterization at single base-pair resolution. *Proc Natl Acad Sci U S A*, *108*(45), 18318-18323. https://doi.org/10.1073/pnas.1110731108

Horz, W., & Altenburger, W. (1981). Sequence specific cleavage of DNA by micrococcal nuclease. *Nucleic Acids Res*, *9*(12), 2643-2658. https://doi.org/10.1093/nar/9.12.2643

Hsieh, F. K., Fisher, M., Ujvari, A., Studitsky, V. M., & Luse, D. S. (2010). Histone Sin mutations promote nucleosome traversal and histone displacement by RNA polymerase II. *EMBO Rep*, *11*(9), 705-710. https://doi.org/10.1038/embor.2010.113

Hughes, A. L., Jin, Y., Rando, O. J., & Struhl, K. (2012). A functional evolutionary approach to identify determinants of nucleosome positioning: a unifying model for establishing the genome-wide pattern. *Mol Cell*, *48*(1), 5-15. https://doi.org/10.1016/j.molcel.2012.07.003

Ioshikhes, I. P., Albert, I., Zanton, S. J., & Pugh, B. F. (2006). Nucleosome positions predicted through comparative genomics. *Nat Genet*, *38*(10), 1210-1215. https://doi.org/10.1038/ng1878

Iyer, V., & Struhl, K. (1995). Poly(dA:dT), a ubiquitous promoter element that stimulates transcription via its intrinsic DNA structure. *EMBO J*, *14*(11), 2570-2579. https://www.ncbi.nlm.nih.gov/pubmed/7781610

Izban, M. G., & Luse, D. S. (1991). Transcription on nucleosomal templates by RNA polymerase II in vitro: inhibition of elongation with enhancement of sequence-specific pausing. *Genes Dev*, *5*(4), 683-696. https://doi.org/10.1101/gad.5.4.683

Jackson, J. D., Falciano, V. T., & Gorovsky, M. A. (1996). A likely histone H2A.F/Z variant in Saccharomyces cerevisiae. *Trends Biochem Sci*, *21*(12), 466-467. https://doi.org/10.1016/s0968-0004(96)20028-3

Jeronimo, C., Angel, A., Nguyen, V. Q., Kim, J. M., Poitras, C., Lambert, E., Collin, P., Mellor, J., Wu, C., & Robert, F. (2021). FACT is recruited to the +1 nucleosome of transcribed genes and spreads in a Chd1-dependent manner. *Mol Cell*, *81*(17), 3542-3559 e3511. https://doi.org/10.1016/j.molcel.2021.07.010

Jiang, C., & Pugh, B. F. (2009). Nucleosome positioning and gene regulation: advances through genomics. *Nat Rev Genet*, *10*(3), 161-172. https://doi.org/10.1038/nrg2522

Jin, C., Zang, C., Wei, G., Cui, K., Peng, W., Zhao, K., & Felsenfeld, G. (2009). H3.3/H2A.Z double variant-containing nucleosomes mark 'nucleosome-free regions' of active promoters and other regulatory regions. *Nat Genet*, *41*(8), 941-945. https://doi.org/10.1038/ng.409

Johnson, S. M., Tan, F. J., McCullough, H. L., Riordan, D. P., & Fire, A. Z. (2006). Flexibility and constraint in the nucleosome core landscape of Caenorhabditis elegans chromatin. *Genome Res*, *16*(12), 1505-1516. https://doi.org/10.1101/gr.5560806

Jones, G. M., Stalker, J., Humphray, S., West, A., Cox, T., Rogers, J., Dunham, I., & Prelich, G. (2008). A systematic library for comprehensive overexpression screens in

Saccharomyces cerevisiae. *Nat Methods*, *5*(3), 239-241. https://doi.org/10.1038/nmeth.1181

Kagalwala, M. N., Glaus, B. J., Dang, W., Zofall, M., & Bartholomew, B. (2004). Topography of the ISW2-nucleosome complex: insights into nucleosome spacing and chromatin remodeling. *EMBO J*, *23*(10), 2092-2104. https://doi.org/10.1038/sj.emboj.7600220

Kaplan, N., Moore, I., Fondufe-Mittendorf, Y., Gossett, A. J., Tillo, D., Field, Y., Hughes, T. R., Lieb, J. D., Widom, J., & Segal, E. (2010). Nucleosome sequence preferences influence in vivo nucleosome organization. *Nat Struct Mol Biol*, *17*(8), 918-920. https://doi.org/10.1038/nsmb0810-918

Kaplan, N., Moore, I. K., Fondufe-Mittendorf, Y., Gossett, A. J., Tillo, D., Field, Y., LeProust, E. M., Hughes, T. R., Lieb, J. D., Widom, J., & Segal, E. (2009). The DNA-encoded nucleosome organization of a eukaryotic genome. *Nature*, *458*(7236), 362-366. https://doi.org/10.1038/nature07667

Kasinathan, S., Orsi, G. A., Zentner, G. E., Ahmad, K., & Henikoff, S. (2014). High-resolution mapping of transcription factor binding sites on native chromatin. *Nat Methods*, *11*(2), 203-209. https://doi.org/10.1038/nmeth.2766

Kireeva, M. L., Hancock, B., Cremona, G. H., Walter, W., Studitsky, V. M., & Kashlev, M. (2005). Nature of the nucleosomal barrier to RNA polymerase II. *Mol Cell*, *18*(1), 97-108. https://doi.org/10.1016/j.molcel.2005.02.027

Klein-Brill, A., Joseph-Strauss, D., Appleboim, A., & Friedman, N. (2019). Dynamics of Chromatin and Transcription during Transient Depletion of the RSC Chromatin Remodeling Complex. *Cell Rep*, *26*(1), 279-292 e275. https://doi.org/10.1016/j.celrep.2018.12.020

Klug, A., Rhodes, D., Smith, J., Finch, J. T., & Thomas, J. O. (1980). A low resolution structure for the histone core of the nucleosome. *Nature*, *287*(5782), 509-516. https://doi.org/10.1038/287509a0

Knezetic, J. A., & Luse, D. S. (1986). The presence of nucleosomes on a DNA template prevents initiation by RNA polymerase II in vitro. *Cell*, *45*(1), 95-104. https://doi.org/10.1016/0092-8674(86)90541-6

Knight, B., Kubik, S., Ghosh, B., Bruzzone, M. J., Geertz, M., Martin, V., Denervaud, N., Jacquet, P., Ozkan, B., Rougemont, J., Maerkl, S. J., Naef, F., & Shore, D. (2014). Two distinct promoter architectures centered on dynamic nucleosomes control ribosomal protein gene transcription. *Genes Dev*, *28*(15), 1695-1709. https://doi.org/10.1101/gad.244434.114

Knoll, K. R., Eustermann, S., Niebauer, V., Oberbeckmann, E., Stoehr, G., Schall, K., Tosi, A., Schwarz, M., Buchfellner, A., Korber, P., & Hopfner, K. P. (2018). The nuclear actin-containing Arp8 module is a linker DNA sensor driving INO80 chromatin remodeling. *Nat Struct Mol Biol*, *25*(9), 823-832. https://doi.org/10.1038/s41594-018-0115-8

Kornberg, R. D. (1974). Chromatin structure: a repeating unit of histones and DNA. *Science*, *184*(4139), 868-871. https://doi.org/10.1126/science.184.4139.868

Kornberg, R. D. (1977). Structure of chromatin. *Annu Rev Biochem*, *46*, 931-954. https://doi.org/10.1146/annurev.bi.46.070177.004435

Kornberg, R. D., & Thomas, J. O. (1974). Chromatin structure; oligomers of the histones. *Science*, *184*(4139), 865-868. https://doi.org/10.1126/science.184.4139.865

Korolev, N., Vorontsova, O. V., & Nordenskiold, L. (2007). Physicochemical analysis of electrostatic foundation for DNA-protein interactions in chromatin transformations. *Prog Biophys Mol Biol*, *95*(1-3), 23-49. https://doi.org/10.1016/j.pbiomolbio.2006.11.003

Krietenstein, N., Wal, M., Watanabe, S., Park, B., Peterson, C. L., Pugh, B. F., & Korber, P. (2016). Genomic Nucleosome Organization Reconstituted with Pure Proteins. *Cell*, *167*(3), 709-721 e712. https://doi.org/10.1016/j.cell.2016.09.045

Krietenstein, N., Wippo, C. J., Lieleg, C., & Korber, P. (2012). Genome-wide in vitro reconstitution of yeast chromatin with in vivo-like nucleosome positioning. *Methods Enzymol*, *513*, 205-232. https://doi.org/10.1016/B978-0-12-391938-0.00009-4

Kubik, S., Bruzzone, M. J., Challal, D., Dreos, R., Mattarocci, S., Bucher, P., Libri, D., & Shore, D. (2019). Opposing chromatin remodelers control transcription initiation frequency and start site selection. *Nat Struct Mol Biol*, *26*(8), 744-754. https://doi.org/10.1038/s41594-019-0273-3

Kubik, S., Bruzzone, M. J., Jacquet, P., Falcone, J. L., Rougemont, J., & Shore, D. (2015). Nucleosome Stability Distinguishes Two Different Promoter Types at All Protein-Coding Genes in Yeast. *Mol Cell*, *60*(3), 422-434. https://doi.org/10.1016/j.molcel.2015.10.002

Kubik, S., O'Duibhir, E., de Jonge, W. J., Mattarocci, S., Albert, B., Falcone, J. L., Bruzzone, M. J., Holstege, F. C. P., & Shore, D. (2018). Sequence-Directed Action of RSC Remodeler and General Regulatory Factors Modulates +1 Nucleosome Position to Facilitate Transcription. *Mol Cell*, *71*(1), 89-102 e105. https://doi.org/10.1016/j.molcel.2018.05.030

Kujirai, T., Ehara, H., Fujino, Y., Shirouzu, M., Sekine, S. I., & Kurumizaka, H. (2018). Structural basis of the nucleosome transition during RNA polymerase II passage. *Science*, *362*(6414), 595-598. https://doi.org/10.1126/science.aau9904

Kujirai, T., & Kurumizaka, H. (2020). Transcription through the nucleosome. *Curr Opin Struct Biol*, *61*, 42-49. https://doi.org/10.1016/j.sbi.2019.10.007

Kunkel, G. R., & Martinson, H. G. (1981). Nucleosomes will not form on double-stranded RNa or over poly(dA).poly(dT) tracts in recombinant DNA. *Nucleic Acids Res*, *9*(24), 6869-6888. https://doi.org/10.1093/nar/9.24.6869

Kuo, M. H., & Allis, C. D. (1998). Roles of histone acetyltransferases and deacetylases in gene regulation. *Bioessays*, *20*(8), 615-626. https://doi.org/10.1002/(SICI)1521-1878(199808)20:8<615::AID-BIES4>3.0.CO;2-H

Kwak, H., Fuda, N. J., Core, L. J., & Lis, J. T. (2013). Precise maps of RNA polymerase reveal how promoters direct initiation and pausing. *Science*, *339*(6122), 950-953. https://doi.org/10.1126/science.1229386

Lai, B., Gao, W., Cui, K., Xie, W., Tang, Q., Jin, W., Hu, G., Ni, B., & Zhao, K. (2018). Principles of nucleosome organization revealed by single-cell micrococcal nuclease sequencing. *Nature*, *562*(7726), 281-285. https://doi.org/10.1038/s41586-018-0567-3

Lai, W. K. M., & Pugh, B. F. (2017). Understanding nucleosome dynamics and their links to gene expression and DNA replication. *Nat Rev Mol Cell Biol*, *18*(9), 548-562. https://doi.org/10.1038/nrm.2017.47

Landschulz, W. H., Johnson, P. F., & McKnight, S. L. (1988). The leucine zipper: a hypothetical structure common to a new class of DNA binding proteins. *Science*, *240*(4860), 1759-1764. https://doi.org/10.1126/science.3289117

Langmead, B., & Salzberg, S. L. (2012). Fast gapped-read alignment with Bowtie 2. *Nat Methods*, *9*(4), 357-359. https://doi.org/10.1038/nmeth.1923

Lantermann, A. B., Straub, T., Stralfors, A., Yuan, G. C., Ekwall, K., & Korber, P. (2010). Schizosaccharomyces pombe genome-wide nucleosome mapping reveals positioning mechanisms distinct from those of Saccharomyces cerevisiae. *Nat Struct Mol Biol*, *17*(2), 251-257. https://doi.org/10.1038/nsmb.1741

Laurent, B. C., Yang, X., & Carlson, M. (1992). An essential Saccharomyces cerevisiae gene homologous to SNF2 encodes a helicase-related protein in a new family. *Mol Cell Biol*, *12*(4), 1893-1902. https://doi.org/10.1128/mcb.12.4.1893-1902.1992

Lawrence, M., Huber, W., Pages, H., Aboyoun, P., Carlson, M., Gentleman, R., Morgan, M. T., & Carey, V. J. (2013). Software for computing and annotating genomic ranges. *PLoS Comput Biol*, *9*(8), e1003118. https://doi.org/10.1371/journal.pcbi.1003118

Le Poul, Y., Xin, Y., Ling, L., Muhling, B., Jaenichen, R., Horl, D., Bunk, D., Harz, H., Leonhardt, H., Wang, Y., Osipova, E., Museridze, M., Dharmadhikari, D., Murphy, E., Rohs, R., Preibisch, S., Prud'homme, B., & Gompel, N. (2020). Regulatory encoding of quantitative variation in spatial activity of a Drosophila enhancer. *Sci Adv*, *6*(49). https://doi.org/10.1126/sciadv.abe2955

Lee, W., Tillo, D., Bray, N., Morse, R. H., Davis, R. W., Hughes, T. R., & Nislow, C. (2007). A high-resolution atlas of nucleosome occupancy in yeast. *Nat Genet*, *39*(10), 1235-1244. https://doi.org/10.1038/ng2117

Levo, M., Zalckvar, E., Sharon, E., Dantas Machado, A. C., Kalma, Y., Lotam-Pompan, M., Weinberger, A., Yakhini, Z., Rohs, R., & Segal, E. (2015). Unraveling determinants of transcription factor binding outside the core binding site. *Genome Res*, *25*(7), 1018-1029. https://doi.org/10.1101/gr.185033.114

Li, M., Hada, A., Sen, P., Olufemi, L., Hall, M. A., Smith, B. Y., Forth, S., McKnight, J. N., Patel, A., Bowman, G. D., Bartholomew, B., & Wang, M. D. (2015). Dynamic regulation of transcription factors by nucleosome remodeling. *Elife*, *4*. https://doi.org/10.7554/eLife.06249

Lieleg, C., Krietenstein, N., Walker, M., & Korber, P. (2015). Nucleosome positioning in yeasts: methods, maps, and mechanisms. *Chromosoma*, *124*(2), 131-151. https://doi.org/10.1007/s00412-014-0501-x

Liu, G., Zhao, H., Meng, H., Xing, Y., & Cai, L. (2021). A deformation energy model reveals sequence-dependent property of nucleosome positioning. *Chromosoma*, *130*(1), 27-40. https://doi.org/10.1007/s00412-020-00750-9

Lorch, Y., LaPointe, J. W., & Kornberg, R. D. (1987). Nucleosomes inhibit the initiation of transcription but allow chain elongation with the displacement of histones. *Cell*, *49*(2), 203-210. https://doi.org/10.1016/0092-8674(87)90561-7

Lorch, Y., Maier-Davis, B., & Kornberg, R. D. (2006). Chromatin remodeling by nucleosome disassembly in vitro. *Proc Natl Acad Sci U S A*, *103*(9), 3090-3093. https://doi.org/10.1073/pnas.0511050103

Lorch, Y., Maier-Davis, B., & Kornberg, R. D. (2014). Role of DNA sequence in chromatin remodeling and the formation of nucleosome-free regions. *Genes Dev*, *28*(22), 2492-2497. https://doi.org/10.1101/gad.250704.114

Lorch, Y., Zhang, M., & Kornberg, R. D. (1999). Histone octamer transfer by a chromatin-remodeling complex. *Cell*, *96*(3), 389-392. https://doi.org/10.1016/s0092-8674(00)80551-6

Lowary, P. T., & Widom, J. (1998). New DNA sequence rules for high affinity binding to histone octamer and sequence-directed nucleosome positioning. *J Mol Biol*, *276*(1), 19-42. https://doi.org/10.1006/jmbi.1997.1494

Luger, K., Mader, A. W., Richmond, R. K., Sargent, D. F., & Richmond, T. J. (1997). Crystal structure of the nucleosome core particle at 2.8 A resolution. *Nature*, *389*(6648), 251-260. https://doi.org/10.1038/38444

Lusser, A., Urwin, D. L., & Kadonaga, J. T. (2005). Distinct activities of CHD1 and ACF in ATP-dependent chromatin assembly. *Nat Struct Mol Biol*, *12*(2), 160-166. https://doi.org/10.1038/nsmb884

MacIsaac, K. D., Wang, T., Gordon, D. B., Gifford, D. K., Stormo, G. D., & Fraenkel, E. (2006). An improved map of conserved regulatory sites for Saccharomyces cerevisiae. *BMC Bioinformatics*, *7*, 113. https://doi.org/10.1186/1471-2105-7-113

Maeshima, K., Ide, S., Hibino, K., & Sasai, M. (2016). Liquid-like behavior of chromatin. *Curr Opin Genet Dev*, *37*, 36-45. https://doi.org/10.1016/j.gde.2015.11.006

Maeshima, K., Rogge, R., Tamura, S., Joti, Y., Hikima, T., Szerlong, H., Krause, C., Herman, J., Seidel, E., DeLuca, J., Ishikawa, T., & Hansen, J. C. (2016). Nucleosomal arrays self-assemble into supramolecular globular structures lacking 30-nm fibers. *EMBO J*, *35*(10), 1115-1132. https://doi.org/10.15252/embj.201592660

Manelyte, L., Strohner, R., Gross, T., & Langst, G. (2014). Chromatin targeting signals, nucleosome positioning mechanism and non-coding RNA-mediated regulation of the chromatin remodeling complex NoRC. *PLoS Genet*, *10*(3), e1004157. https://doi.org/10.1371/journal.pgen.1004157

Mathelier, A., Xin, B., Chiu, T. P., Yang, L., Rohs, R., & Wasserman, W. W. (2016). DNA Shape Features Improve Transcription Factor Binding Site Predictions In Vivo. *Cell Syst*, *3*(3), 278-286 e274. https://doi.org/10.1016/j.cels.2016.07.001

Mavrich, T. N., Jiang, C., Ioshikhes, I. P., Li, X., Venters, B. J., Zanton, S. J., Tomsho, L. P., Qi, J., Glaser, R. L., Schuster, S. C., Gilmour, D. S., Albert, I., & Pugh, B. F. (2008).

Nucleosome organization in the Drosophila genome. *Nature*, *453*(7193), 358-362. https://doi.org/10.1038/nature06929

Meluh, P. B., Yang, P., Glowczewski, L., Koshland, D., & Smith, M. M. (1998). Cse4p is a component of the core centromere of Saccharomyces cerevisiae. *Cell*, *94*(5), 607-613. https://doi.org/10.1016/s0092-8674(00)81602-5

Meneghini, M. D., Wu, M., & Madhani, H. D. (2003). Conserved histone variant H2A.Z protects euchromatin from the ectopic spread of silent heterochromatin. *Cell*, *112*(5), 725-736. https://doi.org/10.1016/s0092-8674(03)00123-5

Mirny, L. A. (2010). Nucleosome-mediated cooperativity between transcription factors. *Proc Natl Acad Sci U S A*, *107*(52), 22534-22539. https://doi.org/10.1073/pnas.0913805107

Mirny, L. A., Imakaev, M., & Abdennur, N. (2019). Two major mechanisms of chromosome organization. *Curr Opin Cell Biol*, *58*, 142-152. https://doi.org/10.1016/j.ceb.2019.05.001

Mishra, P. K., Wood, H., Stanton, J., Au, W. C., Eisenstatt, J. R., Boeckmann, L., Sclafani, R. A., Weinreich, M., Bloom, K. S., Thorpe, P. H., & Basrai, M. A. (2021). Cdc7-mediated phosphorylation of Cse4 regulates high-fidelity chromosome segregation in budding yeast. *Mol Biol Cell*, *32*(21), ar15. https://doi.org/10.1091/mbc.E21-06-0323

Mizuguchi, G., Shen, X., Landry, J., Wu, W. H., Sen, S., & Wu, C. (2004). ATP-driven exchange of histone H2AZ variant catalyzed by SWR1 chromatin remodeling complex. *Science*, *303*(5656), 343-348. https://doi.org/10.1126/science.1090701

Morgunova, E., & Taipale, J. (2017). Structural perspective of cooperative transcription factor binding. *Curr Opin Struct Biol*, *47*, 1-8. https://doi.org/10.1016/j.sbi.2017.03.006

Morozov, A. V., & Siggia, E. D. (2007). Connecting protein structure with predictions of regulatory sites. *Proc Natl Acad Sci U S A*, *104*(17), 7068-7073. https://doi.org/10.1073/pnas.0701356104

Morrison, A. J., & Shen, X. (2009). Chromatin remodelling beyond transcription: the INO80 and SWR1 complexes. *Nat Rev Mol Cell Biol*, *10*(6), 373-384. https://doi.org/10.1038/nrm2693

Morse, R. H. (1989). Nucleosomes inhibit both transcriptional initiation and elongation by RNA polymerase III in vitro. *EMBO J*, *8*(8), 2343-2351. https://www.ncbi.nlm.nih.gov/pubmed/2792088

Moss, T., Langlois, F., Gagnon-Kugler, T., & Stefanovsky, V. (2007). A housekeeper with power of attorney: the rRNA genes in ribosome biogenesis. *Cell Mol Life Sci*, *64*(1), 29-49. https://doi.org/10.1007/s00018-006-6278-1

Moyle-Heyrman, G., Zaichuk, T., Xi, L., Zhang, Q., Uhlenbeck, O. C., Holmgren, R., Widom, J., & Wang, J. P. (2013). Chemical map of Schizosaccharomyces pombe reveals species-specific features in nucleosome positioning. *Proc Natl Acad Sci U S A*, *110*(50), 20158-20163. https://doi.org/10.1073/pnas.1315809110

Narlikar, L., Gordan, R., & Hartemink, A. J. (2007). A nucleosome-guided map of transcription factor binding sites in yeast. *PLoS Comput Biol*, *3*(11), e215. https://doi.org/10.1371/journal.pcbi.0030215

Nijhawan, A., Jain, M., Tyagi, A. K., & Khurana, J. P. (2008). Genomic survey and gene expression analysis of the basic leucine zipper transcription factor family in rice. *Plant Physiol*, *146*(2), 333-350. https://doi.org/10.1104/pp.107.112821

Nishino, Y., Eltsov, M., Joti, Y., Ito, K., Takata, H., Takahashi, Y., Hihara, S., Frangakis, A. S., Imamoto, N., Ishikawa, T., & Maeshima, K. (2012). Human mitotic chromosomes consist predominantly of irregularly folded nucleosome fibres without a 30-nm chromatin structure. *EMBO J*, *31*(7), 1644-1653. https://doi.org/10.1038/emboj.2012.35

Nodelman, I. M., & Bowman, G. D. (2021). Biophysics of Chromatin Remodeling. *Annu Rev Biophys*, *50*, 73-93. https://doi.org/10.1146/annurev-biophys-082520-080201

Nodelman, I. M., Das, S., Faustino, A. M., Fried, S. D., Bowman, G. D., & Armache, J. P. (2022). Nucleosome recognition and DNA distortion by the Chd1 remodeler in a nucleotide-free state. *Nat Struct Mol Biol*, *29*(2), 121-129. https://doi.org/10.1038/s41594-021-00719-x

Noll, M. (1974). Subunit structure of chromatin. *Nature*, *251*(5472), 249-251. https://doi.org/10.1038/251249a0

Oberbeckmann, E., Krietenstein, N., Niebauer, V., Wang, Y., Schall, K., Moldt, M., Straub, T., Rohs, R., Hopfner, K. P., Korber, P., & Eustermann, S. (2021). Genome information processing by the INO80 chromatin remodeler positions nucleosomes. *Nat Commun*, *12*(1), 3231. https://doi.org/10.1038/s41467-021-23016-z

Oberbeckmann, E., Niebauer, V., Watanabe, S., Farnung, L., Moldt, M., Schmid, A., Cramer, P., Peterson, C. L., Eustermann, S., Hopfner, K. P., & Korber, P. (2021). Ruler elements in chromatin remodelers set nucleosome array spacing and phasing. *Nat Commun*, *12*(1), 3232. https://doi.org/10.1038/s41467-021-23015-0

Oberbeckmann, E., Wolff, M., Krietenstein, N., Heron, M., Ellins, J. L., Schmid, A., Krebs, S., Blum, H., Gerland, U., & Korber, P. (2019). Absolute nucleosome occupancy map for the Saccharomyces cerevisiae genome. *Genome Res*, *29*(12), 1996-2009. https://doi.org/10.1101/gr.253419.119

Ocampo, J., Chereji, R. V., Eriksson, P. R., & Clark, D. J. (2016). The ISW1 and CHD1 ATP-dependent chromatin remodelers compete to set nucleosome spacing in vivo. *Nucleic Acids Res*, *44*(10), 4625-4635. https://doi.org/10.1093/nar/gkw068

Ocampo, J., Chereji, R. V., Eriksson, P. R., & Clark, D. J. (2019). Contrasting roles of the RSC and ISW1/CHD1 chromatin remodelers in RNA polymerase II elongation and termination. *Genome Res*, *29*(3), 407-417. https://doi.org/10.1101/gr.242032.118

Olins, D. E., & Olins, A. L. (2003). Chromatin history: our view from the bridge. *Nat Rev Mol Cell Biol*, *4*(10), 809-814. https://doi.org/10.1038/nrm1225

Oudet, P., Gross-Bellard, M., & Chambon, P. (1975). Electron microscopic and biochemical evidence that chromatin structure is a repeating unit. *Cell*, *4*(4), 281-300. https://doi.org/10.1016/0092-8674(75)90149-x

Ozonov, E. A., & van Nimwegen, E. (2013). Nucleosome free regions in yeast promoters result from competitive binding of transcription factors that interact with chromatin modifiers. *PLoS Comput Biol*, *9*(8), e1003181. https://doi.org/10.1371/journal.pcbi.1003181

Papamichos-Chronakis, M., Watanabe, S., Rando, O. J., & Peterson, C. L. (2011). Global regulation of H2A.Z localization by the INO80 chromatin-remodeling enzyme is essential for genome integrity. *Cell*, *144*(2), 200-213. https://doi.org/10.1016/j.cell.2010.12.021

Parnell, T. J., Huff, J. T., & Cairns, B. R. (2008). RSC regulates nucleosome positioning at Pol II genes and density at Pol III genes. *EMBO J*, *27*(1), 100-110. https://doi.org/10.1038/sj.emboj.7601946

Parnell, T. J., Schlichter, A., Wilson, B. G., & Cairns, B. R. (2015). The chromatin remodelers RSC and ISW1 display functional and chromatin-based promoter antagonism. *Elife*, *4*, e06073. https://doi.org/10.7554/eLife.06073

Perisic, O., Collepardo-Guevara, R., & Schlick, T. (2010). Modeling studies of chromatin fiber structure as a function of DNA linker length. *J Mol Biol*, *403*(5), 777-802. https://doi.org/10.1016/j.jmb.2010.07.057

Peterson, C. L., & Laniel, M. A. (2004). Histones and histone modifications. *Curr Biol*, *14*(14), R546-551. https://doi.org/10.1016/j.cub.2004.07.007

Prasad, R., D'Arcy, S., Hada, A., Luger, K., & Bartholomew, B. (2016). Coordinated Action of Nap1 and RSC in Disassembly of Tandem Nucleosomes. *Mol Cell Biol*, *36*(17), 2262-2271. https://doi.org/10.1128/MCB.00195-16

Prunell, A. (1982). Nucleosome reconstitution on plasmid-inserted poly(dA) . poly(dT). *EMBO J*, *1*(2), 173-179. https://www.ncbi.nlm.nih.gov/pubmed/6325153

Quinlan, A. R., & Hall, I. M. (2010). BEDTools: a flexible suite of utilities for comparing genomic features. *Bioinformatics*, *26*(6), 841-842. https://doi.org/10.1093/bioinformatics/btq033

Ramachandran, S., Ahmad, K., & Henikoff, S. (2017). Transcription and Remodeling Produce Asymmetrically Unwrapped Nucleosomal Intermediates. *Mol Cell*, *68*(6), 1038-1053 e1034. https://doi.org/10.1016/j.molcel.2017.11.015

Rawal, Y., Chereji, R. V., Qiu, H., Ananthakrishnan, S., Govind, C. K., Clark, D. J., & Hinnebusch, A. G. (2018). SWI/SNF and RSC cooperate to reposition and evict promoter nucleosomes at highly expressed genes in yeast. *Genes Dev*, *32*(9-10), 695-710. https://doi.org/10.1101/gad.312850.118

Reeves, R., & Nissen, M. S. (1990). The A.T-DNA-binding domain of mammalian high mobility group I chromosomal proteins. A novel peptide motif for recognizing DNA structure. *J Biol Chem*, *265*(15), 8573-8582. https://www.ncbi.nlm.nih.gov/pubmed/1692833

Rhee, H. S., Bataille, A. R., Zhang, L., & Pugh, B. F. (2014). Subnucleosomal structures and nucleosome asymmetry across a genome. *Cell*, *159*(6), 1377-1388. https://doi.org/10.1016/j.cell.2014.10.054

Rhee, H. S., & Pugh, B. F. (2011). Comprehensive genome-wide protein-DNA interactions detected at single-nucleotide resolution. *Cell*, *147*(6), 1408-1419. https://doi.org/10.1016/j.cell.2011.11.013

Ricci, M. A., Manzo, C., Garcia-Parajo, M. F., Lakadamyali, M., & Cosma, M. P. (2015). Chromatin fibers are formed by heterogeneous groups of nucleosomes in vivo. *Cell*, *160*(6), 1145-1158. https://doi.org/10.1016/j.cell.2015.01.054

Rippe, K. (2022). Liquid-Liquid Phase Separation in Chromatin. *Cold Spring Harb Perspect Biol*, *14*(2). https://doi.org/10.1101/cshperspect.a040683

Rippe, K., Schrader, A., Riede, P., Strohner, R., Lehmann, E., & Langst, G. (2007). DNA sequence- and conformation-directed positioning of nucleosomes by chromatin-remodeling complexes. *Proc Natl Acad Sci U S A*, *104*(40), 15635-15640. https://doi.org/10.1073/pnas.0702430104

Rossi, M. J., Kuntala, P. K., Lai, W. K. M., Yamada, N., Badjatia, N., Mittal, C., Kuzu, G., Bocklund, K., Farrell, N. P., Blanda, T. R., Mairose, J. D., Basting, A. V., Mistretta, K. S., Rocco, D. J., Perkinson, E. S., Kellogg, G. D., Mahony, S., & Pugh, B. F. (2021). A high-resolution protein architecture of the budding yeast genome. *Nature*, *592*(7853), 309-314. https://doi.org/10.1038/s41586-021-03314-8

Rossi, M. J., Lai, W. K. M., & Pugh, B. F. (2018). Genome-wide determinants of sequence-specific DNA binding of general regulatory factors. *Genome Res*, *28*(4), 497-508. https://doi.org/10.1101/gr.229518.117

Rudnizky, S., Bavly, A., Malik, O., Pnueli, L., Melamed, P., & Kaplan, A. (2016). H2A.Z controls the stability and mobility of nucleosomes to regulate expression of the LH genes. *Nat Commun*, *7*, 12958. https://doi.org/10.1038/ncomms12958

Saha, A., Wittmeyer, J., & Cairns, B. R. (2002). Chromatin remodeling by RSC involves ATP-dependent DNA translocation. *Genes Dev*, *16*(16), 2120-2134. https://doi.org/10.1101/gad.995002

Santisteban, M. S., Hang, M., & Smith, M. M. (2011). Histone variant H2A.Z and RNA polymerase II transcription elongation. *Mol Cell Biol*, *31*(9), 1848-1860. https://doi.org/10.1128/MCB.01346-10

Satchwell, S. C., Drew, H. R., & Travers, A. A. (1986). Sequence periodicities in chicken nucleosome core DNA. *J Mol Biol*, *191*(4), 659-675. https://doi.org/10.1016/0022-2836(86)90452-3

Schones, D. E., Cui, K., Cuddapah, S., Roh, T. Y., Barski, A., Wang, Z., Wei, G., & Zhao, K. (2008). Dynamic regulation of nucleosome positioning in the human genome. *Cell*, *132*(5), 887-898. https://doi.org/10.1016/j.cell.2008.02.022

Schubert, H. L., Wittmeyer, J., Kasten, M. M., Hinata, K., Rawling, D. C., Heroux, A., Cairns, B. R., & Hill, C. P. (2013). Structure of an actin-related subcomplex of the SWI/SNF chromatin remodeler. *Proc Natl Acad Sci U S A*, *110*(9), 3345-3350. https://doi.org/10.1073/pnas.1215379110

Segal, E., Fondufe-Mittendorf, Y., Chen, L., Thastrom, A., Field, Y., Moore, I. K., Wang, J. P., & Widom, J. (2006). A genomic code for nucleosome positioning. *Nature*, *442*(7104), 772-778. https://doi.org/10.1038/nature04979

Segal, E., & Widom, J. (2009a). Poly(dA:dT) tracts: major determinants of nucleosome organization. *Curr Opin Struct Biol*, *19*(1), 65-71. https://doi.org/10.1016/j.sbi.2009.01.004

Segal, E., & Widom, J. (2009b). What controls nucleosome positions? *Trends Genet*, *25*(8), 335-343. https://doi.org/10.1016/j.tig.2009.06.002

Shivaswamy, S., & Iyer, V. R. (2008). Stress-dependent dynamics of global chromatin remodeling in yeast: dual role for SWI/SNF in the heat shock stress response. *Mol Cell Biol*, *28*(7), 2221-2234. https://doi.org/10.1128/MCB.01659-07

Shrader, T. E., & Crothers, D. M. (1989). Artificial nucleosome positioning sequences. *Proc Natl Acad Sci U S A*, *86*(19), 7418-7422. https://doi.org/10.1073/pnas.86.19.7418

Shrader, T. E., & Crothers, D. M. (1990). Effects of DNA sequence and histone-histone interactions on nucleosome placement. *J Mol Biol*, *216*(1), 69-84. https://doi.org/10.1016/S0022-2836(05)80061-0

Simic, R., Lindstrom, D. L., Tran, H. G., Roinick, K. L., Costa, P. J., Johnson, A. D., Hartzog, G. A., & Arndt, K. M. (2003). Chromatin remodeling protein Chd1 interacts with transcription elongation factors and localizes to transcribed genes. *EMBO J*, *22*(8), 1846-1856. https://doi.org/10.1093/emboj/cdg179

Simon, R. H., & Felsenfeld, G. (1979). A new procedure for purifying histone pairs H2A + H2B and H3 + H4 from chromatin using hydroxylapatite. *Nucleic Acids Res*, *6*(2), 689-696. https://doi.org/10.1093/nar/6.2.689

Simpson, R. T. (1978). Structure of the chromatosome, a chromatin particle containing 160 base pairs of DNA and all the histones. *Biochemistry*, *17*(25), 5524-5531. https://doi.org/10.1021/bi00618a030

Singh, A. K., Schauer, T., Pfaller, L., Straub, T., & Mueller-Planitz, F. (2021). The biogenesis and function of nucleosome arrays. *Nat Commun*, *12*(1), 7011. https://doi.org/10.1038/s41467-021-27285-6

Singh, M., D'Silva, L., & Holak, T. A. (2006). DNA-binding properties of the recombinant high-mobility-group-like AT-hook-containing region from human BRG1 protein. *Biol Chem*, *387*(10-11), 1469-1478. https://doi.org/10.1515/BC.2006.184

Skene, P. J., & Henikoff, S. (2017). An efficient targeted nuclease strategy for high-resolution mapping of DNA binding sites. *Elife*, *6*. https://doi.org/10.7554/eLife.21856

Smith, C. L., & Peterson, C. L. (2005). A conserved Swi2/Snf2 ATPase motif couples ATP hydrolysis to chromatin remodeling. *Mol Cell Biol*, *25*(14), 5880-5892. https://doi.org/10.1128/MCB.25.14.5880-5892.2005

Smolle, M., Venkatesh, S., Gogol, M. M., Li, H., Zhang, Y., Florens, L., Washburn, M. P., & Workman, J. L. (2012). Chromatin remodelers Isw1 and Chd1 maintain chromatin structure during transcription by preventing histone exchange. *Nat Struct Mol Biol*, *19*(9), 884-892. https://doi.org/10.1038/nsmb.2312

Song, F., Chen, P., Sun, D., Wang, M., Dong, L., Liang, D., Xu, R. M., Zhu, P., & Li, G. (2014). Cryo-EM study of the chromatin fiber reveals a double helix twisted by tetranucleosomal units. *Science*, *344*(6182), 376-380. https://doi.org/10.1126/science.1251413

Soria, G., Polo, S. E., & Almouzni, G. (2012). Prime, repair, restore: the active role of chromatin in the DNA damage response. *Mol Cell*, *46*(6), 722-734. https://doi.org/10.1016/j.molcel.2012.06.002

Spivak, A. T., & Stormo, G. D. (2012). ScerTF: a comprehensive database of benchmarked position weight matrices for Saccharomyces species. *Nucleic Acids Res*, *40*(Database issue), D162-168. https://doi.org/10.1093/nar/gkr1180

Stockdale, C., Flaus, A., Ferreira, H., & Owen-Hughes, T. (2006). Analysis of nucleosome repositioning by yeast ISWI and Chd1 chromatin remodeling complexes. *J Biol Chem*, *281*(24), 16279-16288. https://doi.org/10.1074/jbc.M600682200

Stoler, S., Keith, K. C., Curnick, K. E., & Fitzgerald-Hayes, M. (1995). A mutation in CSE4, an essential gene encoding a novel chromatin-associated protein in yeast, causes chromosome nondisjunction and cell cycle arrest at mitosis. *Genes Dev*, *9*(5), 573-586. https://doi.org/10.1101/gad.9.5.573

Struhl, K. (1985). Naturally occurring poly(dA-dT) sequences are upstream promoter elements for constitutive transcription in yeast. *Proc Natl Acad Sci U S A*, *82*(24), 8419-8423. https://doi.org/10.1073/pnas.82.24.8419

Struhl, K., & Segal, E. (2013). Determinants of nucleosome positioning. *Nat Struct Mol Biol*, *20*(3), 267-273. https://doi.org/10.1038/nsmb.2506

Suter, D. M. (2020). Transcription Factors and DNA Play Hide and Seek. *Trends Cell Biol*, *30*(6), 491-500. https://doi.org/10.1016/j.tcb.2020.03.003

Szerlong, H., Hinata, K., Viswanathan, R., Erdjument-Bromage, H., Tempst, P., & Cairns, B. R. (2008). The HSA domain binds nuclear actin-related proteins to regulate chromatin-remodeling ATPases. *Nat Struct Mol Biol*, *15*(5), 469-476. https://doi.org/10.1038/nsmb.1403

Talbert, P. B., & Henikoff, S. (2021). Histone variants at a glance. *J Cell Sci*, *134*(6). https://doi.org/10.1242/jcs.244749

Thastrom, A., Bingham, L. M., & Widom, J. (2004). Nucleosomal locations of dominant DNA sequence motifs for histone-DNA interactions and nucleosome positioning. *J Mol Biol*, *338*(4), 695-709. https://doi.org/10.1016/j.jmb.2004.03.032

Thomas, J. O., & Furber, V. (1976). Yeast chromatin structure. *FEBS Lett*, *66*(2), 274-280. https://doi.org/10.1016/0014-5793(76)80521-2

Tran, Q. H., & Unden, G. (1998). Changes in the proton potential and the cellular energetics of Escherichia coli during growth by aerobic and anaerobic respiration or by fermentation. *Eur J Biochem*, *251*(1-2), 538-543. https://doi.org/10.1046/j.1432-1327.1998.2510538.x

Tremethick, D. J. (2007). Higher-order structures of chromatin: the elusive 30 nm fiber. *Cell*, *128*(4), 651-654. https://doi.org/10.1016/j.cell.2007.02.008

Tropberger, P., Pott, S., Keller, C., Kamieniarz-Gdula, K., Caron, M., Richter, F., Li, G., Mittler, G., Liu, E. T., Buhler, M., Margueron, R., & Schneider, R. (2013). Regulation of transcription through acetylation of H3K122 on the lateral surface of the histone octamer. *Cell*, *152*(4), 859-872. https://doi.org/10.1016/j.cell.2013.01.032

Tsankov, A. M., Thompson, D. A., Socha, A., Regev, A., & Rando, O. J. (2010). The role of nucleosome positioning in the evolution of gene regulation. *PLoS Biol*, *8*(7), e1000414. https://doi.org/10.1371/journal.pbio.1000414

Tsukiyama, T., Palmer, J., Landel, C. C., Shiloach, J., & Wu, C. (1999). Characterization of the imitation switch subfamily of ATP-dependent chromatin-remodeling factors in Saccharomyces cerevisiae. *Genes Dev*, *13*(6), 686-697. https://doi.org/10.1101/gad.13.6.686

Udugama, M., Sabri, A., & Bartholomew, B. (2011). The INO80 ATP-dependent chromatin remodeling complex is a nucleosome spacing factor. *Mol Cell Biol*, *31*(4), 662-673. https://doi.org/10.1128/MCB.01035-10

Ushinsky, S. C., Bussey, H., Ahmed, A. A., Wang, Y., Friesen, J., Williams, B. A., & Storms, R. K. (1997). Histone H1 in Saccharomyces cerevisiae. *Yeast*, *13*(2), 151-161. https://doi.org/10.1002/(SICI)1097-0061(199702)13:2<151::AID-YEA94>3.0.CO;2-5

van Bakel, H., Tsui, K., Gebbia, M., Mnaimneh, S., Hughes, T. R., & Nislow, C. (2013). A compendium of nucleosome and transcript profiles reveals determinants of chromatin architecture and transcription. *PLoS Genet*, *9*(5), e1003479. https://doi.org/10.1371/journal.pgen.1003479

Van Holde, K. E. (2012). *Chromatin*. Springer Science & Business Media.

Vary, J. C., Jr., Gangaraju, V. K., Qin, J., Landel, C. C., Kooperberg, C., Bartholomew, B., & Tsukiyama, T. (2003). Yeast Isw1p forms two separable complexes in vivo. *Mol Cell Biol*, *23*(1), 80-91. https://doi.org/10.1128/MCB.23.1.80-91.2003

Wagner, F. R. (2020). *Structure of SWI/SNF chromatin remodeller RSC bound to a nucleosome and implications for chromatin remodelling* [Dissertation, Max Planck Institute for Biophysical Chemistry].

Wagner, F. R., Dienemann, C., Wang, H., Stutzer, A., Tegunov, D., Urlaub, H., & Cramer, P. (2020). Structure of SWI/SNF chromatin remodeller RSC bound to a nucleosome. *Nature*, *579*(7799), 448-451. https://doi.org/10.1038/s41586-020-2088-0

Wang, F., Ranjan, A., Wei, D., & Wu, C. (2016). Comment on "A histone acetylation switch regulates H2A.Z deposition by the SWR-C remodeling enzyme". *Science*, *353*(6297), 358. https://doi.org/10.1126/science.aad5921

Wang, J. P., & Widom, J. (2005). Improved alignment of nucleosome DNA sequences using a mixture model. *Nucleic Acids Res*, *33*(21), 6743-6755. https://doi.org/10.1093/nar/gki977

Weiner, A., Hsieh, T. H., Appleboim, A., Chen, H. V., Rahat, A., Amit, I., Rando, O. J., & Friedman, N. (2015). High-resolution chromatin dynamics during a yeast stress response. *Mol Cell*, *58*(2), 371-386. https://doi.org/10.1016/j.molcel.2015.02.002

Winger, J., & Bowman, G. D. (2017). The Sequence of Nucleosomal DNA Modulates Sliding by the Chd1 Chromatin Remodeler. *J Mol Biol*, *429*(6), 808-822. https://doi.org/10.1016/j.jmb.2017.02.002

Winger, J., Nodelman, I. M., Levendosky, R. F., & Bowman, G. D. (2018). A twist defect mechanism for ATP-dependent translocation of nucleosomal DNA. *Elife*, *7*. https://doi.org/10.7554/eLife.34100

Wittmeyer, J., Saha, A., & Cairns, B. (2004). DNA translocation and nucleosome remodeling assays by the RSC chromatin remodeling complex. *Methods Enzymol*, *377*, 322-343. https://doi.org/10.1016/S0076-6879(03)77020-7

Woodcock, C. L., Frado, L. L., & Rattner, J. B. (1984). The higher-order structure of chromatin: evidence for a helical ribbon arrangement. *J Cell Biol*, *99*(1 Pt 1), 42-52. https://doi.org/10.1083/jcb.99.1.42

Woodcock, C. L., Safer, J. P., & Stanchfield, J. E. (1976). Structural repeating units in chromatin. I. Evidence for their general occurrence. *Exp Cell Res*, *97*, 101-110. https://doi.org/10.1016/0014-4827(76)90659-5

Workman, J. L., & Roeder, R. G. (1987). Binding of transcription factor TFIID to the major late promoter during in vitro nucleosome assembly potentiates subsequent initiation by RNA polymerase II. *Cell*, *51*(4), 613-622. https://doi.org/10.1016/0092-8674(87)90130-9

Wu, R., & Li, H. (2010). Positioned and G/C-capped poly(dA:dT) tracts associate with the centers of nucleosome-free regions in yeast promoters. *Genome Res*, *20*(4), 473-484. https://doi.org/10.1101/gr.103226.109

Xu, Z., Wei, W., Gagneur, J., Perocchi, F., Clauder-Munster, S., Camblong, J., Guffanti, E., Stutz, F., Huber, W., & Steinmetz, L. M. (2009). Bidirectional promoters generate pervasive transcription in yeast. *Nature*, *457*(7232), 1033-1037. https://doi.org/10.1038/nature07728

Yamada, K., Frouws, T. D., Angst, B., Fitzgerald, D. J., DeLuca, C., Schimmele, K., Sargent, D. F., & Richmond, T. J. (2011). Structure and mechanism of the chromatin remodelling factor ISW1a. *Nature*, *472*(7344), 448-453. https://doi.org/10.1038/nature09947

Yan, C., Chen, H., & Bai, L. (2018). Systematic Study of Nucleosome-Displacing Factors in Budding Yeast. *Mol Cell*, *71*(2), 294-305 e294. https://doi.org/10.1016/j.molcel.2018.06.017

Yang, L., Orenstein, Y., Jolma, A., Yin, Y., Taipale, J., Shamir, R., & Rohs, R. (2017). Transcription factor family-specific DNA shape readout revealed by quantitative specificity models. *Mol Syst Biol*, *13*(2), 910. https://doi.org/10.15252/msb.20167238

Yang, X., Zaurin, R., Beato, M., & Peterson, C. L. (2007). Swi3p controls SWI/SNF assembly and ATP-dependent H2A-H2B displacement. *Nat Struct Mol Biol*, *14*(6), 540-547. https://doi.org/10.1038/nsmb1238

Yuan, G. C., Liu, Y. J., Dion, M. F., Slack, M. D., Wu, L. F., Altschuler, S. J., & Rando, O. J. (2005). Genome-scale identification of nucleosome positions in S. cerevisiae. *Science*, *309*(5734), 626-630. https://doi.org/10.1126/science.1112178

Zentner, G. E., Kasinathan, S., Xin, B., Rohs, R., & Henikoff, S. (2015). ChEC-seq kinetics discriminates transcription factor binding sites by DNA sequence and shape in vivo. *Nat Commun*, *6*, 8733. https://doi.org/10.1038/ncomms9733

Zhang, Y. (2003). Transcriptional regulation by histone ubiquitination and deubiquitination. *Genes Dev*, *17*(22), 2733-2740. https://doi.org/10.1101/gad.1156403

Zhang, Z., Wippo, C. J., Wal, M., Ward, E., Korber, P., & Pugh, B. F. (2011). A packing mechanism for nucleosome organization reconstituted across a eukaryotic genome. *Science*, *332*(6032), 977-980. https://doi.org/10.1126/science.1200508

Zhao, Z., & Shilatifard, A. (2019). Epigenetic modifications of histones in cancer. *Genome Biol*, *20*(1), 245. https://doi.org/10.1186/s13059-019-1870-5

Zhou, C. Y., Johnson, S. L., Gamarra, N. I., & Narlikar, G. J. (2016). Mechanisms of ATP-Dependent Chromatin Remodeling Motors. *Annu Rev Biophys*, *45*, 153-181. https://doi.org/10.1146/annurev-biophys-051013-022819

Zhou, C. Y., Johnson, S. L., Lee, L. J., Longhurst, A. D., Beckwith, S. L., Johnson, M. J., Morrison, A. J., & Narlikar, G. J. (2018). The Yeast INO80 Complex Operates as a Tunable DNA Length-Sensitive Switch to Regulate Nucleosome Sliding. *Mol Cell*, *69*(4), 677-688 e679. https://doi.org/10.1016/j.molcel.2018.01.028

Appendix A:

Table 5 – Primary RSC *in vitro* reconstitution dataset TBPool1 & TBPool2

Sample	Fastq ID	Remodeler	Barrier	Density	Conc. (nM)	Note
1	TBPool1_04	-	-	0.4	10	-
2	TBPool1_042	-	-	0.4	10	-
3	TBPool1_08	-	-	0.8	10	-
4	TBPool1_082	-	-	0.8	10	-
5	TBPool1_1	RSC	-	0.4	10	-
6	TBPool1_10	-	Abf1	0.8	10	-
7	TBPool1_11	-	Rap1	0.8	10	-
8	TBPool1_12	-	Reb1	0.8	10	-
9	TBPool1_13	RSC	Abf1	0.8	10	-
10	TBPool1_14	RSC	Rap1	0.8	10	-
11	TBPool1_15	RSC	Reb1	0.8	10	-
12	TBPool1_16	RSC	-	0.8	10	BamHI
13	TBPool1_17	-	Abf1	0.4	10	-
14	TBPool1_18	RSC	-	0.4	10	-
15	TBPool1_19	-	Rap1	0.4	10	-
16	TBPool1_2	-	Abf1	0.4	10	-
17	TBPool1_20	-	Reb1	0.4	10	-
18	TBPool1_21	-	-	0.4	10	-
19	TBPool1_22	RSC	Abf1	0.4	10	-
20	TBPool1_23	RSC	Rap1	0.4	10	-
21	TBPool1_24	RSC	Reb1	0.4	10	-
22	TBPool1_25	RSC	-	0.4	10	BamHI
23	TBPool1_26	RSC	-	0.8	10	-
24	TBPool1_27	-	Abf1	0.8	10	-
25	TBPool1_28	-	Rap1	0.8	10	-
26	TBPool1_29	-	Reb1	0.8	10	-
27	TBPool1_3	-	Rap1	0.4	10	-
28	TBPool1_30	-	-	0.8	10	-
29	TBPool1_31	RSC	Abf1	0.8	10	-
30	TBPool1_32	RSC	Rap1	0.8	10	-
31	TBPool1_33	RSC	Reb1	0.8	10	-
32	TBPool1_34	RSC	-	0.8	10	BamHI
33	TBPool1_4	-	Reb1	0.4	10	-
34	TBPool1_5	RSC	Abf1	0.4	10	-
35	TBPool1_6	RSC	Rap1	0.4	10	-
36	TBPool1_7	RSC	Reb1	0.4	10	-
37	TBPool1_8	RSC	-	0.4	10	BamHI
38	TBPool1_9	RSC	-	0.8	10	-
39	TBPool2_i5031	-	-	0.4	10	-

40	TBPool2_i50311	RSC	Abf1	0.4	3.3	-
41	TBPool2_i50312	RSC	Abf1	0.4	1.1	-
42	TBPool2_i50313	RSC	Abf1	0.4	0.37	-
43	TBPool2_i50315	RSC	-	0.8	10	-
44	TBPool2_i50316	RSC	-	0.8	3.3	-
45	TBPool2_i50318	RSC	-	0.8	1.1	-
46	TBPool2_i50319	RSC	-	0.8	0.37	-
47	TBPool2_i5032	-	-	0.8	10	-
48	TBPool2_i50321	RSC	Abf1	0.8	10	-
49	TBPool2_i50322	RSC	Abf1	0.8	3.3	-
50	TBPool2_i50323	RSC	Abf1	0.8	1.1	-
51	TBPool2_i50327	RSC	Abf1	0.8	0.37	-
52	TBPool2_i5033	RSC	-	0.4	10	-
53	TBPool2_i5034	RSC	-	0.4	3.3	-
54	TBPool2_i5036	RSC	-	0.4	1.1	-
55	TBPool2_i5037	RSC	-	0.4	0.37	-
56	TBPool2_i5039	RSC	Abf1	0.4	10	-
57	TBPool2_Univ1	RSC	-	0.4	10	-
58	TBPool2_Univ11	RSC	-	0.8	10	-
59	TBPool2_Univ12	-	Abf1	0.8	10	-
60	TBPool2_Univ14	-	Reb1	0.8	10	-
61	TBPool2_Univ15	RSC	Abf1	0.8	10	-
62	TBPool2_Univ18	RSC	Reb1	0.8	10	BamHI
63	TBPool2_Univ2	-	Abf1	0.4	10	-
64	TBPool2_Univ21	-	-	0.8	10	-
65	TBPool2_Univ4	-	Reb1	0.4	10	-
66	TBPool2_Univ6	RSC	Abf1	0.4	10	-
67	TBPool2_Univ7	RSC	Reb1	0.4	10	BamHI
68	TBPool2_Univ9	-	-	0.4	10	-

Acknowledgements

First and foremost, I would like to thank my supervisor PD Dr. Philipp Korber, for having faith in me and entrusting me with the opportunity to work on this project. He demonstrated great patience, generosity of time and a willingness to teach, and I have developed greatly as a scientist as the result of working with Philipp, for which I am extremely grateful.

I'd also like to thank the rest of the Korber group; Iris Langstein, Andrea Schmid and Elisa Oberbeckmann, for helping me settle in my PhD, sharing their scientific expertise and providing a very enjoyable work environment.

A big thanks to my TAC members, Dr. Tobias Straub and Dr. Christoph Kurat, for their generous contributions of expertise and critique toward my work. I learned a great deal of bioinformatics and analytical thinking from Tobias, whilst Christoph taught me invaluable lab skills and was very generous with materials, so to both I am very grateful.

Thank you to my friends in the Molecular Biology department, both past and present, who helped keep my spirits high in more trying times and made the department feel like a second home. A special shoutout to Nikolas, Nadia, Anna, Vera and Janet for the many instances of caffeine fueled laughter.

A huge thank you to Dr. Elizabeth Schroeder-Reiter, for her support in completing my PhD curriculum, monitoring my progress and wellbeing and her open-door policy providing a friendly face to help tackle any of my concerns. I'd certainly not be graduating yet if not for Elizabeth's help, so her support was really appreciated.

Thank you to Prof. Dr. Peter Becker for fostering a fantastic collaborative environment in the Molecular Biology department, leading by example with an infectious enthusiasm for chromatin biology. I've greatly enjoyed my time in the department, and I credit Peter's influence on the culture here heavily for this, so thank you.

Last but certainly not least, I'd like to thank my family for all their support and efforts to feign interest in my work. I wouldn't have the opportunities I have today without the support of my parents Penny and Garry, nor the courage or strength to capitalise on them without my wife Selin by my side. I am a very lucky man!

Affidavit

LMU

LUDWIG-
MAXIMILIANS-
UNIVERSITÄT
MÜNCHEN

Promotionsbüro
Medizinische Fakultät

MMRS

Affidavit

Barnes, Toby

Surname, first name

Grosshaderner Str. 9

Street

82152, Planegg, Germany

Zip code, town, country

I hereby declare, that the submitted thesis entitled:

The role of DNA sequence in *S. cerevisiae* nucleosome organisation as implemented by chromatin remodelers and general regulatory factors

……

is my own work. I have only used the sources indicated and have not made unauthorised use of services of a third party. Where the work of others has been quoted or reproduced, the source is always given.

I further declare that the submitted thesis or parts thereof have not been presented as part of an examination degree to any other university.

Munich, 18.05.2022

place, date

Toby Barnes

Signature doctoral candidate

Confirmation of congruency

LMU

LUDWIG-
MAXIMILIANS-
UNIVERSITÄT
MÜNCHEN

Promotionsbüro
Medizinische Fakultät

MMRS

Confirmation of congruency between printed and electronic version of the doctoral thesis

Barnes, Toby

Surname, first name

Grosshaderner Str. 9

Street

82152, Planegg, Germany

Zip code, town, country

I hereby declare, that the submitted thesis entitled:

The role of DNA sequence in *S. cerevisiae* nucleosome organisation as implemented by chromatin remodelers and general regulatory factors

……………………………………………………………………………………………………….

is congruent with the printed version both in content and format.

Munich, 18.05.2022

place, date

Toby Barnes

Signature doctoral candidate

List of publications

Barnes, T., & Korber, P. (2021). The Active Mechanism of Nucleosome Depletion by Poly(dA:dT) Tracts In Vivo. *Int J Mol Sci*, *22*(15). https://doi.org/10.3390/ijms22158233

Brandstetter, K., Zulske, T., Ragoczy, T., Horl, D., Guirao-Ortiz, M., Steinek, C., Barnes, T., Stumberger, G., Schwach, J., Haugen, E., Rynes, E., Korber, P., Stamatoyannopoulos, J. A., Leonhardt, H., Wedemann, G., & Harz, H. (2022). Differences in nanoscale organization of regulatory active and inactive human chromatin. *Biophys J*, *121*(6), 977-990. https://doi.org/10.1016/j.bpj.2022.02.009